Interaction Dynamics in Oscillator and Human-in-the-loop Systems

by

Bo Yu

A dissertation submitted in partial fulfillment
of the requirements for the degree of
Doctor of Philosophy
(Mechanical Engineering)
in The University of Michigan
2014

Doctoral Committee:

Associate Professor R. Brent Gillespie, Chair
Adjunct Professor Jeffrey A. Cook
Professor James S. Freudenberg
Professor Arthur D. Kuo
Professor Dawn M. Tilbury

© Bo Yu 2014
All Rights Reserved

ACKNOWLEDGEMENTS

I wish to express my greatest appreciation for my advisors, Brent Gillespie and Jim Freudenberg, for their guidance and persistent help throughout my Ph.D. study. I was constantly inspired by their enthusiasm towards research and profound knowledge in science.

I would like to thank Rick Middleton for his in-depth and valuable suggestions for the work in Chapter 2. I am also grateful to Jeff Cook. He has been a great inspiration and I have profited a lot from our discussion for the work in Chapter 3.

I appreciate my committee members Art Kuo and Dawn Tilbury for providing critical and constructive feedback at our meetings. Their insightful advice has greatly improved the work presented in this dissertation. I truly appreciate their time and effort in reviewing this work.

It was a true pleasure to work with the folks at Haptix Lab and Embedded Control Lab. I thank my fellow labmates for the stimulating discussions, for the sleepless nights we were working together before deadlines, and for all the fun we had in the last five years.

I wish to thank all my friends in Ann Arbor. Their friendship makes my life in Ann Arbor meaningful and blissful. My special thanks go to the friends who had been the pilot test subjects for my research projects. I really appreciate their patient participation in my long experiments.

I also gratefully acknowledge the financial support from the Department of Mechanical Engineering, University of Michigan and the National Science Foundation (Grant CNS-1035271).

Finally, and most importantly, I thank my parents for their endless love and support. My deep thanks also go to my wife, Wenwen, and my son, Qiao, for giving me a wonderful family.

TABLE OF CONTENTS

LIST OF FIGURES

Figure

LIST OF TABLES

Table

LIST OF ABBREVIATIONS

ANOVA Analysis of Variance

ARX Autoregressive Exogenous

CLHP Closed-Left Half of the Complex Plane

CRHP Closed-Right halves of the Complex Plane

CNS Central Nervous System

EEG Electroencephalography

FFT Fast Fourier Transform

fMRI Functional Magnetic Resonance Imaging

IAE Integral Absolute Errors

IATE Integrals of the Absolute Values of the Transient Errors

LTI Linear Time-Invariant

MLE Maximum-Likelihood Estimation

OLHP Open-Left Half of the Complex Plane

ORHP Open-Right Half of the Complex Plane

PID Proportional-Integral-Derivative

SSE Steady State Error

ABSTRACT

Interaction Dynamics in Oscillator and Human-in-the-loop Systems
by
Bo Yu

Chair: R. Brent Gillespie

This dissertation addresses control system analysis and system identification in three areas: error propagation in synchronization of harmonic oscillators, modeling of human active movement while grasping objects, and identification of human feedback and feedforward control in manual pursuit tracking. Commonly occurring within systems in these three areas are two types of communication: one-way communication between system elements by information signals and two-way interaction across mechanical contacts (involving force and motion signals in pairs).

While most studies of synchronization in oscillator systems have focused on the existence of synchronous solutions in steady state, many problems pertaining to the transient dynamics have not been fully resolved. We extend the well-established theory of fundamental limitations to study the transient error propagation (string stability) in a string of synchronized harmonic oscillators. We first develop a new Bode integral to accommodate the pure imaginary poles of oscillator dynamics. We then translate design requirements in terms of time-domain response and hardware limitations into a set of constraints on closed-loop frequency response. We further capture the conflict between string stability on the one hand and time-domain design requirements and hardware limitations on the other.

Modeling human active movement is a challenging problem not only because muscle has very sophisticated and highly nonlinear dynamics but also because neural and other signals internal to the body are difficult to observe directly. We seek a simple yet general and competent model to describe active movement in object manipulation tasks. Inspired by the Norton equivalent circuit in electrical engineering, we build a model based on the motion and force/torque signals that may be observed at the

points of contact between a human hand and the environment. The model consists of a motion source to represent a human's motor plan and a spring-mass-damper coupler to capture the time-varying driving point impedance of the human hand. The model is validated using occasional experimental trials in which a participant experiences unexpected loads in a grasp and twist task.

Although a large amount of literature has provided methods to identify feedback control in manual tracking tasks, very little research has been undertaken to experimentally identify feedforward control. We capitalize on the theory of fundamental limitations to study the link between a human's ability to simultaneously reject disturbances and perform pursuit tracking. We further develop an identification method to separate human feedback and feedforward control strategies in sinusoidal tracking tasks.

The control models of human operators in this work have applications in many fields involving a human in the loop. Examples include human interaction with virtual haptic systems, human skill transfer, assist for neurodegenerative disorders, and rehabilitation after neurological injury.

CHAPTER I

Introduction

The rapid proliferation of embedded and networked microprocessors has created many new opportunities for controls. One of these is the replacement of traditional mechanical linkages with cyber (or virtual) connections. Another opportunity is the possibility for multiple independent agents to coordinate their activity through communication networks in order to achieve a common goal. Examples arise in many application domains, including vehicle platooning in transportation systems [90], consensus in formation control [73], synchronization of network-coupled oscillators [21], and the design of steer-by-wire and fly-by-wire systems [83]. In these applications, information exchange takes place through virtual connections instead of physical linkages.

Physical connections inherently provide two-way information flow between agents, through the reaction forces that they impose upon one another [40]. This observation was first made by Newton in his famous third law: "To every action there is always opposed an equal reaction; or the mutual actions of two bodies upon each other are always equal, and directed to contrary parts." Moreover, physical connections fundamentally result in energy exchange through the power-conjugate force and motion variables. On the other hand, virtual connections allow greater flexibility in the information exchanged between agents, yet pose another set of issues not present when agents are connected physically[1]. For example, the failure modes of virtual connections may be poorly understood. If the coupling is virtual, there may be no physical intuition for the behavior of the system as a whole, especially when a human and computer are cooperating to achieve a desired goal. Use of visual feedback by a human driver controlling headway to the preceding vehicle is an example of a virtual link that lacks a simple physical equivalent. Actions transmitted through such a

[1]Two-way interactions may also be present in a virtual connection, but that would be a consequence of design rather than physics.

virtual link need not be accompanied by reactions, and need not carry energy or power. Whether the human or computerized agent is interfaced to a physical link has very important implications in achievable cooperative control performance or human/machine interaction.

The goal in this dissertation is to describe relationships between properties and performance in the framework of controls for systems that mix human and computer and that include physical and virtual links. Specifically, this dissertation aims to study control system analysis and system identification in three different areas:

1) the error propagation phenomenon in synchronization of coupled oscillators;

2) human movement modeling for grasp and twist tasks;

3) identification of human feedback and feedforward control in manual pursuit tracking of sinusoidal signals.

1.1 Synchronization of Coupled Oscillators

Synchronization of a network of coupled oscillators has been a hot topic in various scientific areas ranging from biology, physics, and chemistry to social networks and engineering [93, 45, 21]. Here synchronization means the adjustment of rhythms of oscillating objects to achieve a uniform oscillatory state through inter-agent virtual or physical interactions. Maybe the first observed phenomenon of coupled oscillation in inanimate objects was discovered by the great Dutch scientist Christiaan Huygens in 1665 [7]. He observed the synchronization of two pendulum clocks mounted in one wooden beam: no matter how the pendulums started out, eventually they always ended up swinging in exactly opposite directions; Further, if this agreement was disturbed by some interference, it reestablished itself in a short time. Since then a rich body of literature has grown on synchronization among coupled oscillators and it still fascinates the scientific community nowadays due to the existence of certain applications in science and engineering. Application examples include flashing fireflies, chirping crickets, central pattern generators for animal locomotion, Hodgkin-Huxley model of neurons, phase locking in solid-state circuit oscillators, ground vehicle coordination, synchronization in semiconductor laser arrays, clock synchronization in decentralized computing networks, and network-reduced power system models, to name just a few [67, 22]. The past twenty years have witnessed considerable theoretical progress and novel applications in different disciplines.

The control community has also contributed to the field by providing novel results. Most of the results are focused on synchronization (rather than more complex phenomena) among a finite number of oscillators with simple (e.g. a string structure or tree structure) topologies [56, 88, 14]. Some of the work used graph theory to describe the virtual or physical links in such oscillator systems [103, 81]. A commonly used model of coupled oscillators is the Kuramoto oscillator or its variations [14]. In many studies each oscillator is coupled only to a subset of the others, and the coupling constants are allowed to vary with time, perhaps modeling a situation in which the oscillators are coupled through communication over a switching network. Achieving synchronization in coupled oscillators implies the existence and stability of synchronous solutions in steady state. Various interaction laws and communication topologies have been designed to guarantee synchronization in steady state. However, many problems pertaining to the transient response have received little attention and still need to be fully resolved. The analysis of transient dynamics aims to characterize what happens before a multi-agent system settles to the synchronized states after a disturbance or perturbation. Other research areas in multi-agent systems have illustrated that the poor transient dynamic response may produce alarming behaviors even when the whole system is able to achieve consensus eventually.

String instability in vehicle platooning is one example of a behavior that emerges from a multi-agent system with virtual links and has long been recognized. String instability is an error propagation phenomenon in which a disturbance to the lead vehicle will necessarily be amplified as it propagates along the vehicle platoon. Early studies of string instability were undertaken in the context of specific control laws, such as PID and optimal control [75, 59]. This made comparison between different communication schemes problematic, in that the observed string instability may have been due to a poor choice of controller gains rather than to the particular communication scheme adopted. Only very recently have such statements been made for agents using arbitrary control policies, using analysis from the theory of fundamental design limitations [87, 66]. In these studies the agent model contained a single or double integrator. Significant gaps remain in the determination of fundamental design limits for cyber-physical systems with more complex agent models such as harmonic oscillators.

Our objective is to extend fundamental design limitations theory to cover systems with mixed cyber and physical components. Specifically, we contribute tools that delineate tradeoffs between performance and feedback properties for control systems involving hardware dynamics, controllers, communication topology, and time delays.

We assess the contribution to system behavior (e.g. string stability) of each agent's realization in hardware (whose behavior is subject to the laws of Newton) as well as realization in software and communication (where behavior is subject to the fundamental limitations of Shannon and Bode). The ability to express such relationships for classes of dynamics, controllers, and topologies significantly extends the tools available to predict behaviors emerging within multi-agent systems. The results in this dissertation contribute to the literature of synchronization of linear coupled oscillators by illustrating the fundamental relationship between transient response behavior and system properties.

1.2 Human Movement Modeling for Manual Tasks Involving Anticipatory Control

The maxim of "practice makes perfect"applies widely to our everyday activities that involve the development of motor skills. Dexterous object manipulation is learned from previous body-object interactions. For example, we learn how to make agile and quick maneuvering to play soccer games, which require dexterity with the legs and feet. We also establish well-organized actions to achieve desired outcomes in our daily life. For instance, consider grasping a water cup to take a drink. We use proper grip forces that balance grasp stability and effort to lift cups with different weights. Depending on how full the water cup is, we choose appropriate grip force and trajectories to move the cup and carefully avoid spills.

The simple grasp and lift task has attracted research in the scientific community for decades. Much research has focused on the fine coordination of grip force and load force during grasp and lift tasks [48, 46, 51]. Experimental results have shown that the grip force is precisely controlled so that it is just slightly greater than the minimum grip force needed to prevent slip under normal conditions [47]. Such grip-force load-force coordination also exists when gripping objects with different surfaces [48], curvatures [43], and shapes [44] as well as when gripping objects in virtual haptic environments [26].

The human hand trajectories during these grasp and lift or similar grasp and twist movements have not received much attention compared with the grip-force load-force coordination. Ample research results have shown that human movement trajectories have certain patterns. Some famous examples include Fitts's law [25], the bell-shaped velocity profile in fast reaching tasks, and the minimum jerk performance index [102, 28]. The movement trajectories of human hands in grasp and lift or

grasp and twist tasks probably also display very repeatable patterns, e.g. the smooth velocity profiles [47, 46] and the overshoots in position signals for catch trials [47]. However no mechanical models that can produce such trajectories have been proposed and experimentally tested. In this dissertation, we attempt to establish a simple and competent mechanical model for a prototypical grasp and twist task. Our model is based on the observed interactive behavior in the mechanical domain of motions and forces at the points of contact between human hands and the physical or virtual environments.

The dynamic interaction between the human musculoskeletal system and the environment results in the transmission of power because the force and motion are energetically conjugate at the point of contact. The two-way interaction with power transmission may be partially characterized by mechanical impedance [38, 80, 12]. Mechanical impedance describes the relationship between a displacement imposed on a system and the evoked force. This property is very important for human posture control [20, 97], movement [96], and even the stability of haptic interfaces [105]. Humans can also voluntarily control mechanical impedance to achieve certain goals, such as to stabilize an unstable environment [12]. Sometimes, humans can also choose the appropriate impedance of the body to take advantage of the interactive environment to perform certain tasks.

The structure of various models used to describe mechanical impedance of the human body differs significantly in the literature. The difference is in part due to the intrinsic properties of various body structures. It can be as simple as a pure spring [31] and it can also be as complex as a double spring-damper-mass system that has five parameters [30]. Maybe the most common impedance model is a second-order spring-damper-mass system, which has been used to model the finite impedance of finger tips [34], human hands grasping a knob or a wheel [35], and joint dynamics [55]. Experimental identification of impedance requires mechanical perturbation. Both time-domain identification methods (e.g. least square fit of time-domain data) [97, 34, 35] and stochastic identification methods [91, 105, 58] (e.g. white noise perturbation) have been utilized to characterize the mechanical impedance. Moreover, the human body's mechanical impedance has strong adaptability [12, 1] and evidence shows that in certain tasks the impedance values depend on grip force [34, 35] or postures [97].

The physically measurable mechanical impedance itself cannot fully describe a human's active movement to realize a desired trajectory. Generating active movement requires the participation of some biological actuators like muscles. In engineering, any actuator has two important aspects: the "driving point impedance" and "forward-

path response function" [39, 40]. The forward-path response function for human active movement describes how the neural input from the central nervous system (CNS) affects the movement trajectory. How to characterize the human neural input or motor plan that is generated by the CNS when he or she is interacting with physical or virtual worlds is a common problem in various fields such as biological neuromotor control, haptic interface design, and teleoperation. Even for a simple grasp and twist task, it is not easy to decipher the motor plans produced by the CNS that control active movement. Clearly, when grasping and twisting an object, a human's hands are neither a pure position source nor a pure force source because such pure position or force sources are not backdrivable. The simplest way to incorporate the mechanical impedance and forward-path response function is to combine a position source that represents the motor plans with a mechanical impedance. The position source is coupled to the mechanical impedance in a manner that is analogous to the current source in the Norton-equivalent electrical circuit. Several papers in the literature have attempted to identify such a motion source [37] by designing algorithms to eliminate the interaction torque or force between the motion source and the environment. However, the identified motion source may not be able to model normal human and object interaction due to the presence of interaction force and humans' strong adaptability to different tasks.

Despite the success of identifying the mechanical impedance and motion source, these two important parts have not been put together to predict human active movement nor has the simple model been validated against experimental data. The difficulty in validating this model is partially due to humans' adaptability for different tasks [12, 1]. In this dissertation, we attempt to build an active movement model that captures the adaptability to different environments in a grasp and twist task and also validate this model using "catch trial" experimental data. A motorized haptic device was used to render two different virtual environments that the human user interacted with. One is a heavy load and the other is a light load. We assume the impedance values change with grip force and hence we identify the relationship between impedance values and grip forces from separate system identification experiments. We also assume the same relationship between grip force and twist impedance holds for the active grasp and twist task. An algorithm was formulated to estimate the position sources from the experimental data. We demonstrated that subjects generally use different position source and grip force for these two virtual loads. When the virtual environment changed and the subjects were not aware of the change (we call this a "Catch Trial"), the human hand movement trajectories

would be distorted relative to the normal trajectories with overshoot or undershoot. We checked our proposed model using catch trial data by comparing the predicted trajectory distortion with the experimental data.

Our proposed simple model can be extended to study other human movement behaviors and human-machine interfaces. Of particular interest to us is the phenomena in human interaction with virtual haptic systems in our teaching lab (Embedded Control Lab). Studying interactive behaviors in such systems containing a human in the loop sometimes requires an active human model [105]. Another application is to utilize our proposed model for human skill transfer. The proposed model can be used not only for transferring human movement strategy to robots [42], but also for helping less-skilled humans improve their performance. Automotive industry is another domain that the simple human model can find applications, e.g. the active-steering control system design [95, 68, 4] in which most human models only contain passive driving point impedance or if they contain active control, they lack backdrive impedance [2].

1.3 Human Feedback and Feedforward Control in Manual Pursuit Tracking of Sinusoidal Signals

We carry out various control tasks in our lives that range from the simple grasp and twist tasks like opening a door knob to relatively complex tasks such as driving a vehicle or piloting an airplane. Human operator models are important in integrated man-machine systems. The capabilities and limitations of the human operator in operating the man-machine system need to be measured and described as accurately as possible. An accurate and robust human operator model provides constraints for the design of such man-machine systems and also enables the test of the integrated system with human operator models in a closed-loop fashion.

Models for the human operator can be dated back to 1940s. Early studies in this area were motivated by a need for pilot models that could be used in the design of warplanes and spaceships for space exploration [98, 24, 64]. Most of the research during this early stage was devoted to understanding the characteristics of the human as a controller of single variable, single display linear time-invariant (LTI) systems. The proposed quasi-linear models in [98, 24, 64] are surprisingly adept at predicting human behavior in this simple but important class of tracking tasks.

Some of the recent studies on human operator modeling concentrate on models for drivers' control behavior in part due to the research in advanced active safety

engineering and autonomous vehicles [60, 13, 15, 99]. In the literature, a wide range of driver models employ various modern control methods. These range from the use of optimal control [15] to those using PID controllers [99] or complex models for modelling human behaviour using fuzzy logic and Markov dynamic models [13, 74].

Most of the human operator models focus on the feedback control representation of human operators in response to unpredictable reference signals. Several research papers have indicated that human operators may use a combination of feedforward control on the reference signal and feedback on the remaining error for pursuit display [100, 76, 104, 78]. Here feedforward control is defined as control actions based on the target signal: either from perceiving the target on the display or from memorized or inferred knowledge on the target signal properties. Feedforward control can be made without the sensory feedback information that evolves during the tracking tasks, and may require internal models of the reference signal and the controlled dynamics for accuracy. Hence feedforward control actions can occur rapidly, as no delay from the feedback loop is involved. On the other hand, feedback control involves modification of the ongoing movement to reduce errors using sensory information. Therefore feedback control allows for better accuracy and error correction, but is relatively slow. Despite ample empirical evidence supporting the existence of feedforward control, feedforward behavior has not been found by system identification techniques nor were feedforward models developed and validated by experimental data until the appearance of [23]. The authors of [23] used two independent system identification techniques to identify the feedback and feedforward controllers in human operators when tracking predictable ramp signals. These techniques were ARX model analysis and a time-domain maximum-likelihood method. The feedforward controller identified was similar to the inverse of the system dynamics.

In this dissertation, we propose a different identification method to separate the feedforward and feedback control when human operators track pseudo random signals and single sine waves. In contrast to the approach in [23] in which the methods were developed from the viewpoint of system identification theory, we will capitalize on fundamental limitations theory [89]. It is well-known that human operators can reject low frequency disturbances but not the ability to suppress high frequency disturbances. Through an analysis using fundamental limitations theory, the ability for disturbance rejection determines the ability for reference tracking using feedback control due to a fundamental limit in unity feedback control systems. Once the feedback control is identified from disturbance rejection performance, the feedforward control can be separated from the reference tracking performance. Our

results show that the feedback controller resembles McRuer's "crossover model" [64], and the feedforward controller attempts to invert the system dynamics that the human operator is manipulating if the reference signal is predictable, which matched the results in [23]. And when the reference is not predictable, the feedforward controller loses the ability to invert the system dynamics and the tracking performance mostly depends on the feedback controller.

We have used the proposed identification methods to study the phase lag discrepancies in tracking pseudo-random signals and single sine waves [41, Section 13] in this dissertation. The proposed methods would also have applications in other areas, such as motor control and rehabilitation. The identification method can be incorporated with other observable brain processes through the fMRI or EEG techniques to characterize the motor performance. With these brain processes, researchers have examined which brain regions contribute to feedback and feedforward motor control processes [86]. Also, the pursuit tracking tasks in this dissertation have been used as common tasks to study the impairment of voluntary movement by patients suffering from Parkinson's disease [29, 8, 18, 71]. So far, linear dynamic system approaches to separate the feedback and feedforward behaviors have not been used in human motor control. The proposed novel methods can be further extended for clinical rating scale development and rehabilitation performance estimation for neurodegenerative disorders [71, 5].

1.4 Contributions

The contributions of this dissertation fit directly into the research gaps discussed in the previous sections. In brief, the novel contributions are

1. Development of a new Bode integral for systems with oscillator dynamics

2. Interpretation of design specifications in a synchronized oscillator system as frequency domain constraints imposed on the complementary sensitivity function

3. Analysis of a conflict between certain design specifications and string stability in synchronized oscillator strings

4. Identification of a human active movement model containing a motion source and a grip force dependent mechanical impedance that describes motor behavior in grasp and lift tasks

5. Experimental validation of the human active movement model through the use of catch trials, in which human subjects occasionally experience unexpected loads

6. Development of a novel identification method that incorporates fundamental limitations theory to separate feedback and feedforward control in human manual tracking tasks

7. Analysis of the relationship between disturbance rejection and pursuit tracking in human manual tracking tasks

1.5 Dissertation outline

This dissertation is organized as follows. Chapter II introduces the string instability problem in a string of coupled harmonic oscillators. A new Bode integral is first developed to accommodate the pure imaginary poles of oscillator dynamics. Design requirements in time-domain responses and hardware limitations are then translated into a set of specifications on closed-loop frequency responses. We further analyze conflicts between design specifications, communication time delays, and string stability due to the Bode integral. We capture the severity of string instability in oscillator systems that depends on the design specifications and time delays. Several methods to improve string stability are also discussed.

Grasping and twisting are basic motor skills for the execution of activities in daily life such as opening a door with a door knob. Chapter III studies the relationship between grip force and hand trajectory during a grasp and twist task when unexpected load torques are encountered. The experimental results on grip force development and hand trajectories are consistent with similar studies on grasp and lift tasks in the literature. We also seek to build a simple model to study human feedforward control during grasp and twist movement. Our model includes a position source and driving point impedance. We provide detailed procedures to identify the relationship between the impedance values and grip forces and the algorithm to estimate the position source. We check our model by comparing the model prediction and experimental data on certain catch trial trajectories.

Chapter IV proposes a method to identify human feedback and feedforward control in manual tracking systems. Instead of only using the reference signals in most tracking tasks, we add a disturbance signal in order to investigate the human's ability to suppress output disturbances. Through the theory of fundamental limits,

we illustrate that the ability to reject disturbances also determines the ability for pursuit tracking using feedback control, and then separate the feedforward control based on pursuit tracking performance. The experiments involving tracking pseudo random signals and single sine waves are designed to demonstrate the effectiveness of the proposed method. Our results show that the feedforward controller is similar to the inverse of the system dynamics that the human users are manipulating if the reference signal is predictable while the feedforward controller is no longer the inverse of the controlled dynamics if the reference signal is unpredictable.

In Chapter V, we summarize the results in this work. Future extensions and possible research directions are also provided.

CHAPTER II

Beyond Synchronization: String Instability in Coupled Harmonic Oscillator Systems

2.1 Introduction

Many researchers have studied the problem of synchronization in systems of coupled oscillators. As noted in [72, 82, 107], this problem may be viewed as a special case of consensus control in multi-agent systems, in which each oscillator communicates with a subset of its neighbors for the purpose of achieving synchronization. The synchronization of oscillators finds applications in many different areas [93, 14, 22], e.g. synchronously flashing fireflies, microwave oscillations, and electrical power networks. Depending on the communication topology, the oscillators may or may not be able to achieve synchronization. The ability to do so also depends on the presence of communication time delays and changes in the communication topology. In this chapter, we study the effect of a disturbance on a system of coupled oscillators. Specifically, we wish to know whether the effect of a disturbance to one oscillator will be amplified or diminished as it propagates through the synchronized oscillator system.

Our approach to the problem of disturbance propagation for a system of oscillators is inspired by the literature on the problem of string instability that may arise in vehicle platooning (e.g. [75, 94, 87, 50, 66, 69]). Specifically, we first consider a string of oscillators, in which one is the leader, and with which the remainder attempt to synchronize their oscillations by tracking only their immediate predecessor in the string. It is known that this *predecessor-following* strategy will exhibit string instability under certain conditions for vehicle platoons. More complex communication schemes, on the other hand, may allow the design of control laws that are string stable. For example, when each vehicle may communicate with both its immediate predecessor

and successor a controller supporting string stability exists. Early studies of string instability were undertaken in the context of specific control laws, such as PID [75]. This made comparison between different communication schemes problematic, in that the observed string instability may have been due to a poor choice of controller gains rather than the communication scheme adopted. The authors of [87], on the other hand, show that, under appropriate hypotheses, certain communication topologies will lead to string instability for *any* linear controller. To show this, they applied the theory of fundamental design limitations [89], which enables such general statements to be made assuming only that the controller is stabilizing. In [87], it is assumed that all the vehicles have the same model and use the same control law, and it is shown that the predecessor-following control law will necessarily lead to problems of string instability for constant spacing between vehicles. The authors of [66] greatly extend the results in [87] by considering heterogeneous platoons and more general spacing policies and communication topologies. However, this string instability analysis in vehicle platooning cannot directly be used to study the disturbance response and error propagation problems in synchronized oscillator systems mainly due to the fact that vehicles are modelled by integrators with one or two poles at origin and harmonic oscillators' model has two purely imaginary poles.

Many papers on oscillator synchronization use the first order, nonlinear Kuramoto model [14], or an appropriate extension thereof [82, 72]. In order to apply the theory of fundamental design limitations, we instead use the second order, linear oscillator model described in [81]. This will enable us to use the fact that such oscillators have poles on the imaginary axis, and to generalize the results from the theory of fundamental limitations that were used in [87, 66]. We start our analysis by studying the problem of string instability in a string of identical harmonic oscillators, each trying to track its immediate predecessor using an identical control law corresponding to the predecessor-following strategy used in vehicle platooning studies. By applying the theory of fundamental design limitations [89], we develop a Bode-like integral relation that holds for any stabilizing control law. This integral relation may be used to show that any string of oscillators that satisfies certain time domain performance specifications, bandwidth limitations, and communication delays must necessarily be string unstable.

String instability is clearly not a desirable feature in a string of oscillators. We therefore study strategies that may enable string stability to be present. These are motivated by similar studies of vehicle platooning that include the use of heterogeneous control laws, an extended communication range, and time headway [87, 66].

In this chapter, we develop an extension of the concept of time headway that is applicable to oscillator systems, and show that including such headway in the control law can also result in string stability. We then extend our string instability analysis to consider the heterogeneous controller design and a more general communication range between oscillators.

The remainder of this chapter is outlined as follows. In Section 2.2, we provide some background on oscillator synchronization and review the integral constraint on the complementary sensitivity function that was used in [87] to study the string instability problem in vehicle platooning. This integral constraint is not applicable to our problem, and thus in Section 2.3 we propose a more general integral relation that may be applied to oscillator systems. We use this result to derive three sufficient conditions for string instability in Section 2.4. Specifically, we assume that a controller has been designed that satisfies certain time and frequency domain design specifications, and show that this assumption implies a lower bound on the peak in magnitude response of the complementary sensitivity function; if this lower bound exceeds one, then string instability is present. We then introduce the time headway concept for the oscillator system to improve the string stability and extend our string instability analysis to consider heterogeneous strings and a more general communication range in Section 2.5. The results of the chapter are illustrated with numerical examples in Section 2.6. Conclusions and future research directions are given in Section 2.7.

Notation: Denote by OLHP, CLHP, ORHP, and CRHP respectively the open-left, closed-left, open-right and closed-right halves of the complex plane. We use Re and Im to represent the real and imaginary parts of a complex number, respectively. We use log to denote the natural logarithm and arg to denote the principal branch of the argument of a complex number. The relative degree r of a rational transfer function is the degree of its denominator minus the degree of its numerator polynomial. The notation $P(s) \star u(t)$ is used to denote the time response with zero initial conditions of a linear time-invariant system with transfer function $P(s)$ and input $u(t)$. The notation $\lceil x \rceil$ represents the smallest integer no smaller than x. The product notation that includes matrices is defined as follows: $\prod_{i=1}^{n} M_i \triangleq M_n M_{n-1} \cdots M_2 M_1$.

2.2 Preliminary Results on Synchronization of Oscillators and String Instability

The objective of synchronization is to find the conditions on network topology and coupling algorithms that guarantee the oscillators can collectively achieve syn-

chronized behaviors. The existing literature shows that the ability to achieve synchronization in oscillator systems depends on both the communication topology and the control algorithms that prescribe how one oscillator interacts with its neighbors [81]. Even if an oscillator system can achieve synchronization, other issues such as disturbance response will affect its performance and practicality. In the following, we will demonstrate the problem of disturbance response and error amplification in a synchronized homogeneous oscillator system with a simple communication topology.

Consider the series connection, or *string*, of n single-loop feedback systems depicted in Figure 2.1. We assume that these systems are all identical, with each plant

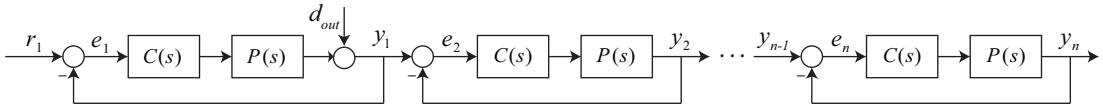

Figure 2.1: Block diagram depicting a string of stabilized oscillators with length n.

described by a proper rational transfer function of the form

$$P(s) = P_0(s)\frac{1}{s^2 + \alpha^2}, \tag{2.1}$$

where $P_0(s)$ has no zeros at $s = \pm j\alpha$, and with rational and stabilizing controller $C(s)$. Each plant thus contains the dynamics of a harmonic oscillator with natural frequency α radians/second.

Suppose that we desire each oscillator in the string to track the position of its immediate predecessor. Following the terminology used in vehicle platooning, we refer to the system in Figure 2.1 as a *predecessor-following* control architecture. Denote the commanded position to the lead oscillator by $r_1(t)$, and the positions and tracking errors of the ith oscillator as $y_i(t)$ and $e_i(t)$, respectively. Let $d_{out}(t)$ denote a disturbance entering at the output of the first oscillator. Each error signal can thus be expressed as

$$e_i(t) = \begin{cases} r_1(t) - y_1(t), & i = 1, \\ y_{i-1}(t) - y_i(t), & i \geq 2. \end{cases} \tag{2.2}$$

Define the *open loop* transfer function $L(s) = P(s)C(s)$, and the *sensitivity* and *complementary sensitivity* functions by

$$S(s) = \frac{1}{1 + L(s)}, \qquad T(s) = \frac{L(s)}{1 + L(s)}, \tag{2.3}$$

respectively. Then the Laplace transforms of the tracking error signals satisfy

$$\begin{aligned} E_1(s) &= S(s)R_1(s) - S(s)D_{out}(s), \\ E_k(s) &= T(s)E_{k-1}(s), \quad k \geq 2, \end{aligned} \tag{2.4}$$

and thus

$$E_k(s) = T^{k-1}(s)E_1(s), \quad k \geq 1. \tag{2.5}$$

The presence of the plant poles at $\pm j\alpha$ implies that $T(\pm j\alpha) = 1$ and $S(\pm j\alpha) = 0$. Hence the steady state error in response to an input of the form $r_1(t) = A\sin(\alpha t + \phi)$ will be equal to zero for each oscillator in the string. In this way the motion of all the oscillators in the string will synchronize to that of the lead oscillator. We see from (2.4) that the command $r_1(t)$ and output disturbance $d_{out}(t)$ affect the system symmetrically, and thus conclusions drawn about the command response also apply to the disturbance response.

In such a homogeneous oscillator system, the synchronization problem reduces to the design of a controller $C(s)$ such that $T(s)$ is stable. Suppose $T(s)$ is stable and there exists a frequency ω for which $|T(j\omega)| > 1$. Then (2.5) implies that any disturbance to the lead oscillator at this frequency will be amplified as it propagates to successive oscillators. As the number of oscillators increases, the error will be amplified without bound, and the string in Figure 2.1 will be *string unstable*.

Similar phenomena of string instability have appeared in vehicle platooning. One approach to study the string instability problem in vehicle platooning is to use theory of fundamental limitations [89] to derive conditions for string instability that apply to all linear time-invariant controllers. In studies of string instability in vehicle platooning, one may derive *sufficient* conditions for string instability using the following integral relation, dual to the Bode sensitivity integral, that must be satisfied by the complementary sensitivity function [89, Theorem 3.1.5].

Theorem II.1. *(a) Consider a unity feedback system with plant $P(s)$ and stabilizing controller $C(s)$. Assume that $L(s)$ is rational and proper, with N_z zeros in the ORHP, $\{z_i : i = 1, \ldots, N_z\}$. Assume further that $L(s)$ may be factored as $L(s) = L_0(s)/s^k$, where $k \geq 1$ and $L_0(s)$ has neither poles nor zeros at $s = 0$. Then*

$$\int_0^\infty \log|T(j\omega)|\frac{d\omega}{\omega^2} = \frac{\pi}{2}T'(0) + \pi\sum_{i=1}^{N_z}\frac{1}{z_i}, \tag{2.6}$$

where $T'(0) = \lim_{s\to 0} dT(s)/ds$.

(b) Suppose, in addition, that $k \geq 2$. Then $T'(0) = 0$, and

$$\int_0^\infty \log|T(j\omega)|\frac{d\omega}{\omega^2} = \pi \sum_{i=1}^{N_z} \frac{1}{z_i}. \tag{2.7}$$

Since complex zeros must occur in conjugate pairs, it follows that the right hand side of (2.7) is real and nonnegative. It follows immediately from (2.7) that if $L(s)$ has a double integrator, then necessarily there must exist a frequency for which $|T(j\omega)| > 1$. This fact was used in [87] to show that a platoon of identical vehicles in the predecessor-following control architecture must be string unstable. Recently, the results of [87] were generalized in [66] to provide sufficient conditions for string instability with heterogeneous platoons and more general control architectures. The assumption of a double integrator is reasonable for study of vehicle platoons to model the vehicle with torque as input and position as output. If only a single integrator is present, then an integral constraint still holds, but need not imply that $|T(j\omega)| > 1$ due to the term $T'(0)$, which may be negative. As discussed in [89], this term is inversely proportional to the *velocity constant* of a Type 1 feedback system.

Theorem II.1 is not applicable to our study of oscillators because it is based on the double integrator model and the harmonic oscillator has a pair of pure imaginary poles. In the following section, we will derive a new generalized complementary sensitivity integral, which can be used for harmonic oscillator systems and includes the integrals in Theorem II.1 as special cases.

2.3 A New Generalized Complementary Sensitivity Integral

We propose a new integral relation that the complementary sensitivity function must satisfy whenever $L(s)$ contains a pair of poles on the imaginary axis.

Theorem II.2. *Consider a feedback system with plant $P(s)$ given by (2.1), and stabilizing controller $C(s)$. Suppose that $L(s)$ has N_z ORHP zeros $\{z_i : i = 1, \ldots, N_z\}$ and may be factored as*

$$L(s) = e^{-s\tau} L_0(s) \frac{1}{(s^2 + \alpha^2)^k}, \tag{2.8}$$

where $k \geq 1$, $L_0(s)\frac{1}{(s^2+\alpha^2)^k}$ is proper, $L_0(s)$ is rational with no zeros at $s = \pm j\alpha$, and

$\tau \geq 0$. *Then*

$$\int_0^\infty \log|T(j\omega)|\, W(\omega,\alpha)d\omega = \frac{\pi}{2}\mathrm{Re}\,(K_\alpha) + \pi\sum_{i=1}^{N_z}\left(\frac{z_i}{z_i^2+\alpha^2}\right) + \frac{\pi}{2}\tau, \tag{2.9}$$

where

$$K_\alpha \triangleq \lim_{s\to j\alpha}\frac{dT(s)}{ds}, \tag{2.10}$$

and the weighting function $W(\omega,\alpha)$ *is defined as*

$$W(\omega,\alpha) = \frac{\omega^2+\alpha^2}{\left(\omega^2-\alpha^2\right)^2}. \tag{2.11}$$

Suppose, in addition, that $k \geq 2$ *and* $\tau = 0$. *Then* $K_\alpha = 0$, *and*

$$\int_0^\infty \log|T(j\omega)|\, W(\omega,\alpha)d\omega = \pi\sum_{i=1}^{N_z}\left(\frac{z_i}{z_i^2+\alpha^2}\right). \tag{2.12}$$

Proof. We prove this theorem by making the integration through a contour that includes the ORHP and imaginary axis. The contour is shown in Figure 2.2. Several indentations are made to avoid the singularities of $\log T(s)$. The integral around the

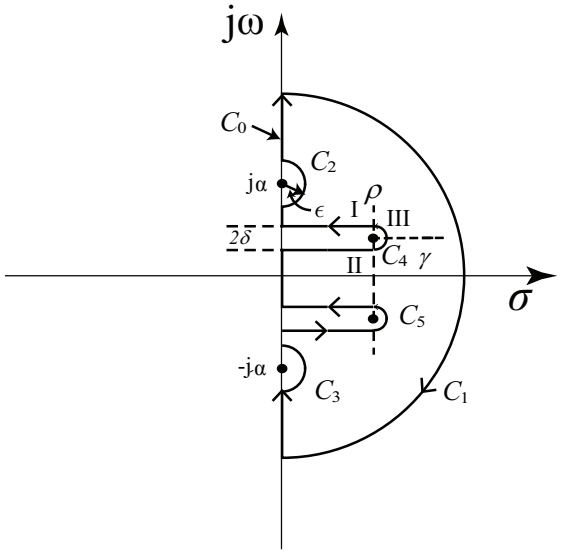

Figure 2.2: Contour for complex s-plane used to prove Theorem II.2.

total contour $C = C_0 + C_1 + C_2 + C_3 + C_4 + C_5$ is zero. The integral along the

imaginary axis, C_0, satisfies

$$\begin{aligned}
&\lim_{\epsilon\to 0}\lim_{\delta\to 0}\lim_{R\to\infty}\int_{C_0}\log\left[T(s)\right]\frac{-s^2+\alpha^2}{\left(s^2+\alpha^2\right)^2}ds\\
=&j\int_{-\infty}^{\infty}\log\left|T(j\omega)\right|\frac{\omega^2+\alpha^2}{\left(\omega^2-\alpha^2\right)^2}d\omega-\int_{-\infty}^{\infty}\arg\left[T(j\omega)\right]\frac{\omega^2+\alpha^2}{\left(\omega^2-\alpha^2\right)^2}d\omega\\
=&2j\int_{0}^{\infty}\log\left|T(j\omega)\right|\frac{\omega^2+\alpha^2}{\left(\omega^2-\alpha^2\right)^2}d\omega.
\end{aligned}\tag{2.13}$$

The curve C_1 is a semicircle, which has infinity radius in the ORHP. Hence $s = Re^{j\theta}$ and $ds = jRe^{j\theta}d\theta$. Then the contribution of this integral C_1 can be evaluated as

$$\lim_{R\to\infty}\int_{C_1}\log\left[T(s)\right]\frac{-s^2+\alpha^2}{\left(s^2+\alpha^2\right)^2}ds=-j\pi\tau.\tag{2.14}$$

The integration for C_2 can be calculated as follows. The radius of the semicircle is ϵ. Hence $s=j\alpha+\epsilon e^{j\theta}$, $-\frac{\pi}{2}\le\theta\le\frac{\pi}{2}$ and $ds=j\epsilon e^{j\theta}d\theta$. Then

$$\lim_{\epsilon\to 0}\int_{C_2}\log\left[T(s)\right]\frac{-s^2+\alpha^2}{\left(s^2+\alpha^2\right)^2}ds=j\int_{-\frac{\pi}{2}}^{\frac{\pi}{2}}\lim_{\epsilon\to 0}\log\left[T(j\alpha+\epsilon e^{j\theta})\right]\frac{1}{-2\epsilon e^{j\theta}}d\theta=-j\frac{\pi}{2}\lim_{s\to j\alpha}\frac{dT(s)}{ds}.$$

Following a similar strategy to calculate the integration for C_3, we have

$$\lim_{\epsilon\to 0}\int_{C_3}\log\left[T(s)\right]\frac{-s^2+\alpha^2}{\left(s^2+\alpha^2\right)^2}ds=-j\frac{\pi}{2}\lim_{s\to -j\alpha}\frac{dT(s)}{ds}.$$

Furthermore, considering the reflection principal of the analytic function, we obtain

$$\lim_{\epsilon\to 0}\int_{C_2+C_3}\log\left|T(s)\right|\frac{-s^2+\alpha^2}{\left(s^2+\alpha^2\right)^2}ds=-j\pi\mathrm{Re}\left[\lim_{s\to j\alpha}\frac{dT(s)}{ds}\right].\tag{2.15}$$

The contribution of integrals for C_4 and C_5 can be calculated as follows. We first assume that the nonminimum phase zeros are $\rho\pm j\gamma$. First, we need to rewrite $T(s)$ as

$$T(s)=\left(s-\rho-j\gamma\right)\left(s-\rho+j\gamma\right)\bar{T}(s).\tag{2.16}$$

Further, we have

$$\int_{C_4,C_5} \log\left[T(s)\right] \frac{-s^2+\alpha^2}{\left(s^2+\alpha^2\right)^2} ds = \int_{C_4,C_5} \log(s-\rho-j\gamma) \frac{-s^2+\alpha^2}{\left(s^2+\alpha^2\right)^2} ds + \int_{C_4,C_5} \log(s-\rho+j\gamma) \frac{-s^2+\alpha^2}{\left(s^2+\alpha^2\right)^2} ds + \int_{C_4,C_5} \log \bar{T}(s) \frac{-s^2+\alpha^2}{\left(s^2+\alpha^2\right)^2} ds. \quad (2.17)$$

The third term in the right hand side of (2.17) is zero because the integrand is analytic inside and on the semicircle C_4 and C_5. Hence we focus on the integration of the first and second terms. Consider the line part I, where $s = x+j(\gamma+\delta),\ 0 \le x \le \rho$. Then $ds = dx$.

$$\begin{aligned}\int_I \log(s-\rho-j\gamma) \frac{-s^2+\alpha^2}{\left(s^2+\alpha^2\right)^2} ds &= \int_\rho^0 \log(x-\rho+j\delta) \frac{-(x+j\gamma+j\delta)^2+\alpha^2}{\left[(x+j\gamma+j\delta)^2+\alpha^2\right]^2} dx \\ &= \int_\rho^0 \ln\sqrt{(\rho-x)^2+\delta^2} \frac{-(x+j\gamma+j\delta)^2+\alpha^2}{\left[(x+j\gamma+j\delta)^2+\alpha^2\right]^2} dx \\ &\quad + j\int_\rho^0 \left[\pi + \arctan\left(\frac{\delta}{x-\rho}\right)\right] \frac{-(x+j\gamma+j\delta)^2+\alpha^2}{\left[(x+j\gamma+j\delta)^2+\alpha^2\right]^2} dx. \quad (2.18)\end{aligned}$$

Following a similar strategy, the integration for II can be calculated as

$$\begin{aligned}&\int_{II} \log(s-\rho-j\gamma) \frac{-s^2+\alpha^2}{\left(s^2+\alpha^2\right)^2} ds \\ &= \int_0^\rho \ln\sqrt{(\rho-x)^2+\delta^2} \frac{-(x+j\gamma-j\delta)^2+\alpha^2}{\left[(x+j\gamma-j\delta)^2+\alpha^2\right]^2} dx \\ &\quad + j\int_0^\rho \left[-\pi + \arctan\left(\frac{-\delta}{x-\rho}\right)\right] \frac{-(x+j\gamma-j\delta)^2+\alpha^2}{\left[(x+j\gamma-j\delta)^2+\alpha^2\right]^2} dx. \quad (2.19)\end{aligned}$$

Now consider the integration for III. Here, $s = \rho + j\gamma + \delta e^{j\theta},\ -\frac{\pi}{2} \le \theta \le \frac{\pi}{2}$ and

$ds = j\delta e^{j\theta} d\theta$.

$$\begin{aligned}
&\lim_{\delta\to 0} \int_{III} \log(s-\rho-j\gamma) \frac{-s^2+\alpha^2}{(s^2+\alpha^2)^2} ds \\
=&\lim_{\delta\to 0} \int_{-\frac{\pi}{2}}^{\frac{\pi}{2}} \log(\delta e^{j\theta}) \frac{-(\rho+j\gamma+\delta e^{j\theta})^2+\alpha^2}{[(\rho+j\gamma+\delta e^{j\theta})^2+\alpha^2]^2} j\delta e^{j\theta} d\theta \\
=&\lim_{\delta\to 0} \int_{-\frac{\pi}{2}}^{\frac{\pi}{2}} (\log\delta + j\theta) \frac{-(\rho+j\gamma)^2+\alpha^2}{[(\rho+j\gamma)^2+\alpha^2]^2} j\delta e^{j\theta} d\theta \\
=&0.
\end{aligned}$$

Note that the first terms in (2.18) and (2.19) cancel out and the second terms are identical when taking $\delta \to 0$. Hence we have

$$\lim_{\delta\to 0} \int_{C_4} \log(s-\rho-j\gamma) \frac{-s^2+\alpha^2}{(s^2+\alpha^2)^2} ds = -2\pi j \left[\frac{\rho+j\gamma}{(\rho+j\gamma)^2+\alpha^2} - \frac{j\gamma}{-\gamma^2+\alpha^2} \right]. \quad (2.20)$$

Similarly, the integration about the curves for $\rho - j\gamma$, e.g. C_5, has the following results

$$\lim_{\delta\to 0} \int_{C_5} \log(s-\rho-j\gamma) \frac{-s^2+\alpha^2}{(s^2+\alpha^2)^2} ds = -2\pi j \left[\frac{\rho-j\gamma}{(\rho-j\gamma)^2+\alpha^2} - \frac{-j\gamma}{-\gamma^2+\alpha^2} \right]. \quad (2.21)$$

Adding (2.20) and (2.21) yields

$$\lim_{\delta\to 0} \int_{C_4+C_5} \log(s-\rho-j\gamma) \frac{-s^2+\alpha^2}{(s^2+\alpha^2)^2} ds = -2\pi j \left[\frac{\rho-j\gamma}{(\rho-j\gamma)^2+\alpha^2} + \frac{\rho+j\gamma}{(\rho+j\gamma)^2+\alpha^2} \right]. \quad (2.22)$$

The final result then follows considering (2.13), (2.14), (2.15), (2.22) and noting that the zeros in Theorem II.2 occur in conjugate pairs. □

In the following section, we will use the integrals in Theorem II.2 to derive three sufficient conditions for string instability for a string of oscillators in Section 2.2. Also it is worth noting that when α is 0, the integrals in Theorem II.2 reduce to those in Theorem II.1.

2.4 Homogeneous Oscillator String

An immediate result of Theorem II.2 is the following sufficient condition for string instability for the homogeneous oscillator system in Section 2.2.

Theorem II.3. *Consider the series connection of feedback systems in Figure 2.1, with plant* (2.1) *and stabilizing compensator* $C(s)$*. If* $L(s)$ *has at least* two *pairs of poles at* $\pm j\alpha$*, then the string of oscillators in Figure 2.1 is string unstable.*

Proof. Note that the right hand side of (2.12) is nonnegative, the time delay term $\frac{\pi}{2}\tau$ is nonnegative and that $W(\omega, \alpha) > 0$ for all frequencies except $\omega = \alpha$. It follows that if $L(s)$ has at least *two* pairs of poles at $\pm j\alpha$, then $K_\alpha = 0$. Hence there must exist a frequency for which $|T(j\omega)| > 1$, and the string of oscillators in Figure 2.1 is string unstable. □

Suppose that $L(s)$ contains only a single pair of poles at $\pm j\alpha$, namely, those due to the plant (2.1). Then K_α defined in (2.10) may be negative and, as a consequence, $|T(j\omega)|$ may be less than one at all frequencies and string instability may not be present.

Recall that the term corresponding to K_α in Theorem II.1 is inversely proportional to the velocity constant that describes the steady state error of a Type 1 feedback system in response to a ramp input. The following result provides a corresponding interpretation for K_α, and shows that it describes the steady state error in response to an input of the form $r_1(t) = t \sin \alpha t$.

Theorem II.4 (Interpretation of K_α)**.** *(a) Consider the series connection of feedback systems in Figure 2.1, with plant* (2.1) *and stabilizing compensator* $C(s)$*. Assume that* $r_1(t) = t \sin \alpha t$*, and define the steady state error for the first system as the response that persists after the transient response decays, denoted by* $e_1^{ss}(t)$*. Then*

$$e_1^{ss}(t) = |K_\alpha| \sin\left(\alpha t + \arg\left(-K_\alpha\right)\right). \tag{2.23}$$

(b) Suppose in addition that $\arg\left(-K_\alpha\right) = 0$*. Then in steady state* $y_1(t)$ *is in phase with* $r_1(t)$*, and the steady state response* $y_1^{ss}(t)$ *is given by*

$$y_1^{ss}(t) = (t - |K_\alpha|) \sin \alpha t. \tag{2.24}$$

Proof. (a) The Laplace transform of $t \sin(\alpha t)$ is given by $2\alpha s / \left(s^2 + \alpha^2\right)^2$. This fact,

together with (2.4), yields

$$E_1(s) = (1 - T(s))\frac{2\alpha s}{(s^2 + \alpha^2)^2}.$$

Noting that $1 - T(s)$ has zeros at $\pm j\alpha$, it follows that the partial fraction expansion of $E_1(s)$ has the form

$$E_1(s) = E_1^{tr}(s) + \frac{a_1 s + b_1}{s^2 + \alpha^2}, \tag{2.25}$$

where $E_1^{tr}(s)$ has poles only in the OLHP, and thus contributes only to the transient response. The constants a_1 and b_1 are given by

$$a_1 = \mathrm{Im}\,(-K_\alpha)\,, \quad b_1 = \alpha \mathrm{Re}\,(-K_\alpha)\,. \tag{2.26}$$

The steady state response $e_1^{ss}(t)$ may be evaluated by computing the inverse Laplace transform of the second term on the right hand side of (2.25).
(b) If $\arg(-K_\alpha) = 0$, then (2.24) follows from (2.2). □

Our next result uses Theorem II.4, together with the fact that all the subsystems in Figure 2.1 are identical, to show that the steady state tracking errors for each subsystem are identical.

Corollary II.5. *(a) Let $e_k^{ss}(t)$ denote the steady state tracking error of the k'th subsystem in Figure 2.1 in response to the input $r_1(t) = t\sin\alpha t$. Then*

$$e_k^{ss}(t) = e_1^{ss}(t), \quad k = 1, \ldots, n. \tag{2.27}$$

(b) Suppose in addition that $\arg(-K_\alpha) = 0$. *Then in steady state $y_k(t)$ is in phase with $r_1(t)$:*

$$y_k^{ss}(t) = (t - k|K_\alpha|)\sin\alpha t, \qquad k = 1, \ldots, n. \tag{2.28}$$

Proof. Theorem II.4 shows that $e_1^{ss}(t)$ is a sinusoid with frequency α, and (a) follows from (2.5) and the fact that $T^{k-1}(j\alpha) = 1$. Together, equations (2.2), (2.24), and (2.27) yield (b). □

Motivated by (2.28), we say that if $\arg(-K_\alpha) = 0$, then the *steady state phase error* for each oscillator is equal to zero. We now show that if the steady state phase error is nonzero, then the string of oscillators will be string unstable. This is another sufficient condition for string instability.

Theorem II.6. *Suppose that* $\arg(-K_\alpha) \neq 0$. *Then there exists a frequency* ω *such that* $|T(j\omega)| > 1$ *and the system of oscillators in Figure 2.1 is string unstable.*

Proof. First consider the case $\arg(-K_\alpha) = \pi$. Then K_α is real and positive and the result follows immediately from (2.9). Suppose next that $\arg(-K_\alpha) \neq 0, \pi$. Then K_α has a nonzero imaginary component. Using the fact that $T(j\alpha) = 1$, we have by definition (2.10) of K_α that

$$K_\alpha = \lim_{s \to j\alpha} \frac{d \log |T(s)|}{ds} + j \lim_{s \to j\alpha} \frac{d \arg T(s)}{ds}.$$

Letting $s = \sigma + j\omega$, it follows from the Cauchy-Riemann equations [11, Section 21],[16, p. 41] that

$$K_\alpha = \lim_{\omega \to \alpha} \frac{\partial \arg T(j\omega)}{\partial \omega} - j \lim_{\omega \to \alpha} \frac{\partial \log |T(j\omega)|}{\partial \omega}.$$

Together, the facts that $|T(j\alpha)| = 1$ and that $\lim_{\omega \to \alpha} \frac{\partial \log |T(j\omega)|}{\partial \omega} \neq 0$ imply that there exists a frequency ω near α such that $|T(j\omega)| > 1$. □

Theorem II.3 and Theorem II.6 provide two sufficient conditions for string instability. Suppose that neither of these sufficient conditions is satisfied. Then it is easy to find examples of systems that are string stable.

Example II.7. Suppose that $P(s) = 1/(s^2 + \alpha^2)$ and $C(s) = ks$, $k > 0$. Then $T(s)$ has stable poles, and $K_\alpha = -2/k$, so that $\arg(-K_\alpha) = 0$. It is easy to verify that $|T(j\omega)| \leq 1$, $\forall \omega$, and thus the system is string stable.

2.4.1 A Lower Bound on the Peak in Complementary Sensitivity

Our goal in the present section is to derive a lower bound on $\sup_\omega |T(j\omega)|$ that holds whenever the system is assumed to satisfy appropriate performance specifications. If this lower bound exceeds unity, then we may conclude that the system in Figure 2.1 is string unstable. We will be interested in the case for which neither sufficient condition for string instability derived in Theorems II.3 and II.6 is satisfied; however, our methods will also yield a lower bound for the case in which $L(s)$ has at least two pairs of poles at $\pm j\alpha$.

We first assume that a specification on the steady state error (SSE) in response to an input $t \sin \alpha t$ must be satisfied.

Assumption II.8 (Magnitude Bound on SSE)**.** *Assume that the steady state error* (2.23) *is uniformly bounded by* $q > 0$*:*

$$|e_1^{ss}(t)| \leq q, \quad \forall t \geq 0. \tag{2.29}$$

Recall from Corollary II.5 that the steady state error for each of the oscillators is identical. The transient error, defined by

$$e_i^{tr}(t) \triangleq e_i(t) - e_i^{ss}(t), \tag{2.30}$$

will in general be different for different oscillators. We assume an *IATE* performance specification on the sum of the integrals of the absolute values of the transient errors (IATE).

Assumption II.9 (IATE Specification)**.** *Let* $e_i^{tr}(t)$ *in* (2.30) *denote the transient error response of the* i*th oscillator in response to the command* $r_1(t) = t\sin(\alpha t)$*. We assume that the sum of the integrals of the absolute values of the transient errors must satisfy the specification*

$$\sum_{i=1}^{n} \int_0^\infty \left|e_i^{tr}(t)\right| dt \leq u(n), \tag{2.31}$$

for some positive function $u(n)$*.*

We now show that Assumptions II.8 and II.9, combined with one additional hypothesis, imply an upper bound on the gain of $T(j\omega)$.

Lemma II.10. *Suppose that Assumptions II.8 and II.9 are satisfied.*

(a) Assume in addition that $C(s)P(s)$ *possesses one pair of poles at* $\pm j\alpha$*, and that the phase error is zero:* $\arg(-K_\alpha) = 0$*. Then*

$$|T(j\omega)| \leq \left(1 + \eta(u(n), q, \alpha, \omega)\left(\omega^2 - \alpha^2\right)^2\right)^{\frac{1}{2n}}, \tag{2.32}$$

where

$$\eta(u(n), q, \alpha, \omega) = \frac{u(n)}{\alpha\omega} + \frac{n^2q^2}{4\omega^2} + \left|\omega^2 - \alpha^2\right| \frac{nu(n)q}{2\alpha\omega^2} + (\omega^2 - \alpha^2)^2 \frac{u(n)^2}{2\alpha^2\omega^2}.$$

(b) Assume instead that $C(s)P(s)$ *possesses at least two pairs of poles at* $\pm j\alpha$*. Then*

$$|T(j\omega)| \leq \left(1 + \frac{\left(\omega^2 - \alpha^2\right)^2}{2\alpha\omega} u(n)\right)^{\frac{1}{n}}. \tag{2.33}$$

Proof. (a) The assumption that $\arg(-K_\alpha) = 0$ implies that $a_1 = 0$ and $b_1 = -\alpha K_\alpha$, where a_1 and b_1 are defined in (2.26). Hence the Laplace transform of each steady state error satisfies

$$E_i^{ss}(s) = \frac{b_1}{s^2 + \alpha^2}. \tag{2.34}$$

Furthermore, it follows from Assumption II.8 and (2.23) that $|b_1| \leq \alpha q$. Recalling from Corollary II.5 that the steady state error is identical for each oscillator, we have, for each $i \geq 1$, that

$$\int_0^\infty e^{-st} e_i^{tr}(t)dt = T(s)^{i-1}(1 - T(s))\frac{2\alpha s}{(s^2 + \alpha^2)^2} - \frac{b_1}{s^2 + \alpha^2}.$$

The sum of all n error signals satisfies

$$\sum_{i=1}^n \int_0^\infty e^{-st} e_i^{tr}(t)dt = (1 - T(s)^n)\frac{2\alpha s}{(s^2 + \alpha^2)^2} - \frac{nb_1}{s^2 + \alpha^2}.$$

Rearranging the previous equation yields

$$T(s)^n = 1 - \frac{(s^2 + \alpha^2)^2}{2\alpha s}\left(\frac{nb_1}{s^2 + \alpha^2} + \sum_{i=1}^n \int_0^\infty e^{-st} e_i^{tr}(t)dt\right),$$

and evaluating this equation at $s = j\omega$ gives

$$T(j\omega)^n = 1 - \frac{(\omega^2 - \alpha^2)^2}{j2\alpha\omega}\left(\frac{-nb_1}{\omega^2 - \alpha^2} + \sum_{i=1}^n \int_0^\infty e^{-j\omega t} e_i^{tr}(t)dt\right).$$

Using Euler's formula, we have

$$\begin{aligned} T(j\omega)^n = 1 + \frac{(\omega^2 - \alpha^2)^2}{2\alpha\omega} \sum_{i=1}^n \int_0^\infty \sin(\omega t) e_i^{tr}(t)dt \\ + j\left(\frac{(\omega^2 - \alpha^2)^2}{2\alpha\omega} \sum_{i=1}^n \int_0^\infty \cos(\omega t) e_i^{tr}(t)dt - \frac{nb_1(\omega^2 - \alpha^2)}{2\alpha\omega}\right). \end{aligned}$$

Furthermore, taking the absolute value, using the fact that $|b_1| \leq \alpha q$, and invoking

(2.31) from Assumption II.9 yield

$$
\begin{aligned}
|T(j\omega)|^{2n} = &\left(1 + \frac{(\omega^2-\alpha^2)^2}{2\alpha\omega}\sum_{i=1}^{n}\int_0^\infty \sin(\omega t)e_i^{tr}(t)dt\right)^2 \\
&+ \left(\frac{(\omega^2-\alpha^2)^2}{2\alpha\omega}\sum_{i=1}^{n}\int_0^\infty \cos(\omega t)e_i^{tr}(t)dt - \frac{nb_1(\omega^2-\alpha^2)}{2\alpha\omega}\right)^2 \\
\leq &\left(1 + \frac{(\omega^2-\alpha^2)^2}{2\alpha\omega}u(n)\right)^2 + \left(\frac{(\omega^2-\alpha^2)^2}{2\alpha\omega}u(n) + \frac{nq\,|\omega^2-\alpha^2|}{2\omega}\right)^2 \\
= &1 + (\omega^2-\alpha^2)^2\left(\frac{u(n)}{\alpha\omega} + \frac{n^2q^2}{4\omega^2}\right) + \left|\omega^2-\alpha^2\right|^3\frac{nu(n)q}{2\alpha\omega^2} + (\omega^2-\alpha^2)^4\frac{u(n)^2}{2\alpha^2\omega^2},
\end{aligned}
$$

from which (2.32) follows immediately.
(b) If the open loop transfer function $C(s)P(s)$ has at least two pairs of complex poles at $\pm j\alpha$, then $E_i^{ss}(s)$ defined in (2.34) is identically zero. Using this fact and following steps similar to those used to prove (2.32) yields (2.33). □

In either case, $T(j\alpha) = 1$ due to the presence of the oscillator poles. The bounds (2.32) and (2.33) constrain the rate at which $|T(j\omega)|$ converges to one as ω approaches α, and are a consequence of the requirement (2.31) that the transient response converges rapidly to zero.

The following assumption implies that the system in Figure 2.1 has the ability to track low frequency commands with a specified error. On the other hand, although Lemma II.10 is applicable for any frequency, system properties in certain frequency ranges tend to be dominated by additional constraints and limitations. For example, at low frequency $T(s)$ may be required to approximate a unity gain low-pass filter. Hence we make the following assumption for the low frequency behavior of $T(s)$.

Assumption II.11 (Low Frequency Behavior)**.** *Let $0 < \omega_l < \alpha$. For $\omega \in (0,\ \omega_l)$, the following inequality holds*

$$|T(j\omega)^n - 1| < \epsilon, \tag{2.35}$$

where $0 \leq \epsilon < 1$.

Finally, we assume that the system satisfies a bandwidth limitation.

Assumption II.12 (Bandwidth Limitation)**.** *The transfer function $T(s)$ obeys the high frequency roll-off constraint*

$$|T(j\omega)| \leq \left(\frac{\omega_h}{\omega}\right)^r, \text{ for all } \omega > \omega_h \tag{2.36}$$

for some $\omega_h > \alpha$ and relative degree $r \geq 1$.

The following theorem shows that Assumptions II.8-II.12, together with one additional hypothesis, imply the existence of a lower bound on the peak magnitude response of the complementary sensitivity function (2.3).

Theorem II.13. *Suppose that Assumptions II.8-II.12 are satisfied.*

(a) Assume in addition that $C(s)P(s)$ possesses one pair of poles at $\pm j\alpha$, and that the phase error is zero: $\arg(-K_\alpha) = 0$. Then for any $\omega_m \in (\alpha, \omega_h)$, we have the following inequality:

$$\max_{\omega \in [\omega_m, \omega_h]} \log |T(j\omega)| \geq \frac{\Omega_H - \Omega_\alpha - \Omega_L - \frac{\pi}{2}q + \pi \sum_{i=1}^{N_z} \left(\frac{z_i}{z_i^2 + \alpha^2} \right) + \frac{\pi}{2}\tau}{\int_{\omega_M}^{\omega_H} W(\omega, \alpha) d\omega}, \tag{2.37}$$

where Ω_L, Ω_α, and Ω_H are bounds on the integral of $\log |T(j\omega)|$ over different frequency ranges:

$$\Omega_L \triangleq \frac{1}{n} \int_0^{\omega_l} \log(1 + \epsilon) W(\omega, \alpha) d\omega, \tag{2.38}$$

$$\Omega_\alpha \triangleq \frac{1}{2n} \int_{\omega_l}^{\omega_m} \log \left(1 + \eta(u(n), q, \alpha, \omega) \left(\omega^2 - \alpha^2 \right)^2 \right) W(\omega, \alpha) d\omega, \tag{2.39}$$

$$\Omega_H \triangleq r \int_{\omega_h}^{\infty} \log \frac{\omega}{\omega_h} W(\omega, \alpha) d\omega. \tag{2.40}$$

(b) Assume instead that $C(s)P(s)$ possesses at least two pairs of poles at $\pm j\alpha$. Then $T(s)$ must satisfy the lower bound (2.37), where Ω_H and Ω_L are as defined in (2.38) and (2.40), and

$$\Omega_\alpha \triangleq \frac{1}{n} \int_{\omega_l}^{\omega_m} \log \left(1 + \frac{\left(\omega^2 - \alpha^2 \right)^2}{2\alpha\omega} u(n) \right) W(\omega, \alpha) d\omega. \tag{2.41}$$

Proof. We establish this result by splitting the integration interval in (2.9). In

particular,

$$\int_{\omega_m}^{\omega_h} \log|T(j\omega)|\, W(\omega,\alpha)d\omega = -\int_{0}^{\omega_l} \log|T(j\omega)|\, W(\omega,\alpha)d\omega - \int_{\omega_l}^{\omega_m} \log|T(j\omega)|\, W(\omega,\alpha)d\omega$$
$$- \int_{\omega_h}^{\infty} \log|T(j\omega)|\, W(\omega,\alpha)d\omega + \frac{\pi}{2}\mathrm{Re}\,(K_\alpha) + \pi \sum_{i=1}^{N_z} \left(\frac{z_i}{z_i^2+\alpha^2}\right) + \frac{\pi}{2}\tau. \quad (2.42)$$

It follows from Assumption II.11 and the triangle inequality that

$$-\int_{0}^{\omega_l} \log|T(j\omega)|\, W(\omega,\alpha)d\omega \geq -\Omega_L.$$

Similarly, Lemma II.10 implies that

$$-\int_{\omega_l}^{\omega_m} \log|T(j\omega)| W(\omega,\alpha)d\omega \geq -\Omega_\alpha,$$

where Ω_α is defined either by (2.39) or (2.41). Together, Assumption II.8 and (2.23) imply that $\mathrm{Re}\,(K_\alpha) \geq -q$. Also note

$$\int_{\omega_m}^{\omega_h} \log|T(j\omega)| W(\omega,\alpha)d\omega \leq \max_{\omega\in[\omega_m,\omega_h]}\{\log|T(j\omega)|\} \int_{\omega_m}^{\omega_h} W(\omega,\alpha)d\omega.$$

The result follows by combining the preceding inequalities and applying the high frequency bound (2.36). □

It follows from Theorem II.13 that time and frequency domain specifications, such as those in Assumptions II.8-II.12, impose a *lower bound* on the peak value of $|T(j\omega)|$. For case (a), should this lower bound prove to be greater than unity, then it provides another sufficient condition for string instability. For case (b), already known to be string unstable, the lower bound provides an estimate of the severity of the instability.

In fact, the lower bound (2.37) is conservative for the purpose of predicting string instability in case (a). To see this, note that the first two terms on the right hand side of (2.42) will be nonnegative if $|T(j\omega)| \leq 1$ in the frequency range $(0, \omega_m)$. (If $|T(j\omega)| > 1$ in this frequency range, then the system is known to be string unstable without considering behavior at other frequencies.) Hence we have the following corollary to the proof of Theorem II.13. For purposes of simplicity, we also assume

that $L(s)$ has no ORHP zeros and the time delay τ is zero.

Corollary II.14. *In addition to the hypotheses of Theorem II.13, assume that* $|T(j\omega)| \leq 1$, $\forall \omega \in (0, \omega_m)$, *and that* $N_z = 0$, $\tau = 0$. *Then, for any* $\omega_m \in (\alpha, \omega_H)$, *we have that*

$$\max_{\omega \in [\omega_m, \omega_h]} \log |T(j\omega)| \geq \frac{\Omega_H - \frac{\pi}{2} q}{\int_{\omega_m}^{\omega_h} W(\omega, \alpha) d\omega}. \tag{2.43}$$

It follows immediately from (2.43) that a necessary condition for string stability is that

$$q > \frac{2}{\pi} \Omega_H, \tag{2.44}$$

where Ω_H is defined by (2.40) and q is defined in Assumption II.8. If (2.44) is not satisfied, then the limit as $\omega_m \to \omega_h$ of the right hand side of (2.43) is equal to infinity, and thus the specifications are infeasible. Hence, the desirability of string stability imposes a tradeoff between bandwidth limitations of the form imposed in Assumption II.12, and steady state tracking error requirements as imposed in Assumption II.8.

2.5 Heterogeneous Feedback Loop and Extended Communication Range

The string instability analysis in the previous section is limited to the homogeneous oscillator string with predecessor-following control architecture depicted in Figure 2.1. It cannot be applied to heterogeneous oscillator strings where the controllers can be designed differently. In such a system, there is no complementary sensitivity function $T(s)$ in (2.4) that describes how the error signal is amplified from one oscillator to its successor. Hence, the heterogeneous oscillator string avoids error amplification at the same frequency and some of the existing works use this approach to improve string stability [6]. Other methods in the area of vehicle platooning to improve and even regain string stability include speed-dependent separation policy and extended communication ranges. We want to extend our analysis in the previous section to include heterogeneous feedback loop design, a new tracking policy, and an extended communication range. For simplicity, we also assume there is no time delay in the feedback loop.

2.5.1 Time Headway Operator for Harmonic Oscillators

We start our analysis by introducing a new separation policy for a heterogeneous oscillator string shown in Figure 2.3. Here, the plants can be different and each contains the dynamics of a harmonic oscillator with natural frequency α radians/second. We write the scalar transfer function $P_i(s)$ as

$$P_i(s) = \bar{P}_i(s)\frac{1}{s^2+\alpha^2}, \quad \text{for } i = 1, 2, \cdots, n, \tag{2.45}$$

where $\bar{P}_i(s)$ has no zeros at $s = \pm j\alpha$. We also assume the controllers can be designed differently and each controller has harmonic oscillator dynamics. That is

$$C_i(s) = \bar{C}_i(s)\frac{1}{s^2+\alpha^2}, \quad \text{for } i = 1, 2, \cdots, n. \tag{2.46}$$

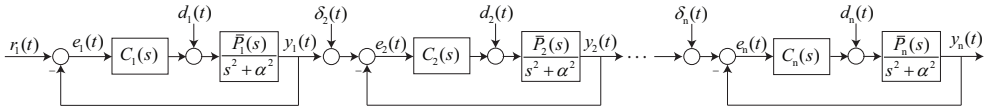

Figure 2.3: Block diagram depicting an oscillator string with time headway.

Due to the presence of the poles at $\pm j\alpha$ in the controller dynamics, the system can achieve asymptotically zero tracking errors for any ramp-enveloped sinusoidal signal of the form $r_1(t) = (At + B)\sin(\alpha t)$ asymptotically and perfect rejection of any disturbance signal $d_i(t)$ of the form $A\sin(\alpha t)$ [17]. Theorem II.3 has shown that if the oscillator string is homogeneous, the whole system is string unstable if $\delta_i(t)$ in Figure 2.3 is zero. $\delta_i(t)$ is the desired distance that the oscillator is kept with its predecessor and this signal represents the separation policy between oscillators.

We can design $\delta_i(t)$ to improve the string stability of the whole system. The concept is similar to the time headway in vehicle platooning, that is to make the intervehicle spacing increase linearly with the vehicle's own velocity. In this section, we limit our discussion to track the ramp-enveloped sinusoidal signal:

$$r_1(t) = (\delta_p + \delta_v t)\sin(\alpha t). \tag{2.47}$$

Here we term δ_v the *amplitude velocity* of this ramp-enveloped sinusoidal signal.

Further, we define the following time headway operator ∇_{TH}:

$$\nabla_{\text{TH}}\left[f(t)\right] \triangleq \frac{1}{2}\int_0^t \left(\frac{d^2}{d\tau^2}f(\tau) + \alpha^2 f(\tau)\right) d\tau \tag{2.48}$$

where $f(t)$ is assumed twice differentiable. It follows that

$$\nabla_{\text{TH}}\left[(\delta_{p,i} + \delta_v t)\sin(\alpha t)\right] = \delta_v \sin(\alpha t),$$

which is not difficult to prove. Note that the transfer function of the time headway operator ∇_{TH} is $\frac{s^2+\alpha^2}{2s}$. Then we propose the following oscillator separation policy that ensures the amplitude of the sinusoidal spacing signal $\delta_i(t)$ linearly increases with the amplitude velocity of $y_i(t)$ in steady state:

$$\delta_i(t) = \bar{\delta}_i - h_i \nabla_{\text{TH}}\left[y_i(t)\right]. \tag{2.49}$$

Here, h_i is the time headway constant for each oscillator, and $\bar{\delta}_i$ is a vector of sinusoidal signals of the form $A\sin(\alpha t)$. The separation policy (2.49) ensures that the amplitude velocities of $y_i(t)$ are all identical in steady state. We assume the time headway constants are the same: $h_i = h$ for each oscillator in this string.

With time headway, the complementary sensitivity function $T_h(s)$ in Figure 2.3 is now given by

$$T_h(s) = \frac{P_i(s)C_i(s)}{1 + P_i(s)C_i(s)\left(1 + h\frac{s^2+\alpha^2}{2s}\right)}. \tag{2.50}$$

The transfer function $T_h(s)$ describes how errors propagate in a manner similar to $T(s)$ in (2.5). Applying Theorem II.2 to the new $T_h(s)$ yields the following integral: [1]

$$\int_0^\infty \log\left|T_h(j\omega)\right| W(\omega,\alpha)d\omega \geq -\frac{\pi}{2}h.$$

The integral above shows that string stability is potentially feasible because the right hand side is negative due to the time headway operator.

Example II.15. Suppose that $P_i(s) = \frac{s+1}{s^2+4}$ and $C_i(s) = \frac{s^2+2s+5}{s^2+4}$. Then $T(s) = \frac{s^3+3s^2+7s+5}{s^4+s^3+11s^2+7s+21}$. By evaluating $\|T(s)\|_{\mathcal{H}_\infty}$, we found that $\sup_\omega |T(j\omega)| = 5.06$ and is achieved at $\omega = 2.87$. Hence we can conclude that the peak magnitude response of

[1] It follows from the proof of Theorem II.2 that the integral relation (2.9) holds for any stable, proper, rational transfer function $T(s)$ that satisfies $T(j\alpha) = 1$. Hence (a) holds for $T_h(s)$ defined in (2.50).

$T(s)$ is greater than 1 and thus the oscillator string is string unstable. By applying the separation policy in (2.49) and letting $h = 2$, we have $T_h(s) = \frac{0.5s^4+1.5s^3+3.5s^2+2.5s}{s^5+2s^4+11s^3+12s^2+24.5s+10}$ and $\sup_\omega |T(j\omega)| = 1$ achieved at $\omega = 2$. Hence the oscillator string regains string stability.

2.5.2 Multi-Variable Representation of the Oscillator String

We also want to consider the more general communication range adopted in [66] and assume that the oscillators are permitted to communicate with a few neighbors forward and backward. This is different from the communication range used in Figure 2.1 and 2.3. With the extended communication strategies, the transfer function from a disturbance at the lead oscillator to the error in the nth oscillator is no longer equal to the product of the individual transfer functions. Hence in this section we examine the disturbance propagation from the first oscillator to the last one for an arbitrarily large string of oscillators. Doing so requires us to use a multi-variable representation of the oscillator string.

We augment the output, control, error, separation, and disturbance variables as:

$$\begin{aligned}
\underline{y}(t) &= \begin{bmatrix} y_1(t) & y_2(t) & \cdots & y_n(t) \end{bmatrix}^{\mathrm{T}}, \\
\underline{u}(t) &= \begin{bmatrix} u_1(t) & u_2(t) & \cdots & u_n(t) \end{bmatrix}^{\mathrm{T}}, \\
\underline{e}(t) &= \begin{bmatrix} e_1(t) & e_2(t) & \cdots & e_n(t) \end{bmatrix}^{\mathrm{T}}, \\
\underline{d}(t) &= \begin{bmatrix} d_1(t) & d_2(t) & \cdots & d_n(t) \end{bmatrix}^{\mathrm{T}}, \\
\underline{\delta}(t) &= \begin{bmatrix} 0 & \delta_2(t) & \cdots & \delta_n(t) \end{bmatrix}^{\mathrm{T}}.
\end{aligned} \tag{2.51}$$

We make the following assumptions by considering the extended communication ranges, heterogeneous feedback loop, and the new separation policy.

Assumption II.16 (Communication Range)**.** *We assume that the ith oscillator is permitted to communicate with c_f oscillators in front and c_r oscillators behind itself. Here c_r, c_f are fixed natural numbers and $c_f \geq 1$. Further, for simplicity, we assume the number of oscillators n to be divisible by the forward communication range c_f, that is $n = Nc_f$.* □

Assumption II.17 (Heterogeneous Feedback Loop)**.** *Considering the extended communication range in Assumption II.16, the control policy can be written using a multivariable transfer function matrix $\mathcal{C}(s)$, where $\mathcal{C}(s)$ is a (c_f, c_r)-banded transfer*

matrix. That is

$$\underline{u}(t) = \mathcal{C}(s) \star \underline{e}(t), \tag{2.52}$$

where $\underline{u}(t)$ *and* $\underline{e}(t)$ *are the augmented control and error signals defined in (2.51). In addition, we assume each non-zero element in* $\mathcal{C}(s)$ *contains the dynamics of a harmonic oscillator with natural frequency* α *radians/second. Thus we write* $\mathcal{C}(s)$ *as*

$$\mathcal{C}(s) = \bar{\mathcal{C}}(s)\frac{1}{s^2 + \alpha^2},$$

with $\bar{\mathcal{C}}(j\alpha)$ *non-singular.* □

Assumption II.18 (Oscillator Separation Policy)**.** *We adopt the separation policy in (2.49). Further, we define* H*, the matrix of time headway, as* $H = diag\{h_i\} \geq 0$*, and* $\underline{\delta}_0 = \begin{bmatrix} 0 & \bar{\delta}_2 & \cdots & \bar{\delta}_n \end{bmatrix}^T$ *to be a vector of sinusoidal signals of the form* $A\sin(\alpha t)$*. The separation policy can be rewritten as*

$$\underline{\delta}(t) = \underline{\delta}_0 - H\nabla_{TH}\left[\underline{y}(t)\right], \tag{2.53}$$

where $\underline{y}(t)$ *and* $\underline{\delta}(t)$ *are the augmented output and separation signals defined in (2.51).* □

To describe the oscillator string under Assumptions II.16 to II.18, we first define the multivariable plant transfer function: $\mathcal{P}(s) = \text{diag}\{P_i(s)\}$, $\bar{\mathcal{P}}(s) = \text{diag}\{\bar{P}_i(s)\}$. Then equation (2.45) can be rewritten as

$$\underline{y}(t) = \mathcal{P}(s) \star \underline{u}(t), \tag{2.54}$$

where $\mathcal{P}(s)$ can be factored as

$$\mathcal{P}(s) = \bar{\mathcal{P}}(s)\frac{1}{s^2 + \alpha^2}.$$

Similarly, we define the error signal as

$$\underline{e}(t) = \underline{\delta}(t) - M\underline{y}(t) + V_1^n r_1(t), \tag{2.55}$$

where $V_1^n = \begin{bmatrix} 1 & 0 & \cdots & 0 \end{bmatrix}^{\mathrm{T}}$ and M denotes the coupling matrix

$$M = \begin{bmatrix} 1 & 0 & \cdots & 0 \\ -1 & 1 & \cdots & 0 \\ \vdots & \ddots & \ddots & 0 \\ 0 & \cdots & -1 & 1 \end{bmatrix}. \tag{2.56}$$

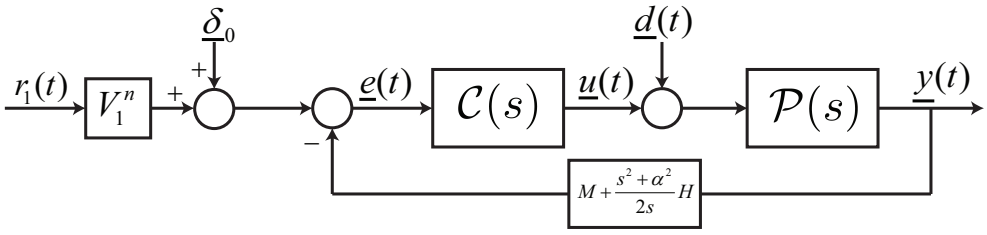

Figure 2.4: Multivariable feedback loop representation of the oscillator string.

The multivariable system representation of the oscillator string is shown in Figure 2.4. Using (2.52)-(2.55), the output variable $\underline{y}(t)$ can be related to the target separation variable $\underline{\delta}_0$ and the lead oscillator target position $r_1(t)$ by the following equation

$$\underline{y}(t) = (I + \mathcal{L}(s))^{-1} \mathcal{P}(s)\mathcal{C}(s) \star (\underline{\delta}_0 + V_1^n r_1(t)), \tag{2.57}$$

where

$$\mathcal{L}(s) = \mathcal{P}(s)\mathcal{C}(s) \left(M + \frac{s^2+\alpha^2}{2s} H \right). \tag{2.58}$$

Hence we can define the closed-loop multivariable transfer function matrix $\mathcal{H}_{yr}(s)$ as

$$\mathcal{H}_{yr}(s) = (I + \mathcal{L}(s))^{-1} \mathcal{P}(s)\mathcal{C}(s) = \left(I - (I + \mathcal{L}(s))^{-1}\right) \left(M + \frac{s^2+\alpha^2}{2s} H \right)^{-1}. \tag{2.59}$$

Assumptions II.16 to II.18 allow us to establish some properties of the closed-loop matrix $\mathcal{H}_{yr}(s)$ at frequency α.

Lemma II.19 (Values of $\mathcal{H}_{yr}$ at $s = j\alpha$)**.** *Consider $\mathcal{H}_{yr}$ as defined in (2.59). Then subject to Assumptions II.16 to II.18, we have*

$$\mathcal{H}_{yr}(j\alpha) = M^{-1}, \tag{2.60}$$

$$\mathcal{H}'_{yr}(j\alpha) = -M^{-1} H M^{-1}. \tag{2.61}$$

Proof. From the definition of $\mathcal{H}_{yr}(s)$ in (2.59) we have

$$\begin{aligned}\mathcal{H}_{yr}(s) &= \left[I + \mathcal{P}(s)\mathcal{C}(s)\left(M + \frac{s^2+\alpha^2}{2s}H\right)\right]^{-1}\mathcal{P}(s)\mathcal{C}(s) \\ &= \left(M^{-1}\left(\mathcal{P}(s)\mathcal{C}(s)\right)^{-1} + I + \frac{s^2+\alpha^2}{2s}M^{-1}H\right)^{-1}M^{-1} \\ &= \left[I + (s^2+\alpha^2)^2 M^{-1}\left(\bar{\mathcal{P}}(s)\bar{\mathcal{C}}(s)\right)^{-1} + \frac{s^2+\alpha^2}{2s}M^{-1}H\right]^{-1}M^{-1}.\end{aligned} \tag{2.62}$$

Evaluating (2.62) at $s = j\alpha$ gives (2.60) and differentiating (2.62) at $s = j\alpha$ gives (2.61). □

The lower left element of $\mathcal{H}_{yr}(s)$ describes the response of the output of the last oscillator to an output disturbance at the first oscillator:

$$\mathcal{H}_{y_n r_1}(s) = (V_n^n)^{\mathrm{T}}\mathcal{H}_{yr}(s)V_1^n, \tag{2.63}$$

where V_1^n and V_n^n are the 1st and nth canonical basis vectors respectively. We then apply Theorem II.2 to the transfer function $\mathcal{H}_{y_n r_1}(s)$ and obtain the following theorem.

Theorem II.20. *Consider $\mathcal{H}_{y_n r_1}(s)$ as defined in (2.63). Then subject to Assumptions II.16 to II.18, we have*

$$\int_0^\infty \log\left|\mathcal{H}_{y_n r_1}(j\omega)\right| W(\omega,\alpha)d\omega \geq -\frac{\pi}{2}n\bar{h}, \tag{2.64}$$

where $\bar{h}$ is the average time headway

$$\bar{h} = \frac{1}{n}\sum_{i=1}^{n} h_i. \tag{2.65}$$

Proof. Note from the definition of M in (2.56) that

$$M^{-1} = \begin{bmatrix} 1 & 0 & \cdots & 0 \\ 1 & 1 & \cdots & 0 \\ \vdots & \ddots & \ddots & 0 \\ 1 & \cdots & 1 & 1 \end{bmatrix}.$$

Then from Lemma II.19, we have

$$\mathcal{H}_{y_n r_1}(j\alpha) = 1, \text{ and } \mathcal{H}'_{y_n r_1}(j\alpha) = -n\bar{h}.$$

The result then follows by using (2.9). □

2.5.3 Lower Bound on Disturbance Amplification

In this section, we present a lower bound on the worst case disturbance amplification along the string when the system is assumed to satisfy certain communication constraints, a high frequency bandwidth limitation, and certain transient performance in response to a ramp-enveloped sinusoidal signal. If this lower bound grows at least linearly with the number of oscillators n, then we may conclude that the system in Figure 2.4 is string unstable.

We first present some assumptions on the system structural properties induced by the communications range and high frequency bandwidth limitation. From Assumption II.16, it is easy to show $\mathcal{L}(s)$ is a (c_f, c_r)-banded transfer matrix. Then $\mathcal{L}(s)$ can be written as an $N \times N$ block matrix, with $N = n/c_f$:

$$\mathcal{L}(s) = \begin{bmatrix} \mathcal{L}_{1,1}(s) & \mathcal{L}_{1,2}(s) & \mathcal{L}_{1,3}(s) & \cdots & 0 \\ \mathcal{L}_{2,1}(s) & \mathcal{L}_{2,2}(s) & \mathcal{L}_{2,3}(s) & \cdots & 0 \\ 0 & \mathcal{L}_{3,2}(s) & \mathcal{L}_{3,3}(s) & \ddots & \vdots \\ \vdots & \ddots & \ddots & \ddots & \mathcal{L}_{N-1,N}(s) \\ 0 & \cdots & 0 & \mathcal{L}_{N,N-1}(s) & \mathcal{L}_{N,N}(s) \end{bmatrix} \tag{2.66}$$

where each block element $\mathcal{L}_{i,j}(s)$ is a $c_f \times c_f$ dimensional transfer function matrix, and $\mathcal{L}_{i,j}(s) = 0$ for $j > i + l_r$, where $l_r = \lceil c_r/c_f \rceil$ is the communication range ratio introduced in Assumption II.16.

It follows that $I + \mathcal{L}(s)$ can be conveniently factorized in a block LU form described in the following lemma [66].

Lemma II.21 (Block LU Factorization of $\mathcal{L}(s)$)**.** *Under Assumption II.16, let $\mathcal{L}(s)$ be the (c_f, c_r)-banded transfer function matrix defined in (2.66). Then*

$$I + \mathcal{L}(s) \triangleq \mathcal{M}_L(s)\mathcal{M}_U(s) \tag{2.67}$$

where $\mathcal{M}_U(s)$ *is given as*

$$\mathcal{M}_U(s) = \begin{bmatrix} I & \mathcal{U}_{1,2}(s) & \mathcal{U}_{1,3}(s) & \cdots & 0 \\ 0 & I & \mathcal{U}_{2,3}(s) & \cdots & 0 \\ 0 & 0 & I & \ddots & \vdots \\ \vdots & \ddots & \ddots & \ddots & \vdots \\ 0 & \cdots & 0 & 0 & I \end{bmatrix} \tag{2.68}$$

and $\mathcal{M}_L(s)$ *as*

$$\mathcal{M}_L(s) = \begin{bmatrix} \tilde{\mathcal{S}}_{1,1}^{-1}(s) & 0 & 0 & \cdots & 0 \\ \mathcal{L}_{2,1}(s) & \tilde{\mathcal{S}}_{2,2}^{-1}(s) & 0 & \cdots & 0 \\ 0 & \mathcal{L}_{3,2}(s) & \tilde{\mathcal{S}}_{3,3}^{-1}(s) & \ddots & \vdots \\ \vdots & \ddots & \ddots & \ddots & 0 \\ 0 & \cdots & 0 & \mathcal{L}_{N,N-1}(s) & \tilde{\mathcal{S}}_{N,N}^{-1}(s) \end{bmatrix} \tag{2.69}$$

and $\tilde{\mathcal{S}}_{k,k}$ *and* $\mathcal{U}_{k,j}$ *are defined recursively by*

$$\begin{aligned} \tilde{S}_{1,1}(s) =& \left(1 + \mathcal{L}_{1,1}(s)\right)^{-1} \\ \mathcal{U}_{1,j}(s) =& \tilde{\mathcal{S}}_{1,1}(s)\mathcal{L}_{1,j}(s) : j = 2, 3, \ldots, N \\ \tilde{\mathcal{S}}_{k,k}(s) =& \left(1 + \mathcal{L}_{k,k}(s) - \mathcal{L}_{k,k-1}(s)\mathcal{U}_{k-1,k}(s)\right)^{-1} : k = 2, 3, \ldots, N \\ \mathcal{U}_{k,j}(s) =& \tilde{\mathcal{S}}_{k,k}(s)\left(\mathcal{L}_{k,j}(s) - \mathcal{L}_{k,k-1}(s)\mathcal{U}_{k-1,j}(s)\right) : 1 < k < j \leq N. \end{aligned} \tag{2.70}$$

From these equations, it follows that the multivariable sensitivity function $\mathcal{S}(s) = \left(I + \mathcal{L}(s)\right)^{-1}$ can be written as a product of upper and lower block triangular matrices

$$\mathcal{S}(s) = \mathcal{M}_U^{-1}(s)\mathcal{M}_L^{-1}(s) = \begin{bmatrix} I & * & \cdots & * \\ 0 & I & \ddots & \vdots \\ \vdots & \ddots & \ddots & * \\ 0 & \cdots & 0 & I \end{bmatrix} \begin{bmatrix} \tilde{\mathcal{S}}_{1,1}(s) & 0 & \cdots & 0 \\ \tilde{\mathcal{S}}_{2,1}(s) & \tilde{\mathcal{S}}_{2,2}(s) & \ddots & \vdots \\ \vdots & \ddots & \ddots & 0 \\ \tilde{\mathcal{S}}_{N,1}(s) & \cdots & \tilde{\mathcal{S}}_{N,N-1}(s) & \tilde{\mathcal{S}}_{N,N}(s) \end{bmatrix} \tag{2.71}$$

where $*$ denotes possibly non-zero transfer function blocks within the matrix $\mathcal{M}_U^{-1}(s)$. Further, we have

$$\mathcal{S}_{N,i}(s) = \tilde{\mathcal{S}}_{N,i}(s) = \tilde{\mathcal{S}}_{N,N}(s) \prod_{k=i}^{N-1} \tilde{\mathcal{T}}_{k+1,k}(s) \tag{2.72}$$

where

$$\tilde{\mathcal{T}}_{k+1,k}(s) \triangleq -\mathcal{L}_{k+1,k}(s)\tilde{\mathcal{S}}_{k,k}(s) \quad \text{for } k = 1, 2, \cdots, N-1. \tag{2.73}$$

Further, noting that $\tilde{\mathcal{S}}_{k,k}(s)$ is exactly the lower right hand block of the multivariable sensitivity function $\mathcal{S}(s)$ in (2.71), we assume the following uniform bounds on $\tilde{\mathcal{S}}_{k,k}(s)$.

Assumption II.22 (Uniform Bounds on $\tilde{\mathcal{S}}_{k,k}(s)$)**.** *There exists a finite number $\sigma \geq 0$ such that*

$$\left\|\tilde{\mathcal{S}}_{k,k}(s)\right\|_{\mathcal{H}_\infty} \leq \sigma \quad \text{for } k = 1, 2, \cdots, N. \qquad \square$$

We also assume each $\tilde{\mathcal{T}}_{k+1,k}(j\omega)$ satisfies a high frequency bandwidth limitation based on its definition in (2.73).

Assumption II.23 (Loop High Frequency Bound)**.** *The loop transfer functions $\tilde{\mathcal{T}}_{k+1,k}(s)$ with $k \in \{1, 2, \ldots, N-1\}$, defined in (2.73), obey the uniform high frequency bound*

$$\left\|\tilde{\mathcal{T}}_{k+1,k}(j\omega)\right\| \leq \left(\frac{\omega_H}{\omega}\right)^r, \quad \text{for all } \omega > \omega_H \tag{2.74}$$

for some $\omega_H > 0$ independent of N and (relative degree) $r \geq 1$ and all $k \in \{1, 2, \ldots, N-1\}$. In addition, we assume that $\forall \omega \geq \omega_H$

$$\left\|\left(\mathcal{P}(s)\mathcal{C}(s)\right)_{1,1}(j\omega)V_1^{c_f}\right\| \leq \bar{p} \tag{2.75}$$

for some $\bar{p} < \infty$. $\square$

We now show that Assumptions II.22 and II.23 imply a bound on the integral of the magnitude response of $\mathcal{H}_{y_n r_1}(s)$ over a high frequency range.

Corollary II.24. *Under Assumptions II.16 to II.23, we have*

$$\int_{\omega_H}^{\infty} \log\left|\mathcal{H}_{y_n r_1}(j\omega)\right| W(\omega, \alpha) d\omega \leq \log(\sigma\bar{p}) \frac{\omega_H}{\omega_H^2 - \alpha^2} + \frac{(N-1)r}{2\alpha} \log \frac{\omega_H - \alpha}{\omega_H + \alpha}. \tag{2.76}$$

Proof. The proof is similar to the proof of Corollary 5 in [66]. By following the same line of logic, we have the following inequality:

$$\left|\mathcal{H}_{y_n r_1}(j\omega)\right| \leq \sigma\bar{p}\left(\frac{\omega_H}{\omega}\right)^{r(N-1)}, \quad \text{for all } \omega > \omega_H. \tag{2.77}$$

Then we have

$$\int_{\omega_H}^{\infty} \log|\mathcal{H}_{y_n r_1}(j\omega)|\, W(\omega,\alpha)d\omega \leq [\log(\sigma\bar{p}) + (N-1)r\log\omega_H] \int_{\omega_H}^{\infty} W(\omega,\alpha)d\omega - (N-1)r\int_{\omega_H}^{\infty} W(\omega,\alpha)\log\omega d\omega.$$

The result in (2.76) follows by solving the integrals in the inequality above. □

As $\mathcal{P}(s)\mathcal{C}(s)$ contains a double oscillator dynamics in Assumption II.17, the oscillator string can achieve asymptotically zero tracking error for a sinusoidal signal in the form of (2.47). We assume the oscillator string satisfies a performance specification on the sum of integral absolute errors (IAE) that describes how fast the errors converge to zero.

Assumption II.25 (IAE Specification on Transient Response)**.** *For $i = 1,\ 2, \cdots,\ n$, let $e_i^{ramp}(t)$ be the error response of the ith oscillator to a ramp-enveloped sinusoidal signal: $r_1(t) = t\sin(\alpha t)$. We assume that for all n oscillators the integral of the absolute value of $e_i^{ramp}(t)$ is bounded as*

$$\sum_{i=1}^{n} \int_0^{\infty} |e_i^{ramp}(t)|\, dt \leq u(n) \tag{2.78}$$

for some positive function $u(n)$. □

One immediate consequence of Assumption II.25 is a bound on the frequency response of $\mathcal{H}_{y_n r_1}(s)$.

Lemma II.26. *Let Assumption II.25 hold. Then, for all $\omega \in \mathbb{R}$*

$$|\mathcal{H}_{y_n r_1}(j\omega)| \leq 1 + u(n)\frac{(\omega^2-\alpha^2)^2}{2\alpha\omega}. \tag{2.79}$$

Proof. This lemma can be proved by following a line similar to the proof of Lemma 6 in [66]. □

In addition, $\mathcal{H}_{y_n r_1}(s)$ typically has low-pass characteristics. Hence we make the following assumption for the low frequency behavior of $\mathcal{H}_{y_n r_1}(s)$.

Assumption II.27 (Low Frequency Behavior)**.** *Let* $0 < \omega_L < \alpha$*. For* $\omega \in (0,\ \omega_L)$*, the following inequality holds*

$$|\mathcal{H}_{y_n r_1}(j\omega) - 1| < \epsilon, \tag{2.80}$$

where $0 \leq \epsilon < 1$*.* □

The following theorem provides a lower bound on the peak magnitude response of $\mathcal{H}_{y_n r_1}(s)$.

Theorem II.28. *Consider a system subject to Assumptions II.16 to II.27. Then for any* $\omega_M \in (\alpha, \omega_H)$*, we have the following inequality:*

$$\max_{\omega \in [\omega_M, \omega_H]} \log |\mathcal{H}_{y_n r_1}(j\omega)| \geq \frac{\bar{\Omega}_H - \bar{\Omega}_\alpha - \bar{\Omega}_L - \frac{\pi}{2} n\bar{h}}{\int_{\omega_M}^{\omega_H} W(\omega, \alpha) d\omega}, \tag{2.81}$$

where $\bar{\Omega}_L$*,* $\bar{\Omega}_\alpha$*,* $\bar{\Omega}_H$ *are bounds on different frequency ranges of the integral of* $\log |\mathcal{H}_{y_n r_1}(j\omega)|$ *and defined as*

$$\begin{aligned}
\bar{\Omega}_L &\triangleq \int_0^{\omega_L} \log(1+\epsilon) W(\omega, \alpha) d\omega = -\log(1+\epsilon) \frac{\omega_L}{\omega_L^2 - \alpha^2}, \\
\bar{\Omega}_\alpha &\triangleq \int_{\omega_L}^{\omega_M} \log \left[1 + u(n) \frac{\left(\omega^2 - \alpha^2\right)^2}{2\alpha\omega} \right] W(\omega, \alpha) d\omega \\
\bar{\Omega}_H &\triangleq -\log(\sigma\bar{p}) \frac{\omega_H}{\omega_H^2 - \alpha^2} + \frac{(N-1)r}{2\alpha} \log \frac{\omega_H + \alpha}{\omega_H - \alpha}.
\end{aligned}$$

In addition, assume that $|\mathcal{H}_{y_n r_1}(j\omega)| \leq 1$*,* $\forall \omega \in (0, \alpha)$*. Then if* $\bar{\Omega}_H - \frac{\pi}{2} n\bar{h} > 0$*, we have*

$$\max_{\omega \in (\omega_M, \omega_H)} |\mathcal{H}_{y_n r_1}(j\omega)| \geq \exp\left(\frac{\alpha^3 (\bar{\Omega}_H - \frac{\pi}{2} n\bar{h})^2}{\omega_H u(n) (\omega_H^2 + \alpha^2)} \right). \tag{2.82}$$

Furthermore, if $u(n) < n\bar{u}$ *and* n *is sufficiently large, then*

$$\max_{\omega \in (\omega_M, \omega_H)} |\mathcal{H}_{y_n r_1}(j\omega)| \geq \exp\left(n\beta\left(\alpha, \omega_H, \bar{u}, r, c_f, \bar{h}\right) \right), \tag{2.83}$$

where $\beta\left(\alpha, \omega_H, \bar{u}, r, c_f, \bar{h}\right)$ *represents the lower bound of the growth per oscillator in the peak of the frequency response and is defined as*

$$\beta\left(\alpha, \omega_H, \bar{u}, r, c_f, \bar{h}\right) = \frac{\alpha^3}{\omega_H \bar{u} (\omega_H^2 + \alpha^2)} \left(\frac{r}{2\alpha c_f} \log \frac{\omega_H + \alpha}{\omega_H - \alpha} - \frac{\pi}{2} \bar{h} \right)^2.$$

Proof. The inequality (2.81) can be proved following the same line of logic as the proof of Theorem II.13.

From Lemma II.26, we have

$$\begin{aligned}
&\int_{\alpha}^{\omega_M} \log\left|\mathcal{H}_{y_n r_1}(j\omega)\right| W(\omega,\alpha)d\omega \\
\leq &\int_{\alpha}^{\omega_M} \log\left(1+u(n)\frac{(\omega^2-\alpha^2)^2}{2\alpha\omega}\right)\times\frac{\omega^2+\alpha^2}{(\omega^2-\alpha^2)^2}d\omega \\
\leq &\left(\omega_M-\alpha\right)\left(\omega_H^2+\alpha^2\right)\max_{\omega\in(\alpha,\omega_M)}\frac{\log\left(1+u(n)\frac{(\omega^2-\alpha^2)^2}{2\alpha\omega}\right)}{(\omega^2-\alpha^2)^2}.
\end{aligned}$$

Then it is not difficult to prove

$$\max_{\omega\in(\alpha,\omega_M)}\frac{\log\left(1+u(n)\frac{(\omega^2-\alpha^2)^2}{2\alpha\omega}\right)}{(\omega^2-\alpha^2)^2}=\frac{u(n)}{2\alpha^2}.$$

Hence, we obtain

$$\int_{\alpha}^{\omega_M}\log\left|\mathcal{H}_{y_n r_1}(j\omega)\right| W(\omega,\alpha)d\omega\leq\frac{u(n)(\omega_H^2+\alpha^2)}{2\alpha^2}\left(\omega_M-\alpha\right). \tag{2.84}$$

Applying (2.84) to inequality (2.81) yields the following inequality

$$\begin{aligned}
\max_{\omega\in(\omega_M,\omega_H)}\log\left|\mathcal{H}_{y_n r_1}(j\omega)\right| \geq &\frac{\bar{\Omega}_H-\frac{\pi}{2}n\bar{h}-\frac{u(n)(\omega_H^2+\alpha^2)}{2\alpha^2}\left(\omega_M-\alpha\right)}{\int_{\omega_M}^{\infty}W(\omega,\alpha)d\omega} \\
\geq &\frac{2\alpha}{\omega_H}(\omega_M-\alpha)\left(\bar{\Omega}_H-\frac{\pi}{2}n\bar{h}-\frac{u(n)(\omega_H^2+\alpha^2)}{2\alpha^2}\left(\omega_M-\alpha\right)\right) \\
= &\frac{2\alpha}{\omega_H}\left[-\frac{u(n)(\omega_H^2+\alpha^2)}{2\alpha^2}(\omega_M-\alpha)^2+\left(\bar{\Omega}_H-\frac{\pi}{2}n\bar{h}\right)\left(\omega_M-\alpha\right)\right].
\end{aligned}$$

If we take $\omega_M=\alpha+\frac{\alpha^2(\bar{\Omega}_H-\frac{\pi}{2}n\bar{h})}{u(n)(\omega_H^2+\alpha^2)}$, the inequality (2.82) is obtained. □

Theorem II.28 shows that the lower bound of $\max_{\omega\in(\omega_M,\omega_H)}\log\left|\mathcal{H}_{y_n r_1}(j\omega)\right|$ will increase at least linearly with the number of oscillators under certain conditions. Hence the peak will grow without bound and the oscillator string will be string unstable.

2.6 Numerical Examples

We present a few examples to illustrate the results.

2.6.1 Homogeneous Oscillator String

We present a numerical example to illustrate the results in Theorem II.13. Consider a string of n identical oscillators with frequency $\alpha = 1$ and plant transfer function $P(s) = (s + 0.5)/(s^2 + 1)$. A controller that achieves zero steady state phase error, $\arg(-K_\alpha) = 0$, is given by

$$C(s) = \frac{40(s + 10)(s + 2)}{s^2 + 0.05s + 1.5}. \tag{2.85}$$

A plot of the lower bound (2.37) as a function of ω_h, the frequency at which the bandwidth limitation becomes effective, is given in Figure 2.5 for various values of the parameter q that governs the size of the tracking error via (2.29). As expected, smaller values of ω_h increase the size of the lower bound, and for a given value of ω_h, the bound increases as the constraint on the tracking error decreases.

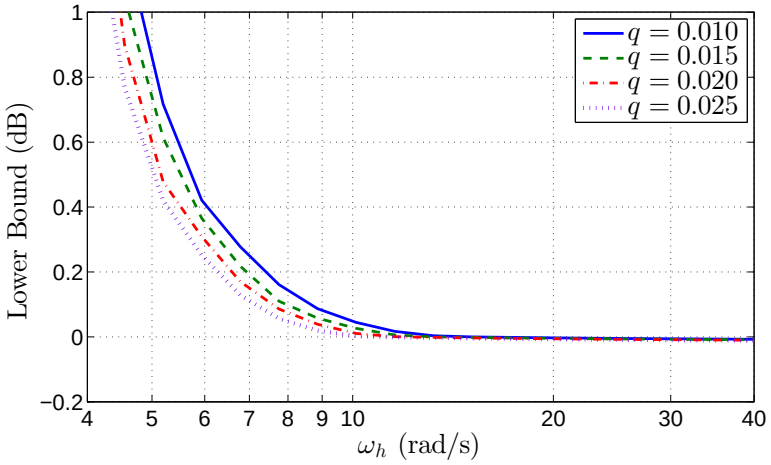

Figure 2.5: The lower bound (2.37) vs. ω_h, for parameters $n = 10$, $r = 1$, $\epsilon = 0.1$, $u(10) = 1$, and $\omega_l = 0.6$.

The corresponding complementary sensitivity function is

$$T(s) = \frac{40s^3 + 500s^2 + 1040s + 400}{s^4 + 40.05s^3 + 502.5s^2 + 1040s + 401.5}. \tag{2.86}$$

As it happens, the DC gain of $|T(j\omega)|$ is nearly unity, and it is straightforward to verify that $T(j1) = 1$ and $K_\alpha = -0.001$. The Bode magnitude plot for (2.86),

depicted in Figure 2.6, shows a peak value of 1.70 dB, or 1.22 in absolute terms. As a consequence, the string of oscillators is string unstable. The tracking errors (2.2)

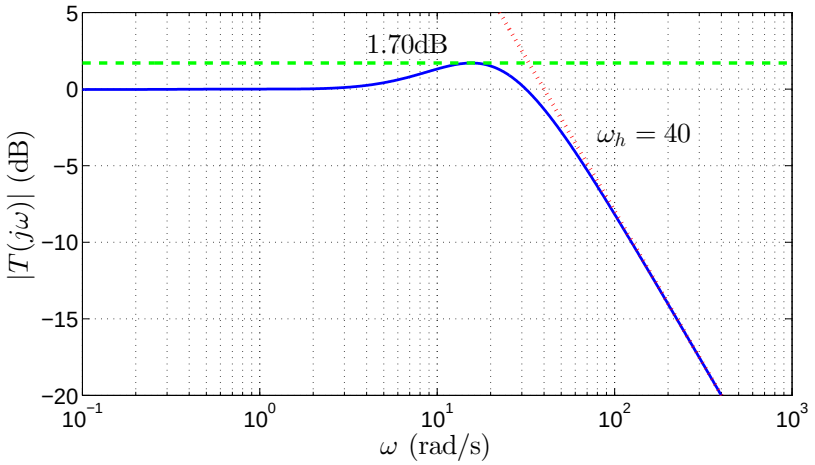

Figure 2.6: Magnitude response of $T(s)$.

in response to an input $r_1(t) = t \sin t$ are plotted in Figure 2.7, and show transient peaks that, as expected, increase in magnitude along the string. In all cases, the steady state value of the tracking error is given by $e_k^{ss}(t) = 0.001 \sin t$, as predicted from Theorem II.4 and Corollary II.5.

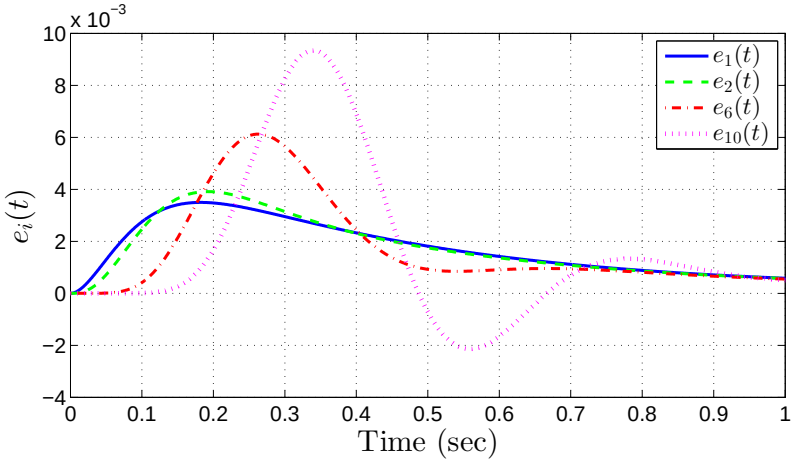

Figure 2.7: Tracking errors $e_i(t)$ defined in (2.2).

To illustrate the bound (2.37), we find that the various parameters used to construct the bound have the values depicted in Table 2.1. With these parameter values, we predict that $|T(j\omega)|$ must have a peak greater than 1.0146 (0.126 dB), which is less than the observed peak value of 1.70 dB. The difference is due in part to conservativeness in the lower bound (2.37), and in part due to controller design. A

different controller might yield a smaller peak, but no smaller than the guaranteed lower bound provided that the rest of the design satisfies the parameter values from Table 2.1.

Table 2.1: Parameters to Calculate the Lower Bound

n	ϵ	$u(n)$	q	r	ω_h	ω_l	ω_m
10	0.0367	0.072	0.001	1	40	0.536	1.95

2.6.2 Heterogeneous Oscillator String

We will illustrate the result in Theorem II.28 in this section. We first show the lower bound on peak growth of the frequency response per oscillator for different bandwidth limitations ω_H and IAE specifications $\bar{u}$ in (2.83). The plot is shown in Figure 2.8. The parameter values are $r = 1$, $c_f = 2$, $\alpha = 1$, and $\bar{h} = 0.1$.

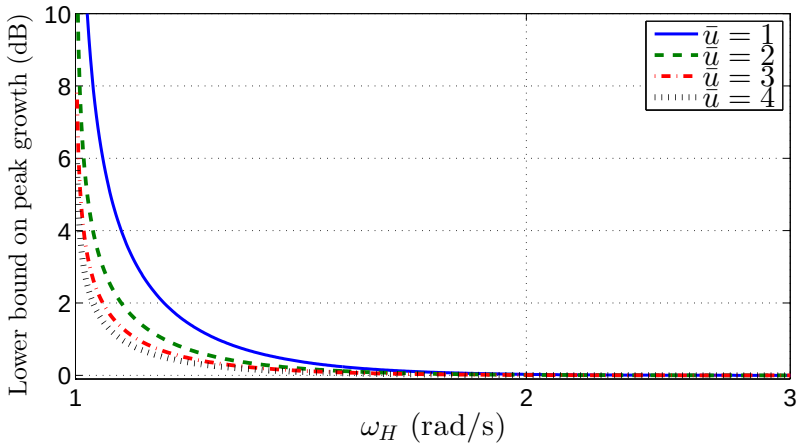

Figure 2.8: Lower bound on peak growth of magnitude response per oscillator v.s. ω_H for different values of $\bar{u}$.

We can see from Figure 2.8 that the lower bound on peak growth per oscillator in (2.83) $\left(20 \times \beta\left(\alpha, \omega_H, \bar{u}, r, c_f, \bar{h}\right)\right.$ in dB) increases as the value of ω_H becomes smaller. For the same value of ω_H, the lower bound increases as the tracking error $\bar{u}$ decreases. This conclusion is similar to the results in the homogeneous case.

We also present several design examples to illustrate the results in Section 2.5. Consider a string of n identical harmonic oscillators with frequency $\alpha = 1$ defined by the plant transfer function

$$P_i(s) = \frac{5(s+2)}{s^2+1}, \quad \text{for } i = 1, 2, \cdots, n. \tag{2.87}$$

We first consider the homogeneous string with a predecessor following control strategy and assume no time headway policy, that is $\delta_i(t) = 0$. In this case, we have already shown that the system is string unstable from the analysis in Section 2.4. Here we apply Theorem II.28 for the analysis of string instability. The control policy for each oscillator is fully decentralized, that is $C(s) = C_i(s)I$ and

$$C_i(s) = \frac{10(s^2 + 2s + 6)}{s^2 + 1}, \quad \text{for } i = 1, 2, \cdots, n. \tag{2.88}$$

In this case, we can show that $\tilde{T}_{k+1,k}(s) = (50s^3 + 200s^2 + 500s + 600)/(s^4 + 50s^3 + 202s^2 + 500s + 601)$, for $i = 1, 2, \cdots, n$. This transfer function has relative degree $r = 1$, with $\omega_H = 50$ as shown in Figure 2.9 (left).

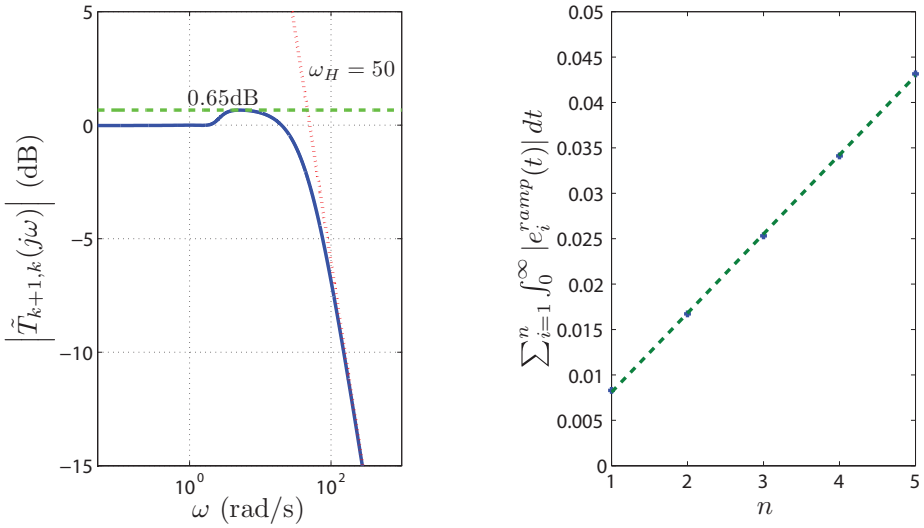

Figure 2.9: String transfer function $\tilde{T}_{k+1,k}(s)$ (left) and numerical evaluation of IAEs (right) for an homogeneous string.

By examining the transient response for a small range of string sizes, we obtain the IAE values shown in Figure 2.9 (right). If we assume that $u(n) = 0.009n$, then we predict from Theorem II.28

$$|H_{y_n r_1}(j\omega)|_{\mathcal{H}_\infty} \geq \exp\left(\frac{n\alpha r^2}{4\omega_H \bar{u} c_f^2(\omega_H^2 + \alpha^2)}\left(\log\frac{\omega_H + \alpha}{\omega_H - \alpha}\right)^2\right).$$

Hence, we predict string instability with a growth in the peak of the frequency response of at least a factor of $\exp(3.56 \times 10^{-7})$, that is 3.09×10^{-6}dB per oscillator. It is worth noting that the predicted string instability growth per oscillator in this case is a lower bound. The growth of $|H_{y_n r_1}(j\omega)|_{\mathcal{H}_\infty}$ per oscillator may be more severe

than the predicted value. For example, the observed of $|\tilde{T}_{k+1,k}(j\omega)|_{\mathcal{H}_\infty}$ is 0.65dB and it is clear the peak in disturbance response grows at this rate. The difference is due to conservativeness in the lower bound in Theorem II.28.

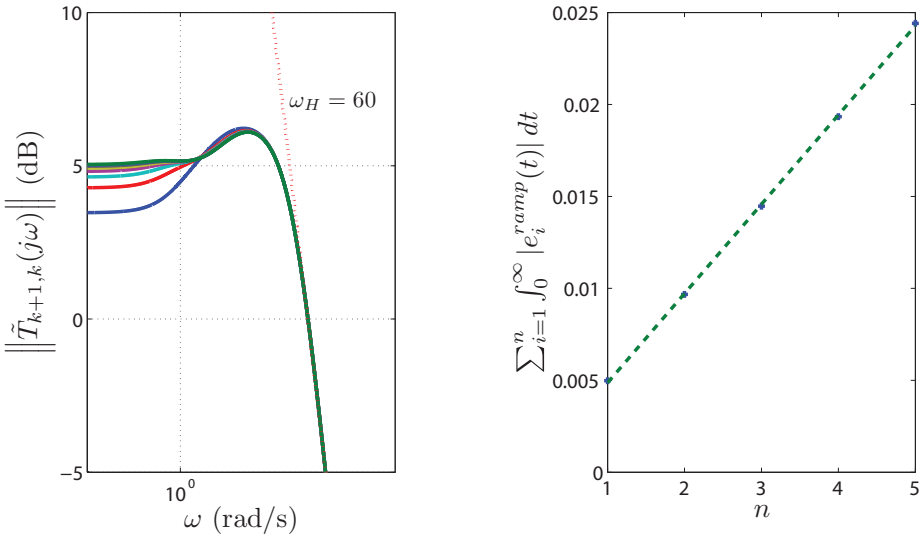

Figure 2.10: String transfer function $\tilde{T}_{k+1,k}(s)$ (left) and numerical evaluation of IAEs (right) for an heterogeneous string.

We now turn to the effect of heterogeneous control and an increased forward communications range of 2. The control law we consider is

$$u_i(t) = \frac{10(s^2 + 4s + \frac{10}{i} + 1)}{s^2 + 1} \star e_i(t) + \frac{s^2 + 4s + 1}{s^2 + 1} \star e_{i-1}(t), \quad \text{for } i = 2, 3, \cdots, n. \tag{2.89}$$

This results in a (2×2) multivariable transfer function $\tilde{T}_{k+1,k}(s)$, whose magnitude plot is shown in Figure 2.10 (left). Also if we compute numerically the IAE performance for this situation, we obtain $\bar{u} = 0.005$ as illustrated in Figure 2.10 (right). By applying Theorem II.28, we predict string instability with a growth of 2.23×10^{-6}dB per oscillator. Numerical evaluation of the frequency response gives the results in Figure 2.11.

We further introduce the time headway policy. We assume the controllers are (2.89) and take $h_i = 0.5$, for $i = 2, 3, \cdots, n$. The simulation results on error responses are shown in Figure 2.12 and it is shown we can recover string stability in this case.

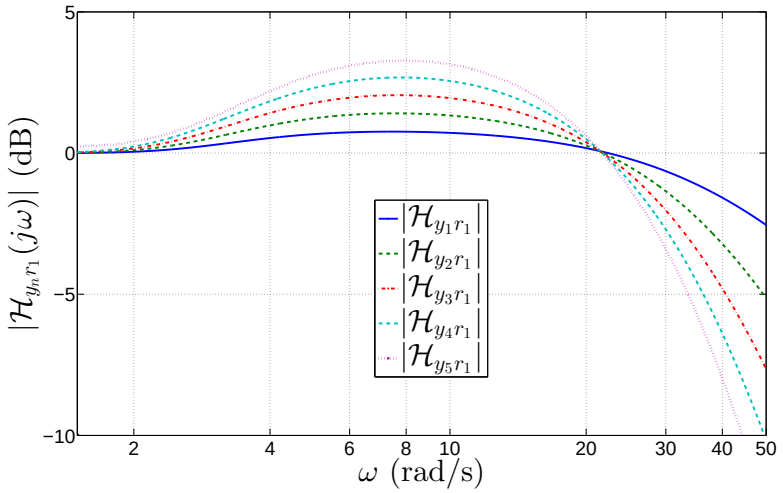

Figure 2.11: Frequency response of $\mathcal{H}_{y_n r_1}(j\omega)$ in an heterogeneous oscillator string.

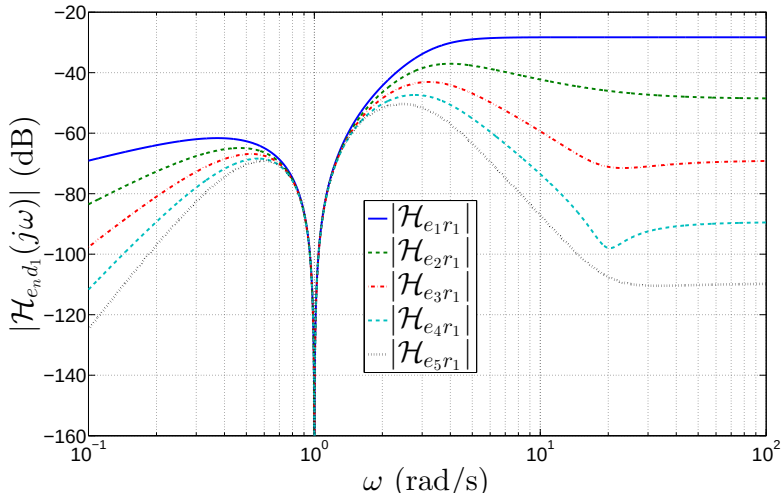

Figure 2.12: Frequency response of $\mathcal{H}_{e_n r_1}(j\omega)$ in an heterogeneous oscillator string with time headway spacing.

2.7 Conclusion

In this chapter we have studied the problem of string instability in synchronized harmonic oscillator systems. By using a new integral relation that must be satisfied by the complementary sensitivity function, we provided three sufficient conditions for string instability in homogeneous oscillator systems. We also extended our string instability analysis to heterogeneous oscillator systems where the controllers for different oscillators may be tuned differently and each oscillator can communicate with a few neighbors.

CHAPTER III

Identification of Human Feedforward Control in Grasp and Twist Tasks

3.1 Introduction

People are not very good at holding their position. The human body, whether considered at a finger, hand, or even shoulder, *gives* or *bends* under load. Even when a person co-contracts their muscles or changes posture to gird a hand with the weight of their torso, a sufficiently large unexpected force will still produce an excursion in intended position. Likewise, deviations accompany position trajectories if a load is encountered while moving. Since the human motor system cannot impose a motion on the environment independent of the loads encountered, it can hardly be described as a pure motion source. Modeling the motor system as a pure force source has similar shortcomings[1]. A truly competent model of the arm and hand as a motor system must contain a description of how the hand moves in response to a force applied through a contact with the environment. That is, a competent model will contain a finite mechanical admittance to describe the relationship between applied force and response motion that the environment *sees* of the body at the point of contact. Alternatively, a model in the dual operational form can be given, which would contain a finite impedance to describe the relationship between applied motion and response force that the environment sees of the body.

But the motion (force) at a point of contact with the environment depends on the neural activation of muscle in addition to the contact force (motion). That is, a competent model of the human motor system must also describe an actuator—a

[1] A pure force source imposes a force trajectory at a contact with the environment no matter the motion response. Thus modeling the motor system as a force source would not capture the manner in which a contact force drops if the environment suddenly moves away.

system capable of driving motion or force at a point of contact with the environment. While we have argued against the use of a pure force or motion source, a source of some kind is nevertheless needed alongside the immittance[2] that describes the relationship between contact force and motion. A source is required to drive energy into the mechanical system comprising the body in contact with a part of the environment or the body by itself.

To develop a model that can both drive energy across a mechanical contact and bend appropriately under a load, we may draw on the theory of Equivalent Networks. In particular, the Norton equivalent network allows us to build a linear model of the human motor system that generalizes all other linear models using a single motion source connected in series with an immittance. Owing to the fundamental role of the Norton equivalent network in systems theory and its general applicability across electrical, mechanical, and other domains, a model of the neural response and mechanics of the human motor system in the form of a Norton network cannot be claimed as a novel contribution. Hodgson and Hogan [37] used a Norton network to model the upper limb moving a manipulandum in the horizontal plane. To identify the motion trajectory generated by the motion source in the model, Hodgson and Hogan adapted the motor drive on the manipulandum to null the interaction force while human subjects repeated a reaching motion several times. Like short-circuiting the output terminals of a Norton circuit, nulling the interaction force enables direct measurement of the sourced motion without having an estimate of the Norton impedance. Recently, Hogan [40] has generalized the Norton Equivalent to *nonlinear* systems, showing that the forces acting on inertia elements combine linearly. The Norton network also generalizes the equilibrium point model [31] and so-called virtual trajectory model [37] of the human motor system.

In this chapter we develop a complete Norton-type model of the human motor system, identifying both the impedance and the motion source. Note that in the work by Hodgson and Hogan [37], only the sourced motion was identified. The resulting model captures all observable aspects of the arm functioning as an actuator driven by a neural command and subject to loading.

[2]After Bode [9], we use the term *immittance* to stand for either *admittance* or *impedance*, as appropriate to the operational form of a model. An admittance function describes a relationship in which motion is input and force is output whereas an impedance function describes a relationship in which force is input and motion is output.

3.1.1 Feedback and Feedfoward Control

An actuator under neural control can be used to close a loop—to realize feedback control. Feedback control can contribute several useful properties to a system—one of the most useful being the ability to reject disturbances. Thus feedback control can minimize the deviations from intended motion that are induced by disturbance loads by commanding muscles with a neural signal that depends on sensory readings of the deviation or the disturbance load itself (or both). However, feedback control in the human neuromotor system is hampered by slow neural communication speeds that contribute at least 100ms of loop delay [19, 85]. Even reflex loops suffer 40-70ms of loop delay [48, 53, 85], limiting the degree to which feedback can be used to eliminate position errors. Thus feedback control is not available in the first 40-100ms of any response to a sudden onset load.

The only sure-fire way to eliminate the effects of load on the mechanics of the body is to *anticipate* those loads and cancel them with carefully timed and scaled muscle activations. This is feedforward control, often called *anticipatory* control in the motor behavior literature. Muscle actions can be harnessed to drive the impedance so that the applied loads are perfectly balanced at the point of contact and their effects nulled. The existence proof for anticipatory control is provided by the tight link between whether the size and timing of a load can be anticipated, and whether excursions are eliminated from the intended motion trajectory.

The challenge, then, is to estimate both the sourced motion and the driving point impedance from measurements of force and motion at the point of contact with the environment. Measuring the sourced motion directly is not possible, at least not by ethical means. Thus we shall seek a means to identify the sourced motion and series immittance by manipulating and observing the force and motion at the interaction port (point of contact with the environment). Once the sourced motion and immittance are identified, however, it will be imperative to validate the model in both of its parts under different conditions than those used for identification. By manipulating the expectations of our experiment participants, we can create such altered conditions. The opportunities to manipulate expectation are provided by the grasp and lift task, as we describe next.

3.1.2 The Grasp and Lift Task

A great deal of insight into human motor control can be generated from the study of object manipulation. In the case of manipulating known objects, certain principles

contribute to one's ability to anticipate loads applied by the object. First, loads follow from the motor actions imposed on the object according to invariant laws of physics. Second, insofar that a person knows their own actions and has prior experience with a given object, a mental representation of the relationship between action and object response can be used to predict the ensuing load produced by a given object acted upon in certain ways. Loads that are predictable can be accounted for in adjusted motor plans so that these loads do not produce deviations from the intended object motion.

A very common object manipulation activity in which loads must be anticipated to enable their accommodation is the grasp and lift task. Grasp and lift is particularly valuable for the study of anticipatory (feedfoward) control because the easily measured grip force can be considered a reading of the anticipated load. Starting with the paper by Johansson and Westling [48], many papers have shown that grip forces are finely coordinated with lifting actions to prevent slip under the load force that develops as the object leaves a tabletop [26, 46, 43].

In particular, Johansson and Westling [47] showed that grasp forces are finely coordinated with the load forces produced during lifting. Even the peaks in the grip force rate and load force rate are carefully timed within the first 100 ms when adults grasp and lift objects. The grip force in the contact normal direction is just sufficient to produce a friction force in the direction of motion that will prevent slip. This fine coordination is clear evidence that muscle activations are pre-planned—a feedforward controller is acting to balance expected loads and produce the desired outcome. Studies have shown that the CNS can accommodate expected changes in weight [47], friction properties [48], and shape [44], so long as prior experience is available to build a feedforward control strategy. Unexpected changes in load result in the application of insufficient or excessive grip forces and distortions in hand/object movement trajectories. Nonetheless, within one or two subsequent lifts with the same object, an appropriate feedforward control strategy is recalled and employed to re-establish the characteristic coordination patterns. Even after 100ms within the same lift, the characteristic patterns can appear, indicating the appropriate feedforward control can be quickly swapped into play based on the sensory feedback [101]. Virtual environments rendered through haptic devices have also been used to show that the CNS can accommodate stiffness, damping, and inertial loads in addition to gravity loads [26] and the object can be twisted or turned like a door knob as well as lifted [46].

In this chapter we measure the position of an object as it is grasped and lifted

in addition to the grip and load forces. From published studies [47] we can expect the position trajectory to be perturbed if the weight of the object (load) is different than expected (not properly anticipated). We can also expect the grip force to be insufficient or excessive to prevent slip depending on whether the load is greater or smaller than anticipated. But even further, we can expect that the impedance in the axis of lift will vary with the anticipated load, because (as has been shown in an altogether different body of research) the driving point impedance depends on grip force [35, 34].

3.1.3 Model Validation

The perturbations that occur in the lift trajectory when unexpected loads are encountered can serve as test cases for a model of human motor control. In particular, both the motion trajectory (unloaded motion) and the impedance (tendency to bend under load) features of our proposed model can be tested using lifts of an object in which a different load is expected than that encountered. As in many motor behavior experiments, we call trials in which the human participant prepares for one load but encounters another "catch trials". We use catch trials to test our proposed model. We use a set of experiments in which the participant correctly anticipates the load to determine the sourced motion. In particular, we formulate an input estimation problem to determine the sourced motion, but for this problem the driving point impedance must already be known. Using a separate experiment in which the lift-axis impedance is measured as a function of grip force, we assume the same impedance may be used to describe how the hand bends under unexpected loads in short time-scales.

In fact we use a grasp and *twist* task, rendered in a virtual environment, rather than a grasp and lift task. Both tasks involve grip forces that must be modulated to prevent slip during the development of load forces, as highlighted in Figure 3.1.

The remainder of the chapter is organized as follows. The proposed model of human hand movement for grasp and twist tasks is developed in Section 3.3. We also provide detailed experimental procedures to set parameters of the impedance model in Section 3.3. Section 3.4 details the experimental results including a relationship between impedance values and grip force, the grip force profiles, and the comparison of our model prediction to experimental data. This chapter ends with a discussion and concluding remarks.

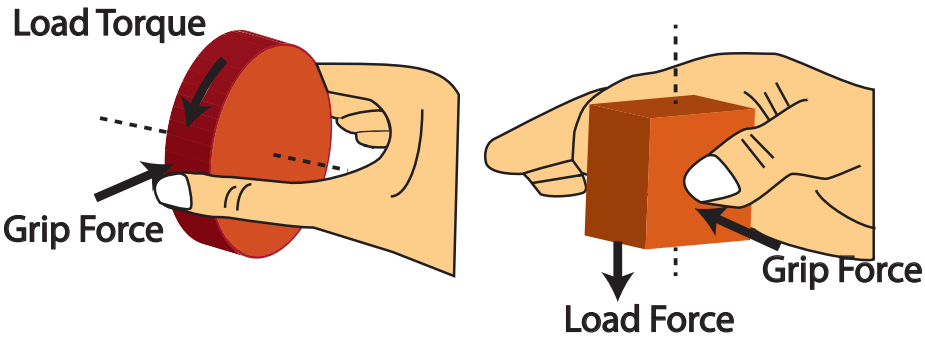

Figure 3.1: Schematics of grasp and twist, grasp and lift tasks.

3.2 Background

3.2.1 Equivalent Networks: A General Model

Network theory was first developed to describe the behavior of linear circuits in the early 20th century. A theorem by Norton [49] (developed independently by Mayer [49]) states (in mechanical terms) that any linear interconnection of force sources, motion sources, and inertia, damping, or stiffness elements may be replaced by an equivalent parallel interconnection of a single pure motion source with a single impedance. This simple interconnection will be indistinguishable from the more complicated network that it replaces when *viewed* from its connections—the (neural) command signal and the (mechanical) input/output signals at the mechanical contact (interaction port). The dual Thévinin Theorem states that a given network is indistinguishable from a mechanical parallel interconnection of a pure force source and an impedance, when observed from its connections. Thus the Thévinin actuator model contains a force source (driven by neural command) connected in parallel with an impedance.

Note that the input and output variables associated with an impedance model both pertain to a common point of contact, and are called power-conjugate variables or port variables, since their product expresses power (when the motion variable is velocity). The neural input, on the other hand, is a signal without an associated power-conjugate output signal.

The source motion and driving point immittance in the Norton model can be identified using various methods, though most of these require two identification experiments. In complete analogy with circuit theory, the sourced motion can be determined if the load is completely removed from the contact port. This corresponds to measuring the "closed circuit" current flow. This is basically the approach adopted

by Hodgson and Hogan [37]. Subsequently the immittance can be found if the motion and force at the contact port are both known. Note that Hodgson and Hogan did not estimate the Norton immittance.

In our work we adopt an alternative approach. We first estimate the immittance using measurements of force and motion at the contact point when the participant is not moving. Human participants can be instructed to not move while a perturbing force pulse is administered and the response motion recorded. We are careful to characterize the immittance under various grip forces, however, since it is known that impedance varies with grip force [34]. Once the immittance is known, it is possible to estimate the sourced motion by formulating an input estimation problem, as we describe below. It is necessary, however, to assume that the immittance measured when the participant's hand is stationary remains the same for a task in which the participant's hand is moving.

3.2.2 Identifying the Impedance Component

Impedance models of the body have been fit to force and motion recordings from experiments conducted with instrumented and actuated plates, handles, and braces. Reported models describe a finger pressing a plate [34], a finger and thumb pinching a rotary knob [35], a hand grasping a handle [105] and others. Also, measurements of torque and angular motion across a joint can be used to determine the impedance of individual joints [97, 55, 57]. Impedance can even be characterized during motion or task execution using small perturbations on a handle[61]. When two or more dimensions are involved, as in the grip of a handle moving in a plane, an impedance matrix is required to describe the relationship of all combinations of force and motion in the various directions [32]. The impedance has been shown to systematically vary with configuration (posture) [97] and muscle activation. For small motions, a linear description of the impedance (or each entry in an impedance matrix) can be justified, reportable using stiffness, damping, and inertial components that correspond to the displacement, velocity, and acceleration components of motion. In particular, with increasing contact force or [34] or grip force [35] or with increasing co-contraction [77], the inertia remains relatively constant; the damping increases; and the stiffness increases. Impedance models such as these, however, must assume that neural control is not at play and reflex loops, if any, operate at steady state.

3.2.3 Identifying the Motion Source: Input Estimation

From a system viewpoint, the motion source is the input that drives the human hand through the impedance model to interact with the loads. As the loads and the output trajectories are recorded in our experiment and the impedance is already available as a function of grip force, the identification of the motion source can be formulated as an input estimation problem. To facilitate this input estimation problem, the velocity and acceleration variables during hand movement that are associated with the damping and inertia components in the impedance model can be obtained through the differentiation and filtering techniques in signal processing.

3.3 Model and Methods

3.3.1 Model of Human Hand Movement

Our model consists of a position source and a spring-damper coupler that captures the variable driving-point impedance of the hand. The position source is an embodiment of a human user's volitional control, in this case control of the twisting movement.

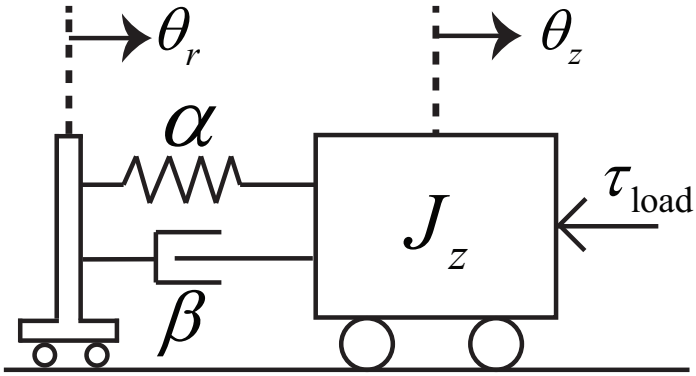

Figure 3.2: Coupled model of human hand, wheel, and external loads

Although we study the rotational motion of the human hand holding the haptic wheel, for convenience we draw the motion as an equivalent translational motion system, as depicted in Figure 3.2. Figure 3.2 shows a mechanical system translating along a single axis that models the arm, hand, and wheel that rotate about a single axis[3]. Here α and β are the stiffness and damping coefficients of a torsional spring and damper. The parameter J_z captures the combined inertia of the hand and the

[3]A similar model of the human hand is used in [105] to explain dissipativity in a system comprising a hand and virtual harmonic oscillator.

wheel gripped by the hand. The variable θ_z is the angular position of the hand and wheel. The signal θ_r is a smooth reference angular position source that is planned and imposed by the human neuromuscular system. The signal τ_{load} is the external load torque generated by the motor through the wheel. In this study, τ_{load} is one of two saturated springs, that present what we call a Light load and Heavy load as shown in Figure 3.3. We will quantify differences in the way our study participants grasp and twist the Light Load and the Heavy Load. The two loads are designed to lift off from zero and saturate already when the wheel passes 0.1 rad (5.7 degrees).

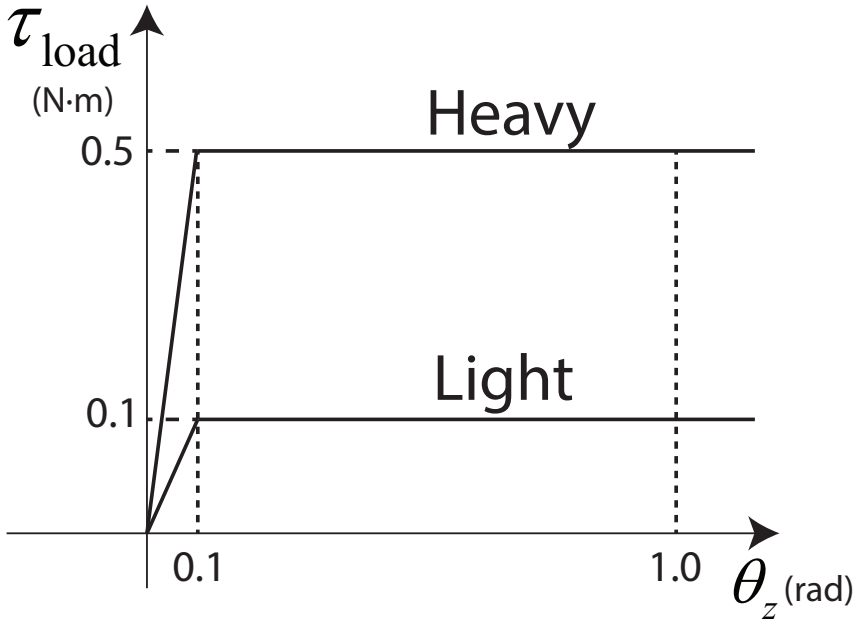

Figure 3.3: External loads: Heavy and Light.

Previous work [35] has shown that the impedance (in particular, values for J_z, α, β) changes with grip force when humans grasp a small knob. Here, we also assume that the values of J_z, α, and β are grip-force dependent (this will be shown experimentally in Section 3.3.3 and Section 3.4.1). Hence our model is a parameter-varying system. To highlight this parameter-dependence, we write the equation of motion for the system in Figure 3.2 with the parameter-dependence shown explicitly:

$$J_z(f_{\text{grip}})\ddot{\theta}_z + \beta(f_{\text{grip}})\dot{\theta}_z + \alpha(f_{\text{grip}})\theta_z = \alpha(f_{\text{grip}})\theta_r + \beta(f_{\text{grip}})\dot{\theta}_r - \tau_{\text{load}}(\theta_z), \qquad (3.1)$$

where f_{grip} is the grip force.

The proposed model in Figure 3.2 may have some connections with other research areas such as muscle models [62]. We might hypothesize that there are two sets

of muscles in the forearm that work cooperatively to realize the grasp and twist movement. One set of muscles is responsible for grasping and the other set of muscles in the forearm is for twisting. These two sets of muscles are closely coordinated during the movement. To activate the movement, the CNS first sends neural signals to muscles and the muscles change their lengths depending on the firing rate of the neuron signals. The change of length in muscles generates forces and drives the limbs to achieve certain movements. Figure 3.4 shows a schematic of the Hill muscle model that describes how muscle drives a limb. The set of muscles responsible for the twist movement can be abstracted into a muscle model that includes a contractile component, a parallel elastic component, and a series elastic component [62]. Hence θ_r in our model might be considered as the length of the contractile element and the spring of stiffness α is the series elastic element in the Hill muscle model.

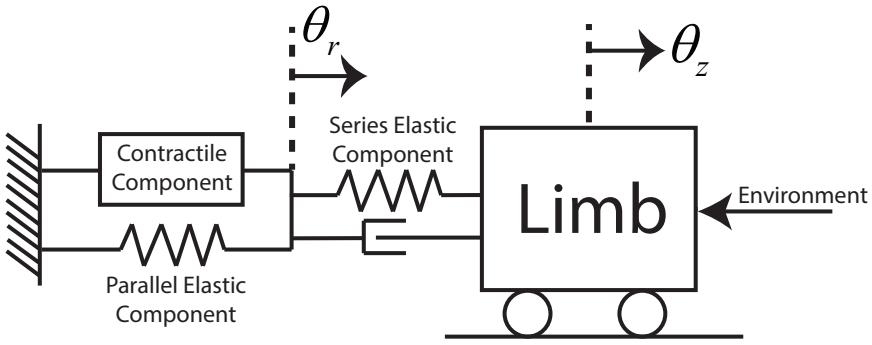

Figure 3.4: Schematic of the limb and muscle system.

3.3.2 Apparatus

We asked our study participants to grasp the wheel shown in Figure 3.5 using thumb and middle finger in the grip position shown. The grip force was measured by a load cell (Transducer Techniques, LSP-10). The wheel with the integrated load cell was connected to a DC motor (Maxon Motor, RE63). The motor was powered by a power amplifier (Maxon Motor, ADS 50/10) and the angular position of the wheel is reported by an optical encoder attached to the motor (Avago Technologies, HEDL-556x series). The resolution of the angular position is 0.09 degree (4000 counts per revolution in quadrature mode).

A PC computer with a Sensoray Model 626 data acquisition card was used to sample the position at 10 kHz and the grip force measured by the load cell was sampled at 1 kHz. The computer was used to control the load torque shown in

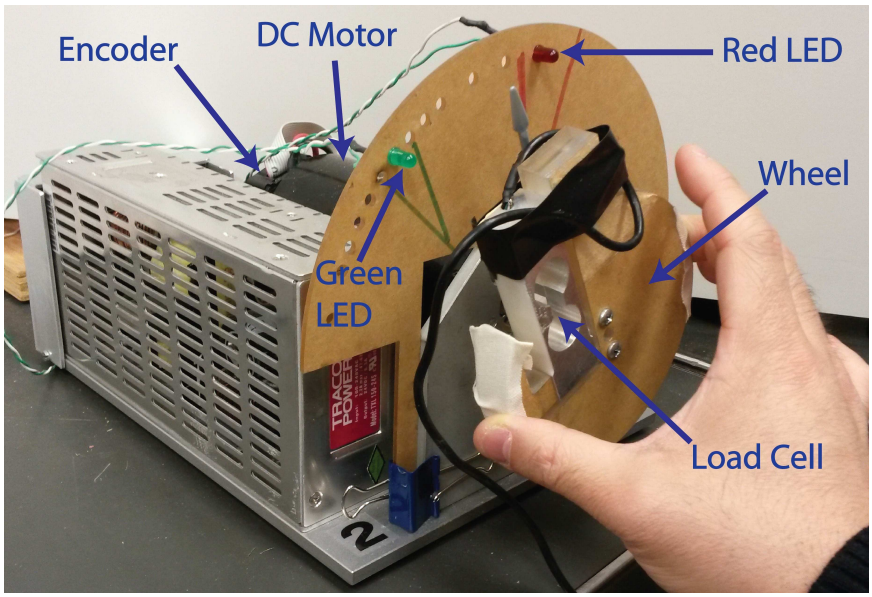

Figure 3.5: Experimental device.

Figure 3.3, resisting the movement on the basis of the angular position of the wheel. The torque servo rate was 10 kHz.

3.3.3 Experimental Protocol

Nine test participants (all males, 20 to 50 years old, right-handed) participated in this study. Prior to starting the study, each participant was consented according to the University of Michigan's Institutional Review Board and given an overview of the study. The IRB Registration Number was IRB00000245.

The experimental procedure consists of two parts. The first part is to obtain the participants' impedance values in the twist axis which depend on the grip force. The second part is the grasp and twist task.

3.3.3.1 System Identification for Human Hands

The participant was asked to grip the wheel using thumb and middle finger, to slowly increase the grip force, and keep the hand still. When the participant's grip force reached a preset threshold, the motor applied a 70 ms counterclockwise torque pulse to perturb the participant's hand. The magnitude of the pulse increased with the grip force thresholds, ranging from 0.5 to 1 N·m. The values of pulse magnitude were chosen to ensure that the displacement of the participant's rotation was roughly the same for different grip forces. The range of rotation was $20 - 30$ degrees, large

enough to engage rotation of the participant's forearm.

Each participant completed six identical blocks with ten trials each. Each block of ten trials included force thresholds of 5.0, 7.5, 10.0, 12.5, 15, 17.5, 20.0, 22.5, 25.0, 27.5 Newtons, in order. The participant was invited to rest between blocks. Acquired data included wheel displacement, the pulse perturbing signal, and the grip force.

3.3.3.2 Grasp and Twist Task

Each participant performed five to eight blocks of grasp and twist movements. In each block, the participants repeatedly grasped the wheel using thumb and middle finger when the green LED was illuminated, turned the wheel clockwise against the external load torques shown in Figure 3.3 to the end position, and then turned the wheel back to the initial position. The initial position was marked by the green LED and the end position with the red LED. The angle between the green and red LEDs was 45 degrees. In each grasp and twist movement, the rise time, defined as the time of movement from 5 degrees to 40 degrees, was calculated. If the rise time was less than 65 ms, the red LED was illuminated. We used the rise time configuration to regulate the speed and consistency of participants' movement. Participants were instructed to make each movement a single action and were told not to be too concerned about the accuracy of end point positioning. Each block lasted for three minutes, and the participants usually grasped and twisted about 40 times in one block.

During the experiments, we presented two types of external loads: a heavy load torque of 0.5 N·m and a light load torque of 0.1 N·m as already described in Figure 3.3. One external load (heavy or light) appeared repeatedly between 3 and 7 times without change, where the number between 3 and 7 was chosen randomly. Then the external load switched from light to heavy or heavy to light and repeated without change 3-7 times, and then switched back again. Thus the participants could not anticipate the changes in load torque. One sample sequence of the load torque type is

$$\overbrace{\underbrace{LLL}_{3}\ \underbrace{HHHHH}_{5}\ \underbrace{LLLL}_{4}\ \underbrace{HHHHHHH}_{7}\ \underbrace{LLLLLL}_{6}\cdots}^{\text{One Block}},$$

where L stands for light load torque and H represents heavy load torque. The participants were also instructed to try their best to turn the wheel quickly so that the red LED is illuminated after each movement.

Each participant completed five to eight blocks for the grasp and twist task. Only

the data of the last three blocks were used for analysis. All test data including the displacement of handle, the load torque signal, and grip force were saved.

3.3.4 Data Analysis

3.3.4.1 System Identification of Human Hand Impedance

The objective of the experiments described in Section 3.3.3.1 is to obtain the dependence of the impedance parameters (α, β, J_z) on grip force. Because 70 ms is too short for the subject to voluntarily change the motor command, only the arm and hand's passive biomechanics and short-latency reflexes contribute to the estimated impedance values. In this chapter, we assume that the grip force and with it the hand inertia, viscosity, and stiffness remain constant after the onset of the pulse signal in each trial. Recordings showed that the grip force stayed relatively constant. Then we have the linear impedance model of the hand dynamics

$$J_z\ddot{\theta}_z + \beta\dot{\theta}_z + \alpha\theta_z = \tau_{\text{pulse}}, \tag{3.2}$$

where τ_{pulse} is the 70ms long pulse torque signal used to perturb the participant's hand. Since the equation is linear in the parameters, the estimation problem can be solved using the standard least squares procedure. Also considering that integration is numerically a more robust operator than differentiation and we only have position signals, we applied the least squares method to the following equation, obtained by integrating (3.2) twice over time

$$J_z\theta_z + \beta\int\theta_z dt + \alpha\iint\theta_z dt^2 = \iint\tau_{\text{pulse}}dt^2. \tag{3.3}$$

Using this method, we can obtain the impedance parameters of the human hand for all grip force thresholds. Also the participants performed six identical blocks for the impedance identification task and hence we can compute the means and standard deviations.

3.3.4.2 Grasp and Twist Data Analysis

Using the characterization of impedance as a function of grip force from the first part of the experiment, we can assume that the same impedance estimate describes the twisting action during the grasp and twist task. And we assume the same dependence of twist action impedance on grip force. Thus the impedance can be estimated so

long as a grip force measurement is available. The load τ_{load} is known because it is programmed through the PC. It now remains to estimate the position source $\theta_r(t)$.

Before we introduce the method to estimate $\theta_r(t)$, we first classify trials into four categories depending on the loads encountered in the current and previous trials. We assume that the participant prepares for the current trial based on the experience in the previous trial. If the previous trial load is light and the current trial load is light, we call this a normal Light trial because the participant has prepared for the light load. Similarly, if the previous and current trial load is heavy, we call this is a normal Heavy trial. If the previous is light and the current is heavy, this is a catch trial and called a Light-Heavy trial because the participant erroneously prepares for light torque when in fact the load torque is heavy. Similarly, the other catch trial is when the previous is heavy and current is light, and called a Heavy-Light trial. The classification of the trials with the sample sequence in Section 3.3.3.2 is shown below

$$\overbrace{LLL}^{\text{Light}}\ \overbrace{H}^{\text{Light-Heavy}}\ \overbrace{HHHH}^{\text{Heavy}}\ \overbrace{L}^{\text{Heavy-Light}}\ \overbrace{LLL}^{\text{Light}}\ \overbrace{H}^{\text{Light-Heavy}}\ \overbrace{HHHHHH}^{\text{Heavy}}\ \overbrace{L}^{\text{Heavy-Light}}\ \overbrace{LLLLL}^{\text{Light}}\cdots.$$

The data of normal Light and Heavy are used to estimate θ_r. The data of catch trials Heavy-Light and Light-Heavy are used to check the proposed model.

The calculation of θ_r based on θ_z and impedance values is an input estimation problem, to which we apply a two-step process. The first step is to calculate the auxiliary signal θ_r^{aux}

$$\theta_r^{\mathsf{aux}} = \frac{J_z(f_{\text{grip}})\ddot{\theta}_z + \beta(f_{\text{grip}})\dot{\theta}_z + \alpha(f_{\text{grip}})\theta_z + \tau_{\text{load}}(\theta_z)}{\alpha(f_{\text{grip}})}, \tag{3.4}$$

where $\dot{\theta}_z$ is obtained by digitally differentiating and then smoothing the position signal θ_z (using an equiripple FIR lowpass filter and also the *filtfilt* function in matlab) and $\ddot{\theta}_z$ is obtained in same way based on $\dot{\theta}_z$. Then we have the following differential equation

$$\theta_r + \frac{\beta(f_{\text{grip}})}{\alpha(f_{\text{grip}})}\dot{\theta}_r = \theta_r^{\mathsf{aux}}. \tag{3.5}$$

θ_r can be calculated from θ_r^{aux} using the Forward Rectangular rule, that is $\dot{\theta}_r(k) \approx \frac{\theta_r(k+1)-\theta_r(k)}{t_s}$, where t_s is the sampling period.

Since we have two kinds of load torques shown in Figure 3.3, we can derive two θ_r signals: one for normal Heavy and one for normal Light trials, which we name: θ_r(Heavy) and θ_r(Light), respectively. Based on these two θ_rs together with the grip

forces, we can predict the human hand movement during a catch trial and test our model by comparing the predicted trajectories with the experimental trajectories.

3.4 Experimental Results

The results are presented in two sections. The first focuses on the impedance values of the human hand. In the second section, we build a model of human hand movement during grasp and twist tasks based on the impedance profiles and the data in grasp and twist trials. We also use this model to predict the trajectories of catch trials and check these against experimental data from catch trials.

3.4.1 Human Hand Impedance Profile

We use the least squares algorithm in Section 3.3.4.1 to estimate the impedance values. Figure 3.6 shows the inertia, damping, and spring value estimates vs. different grip force thresholds for Participant 4. Each participant completed six blocks of the impedance identification task. Here, the units for J_z, β, and α are $\mathrm{kg}\cdot\mathrm{m}^2$, $\mathrm{N}\cdot\mathrm{m/rad/s}$, and α are $\mathrm{N}\cdot\mathrm{m/rad}$, respectively.

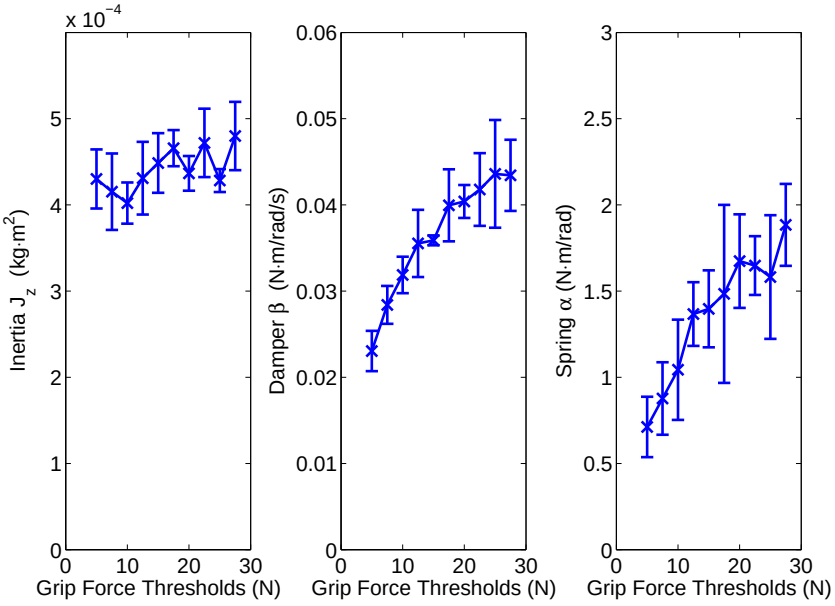

Figure 3.6: Impedance estimate vs. grip force thresholds for Subject 4. Error bars represent one standard deviation of the mean.

All other participants' impedance profiles are very similar to the results in Figure 3.6. The mean values of all participants' impedances are shown in Figure 3.7. We

can see that the inertia estimate is almost constant and the damping and spring estimates increase approximately linearly with grip force. It is also worth noting that the trends of the impedance values are consistent with previous research results on human hand/finger impedance [34, 35]. The human hand impedance when grasping a small knob [35] and the finger tip impedance [34] show similar trends.

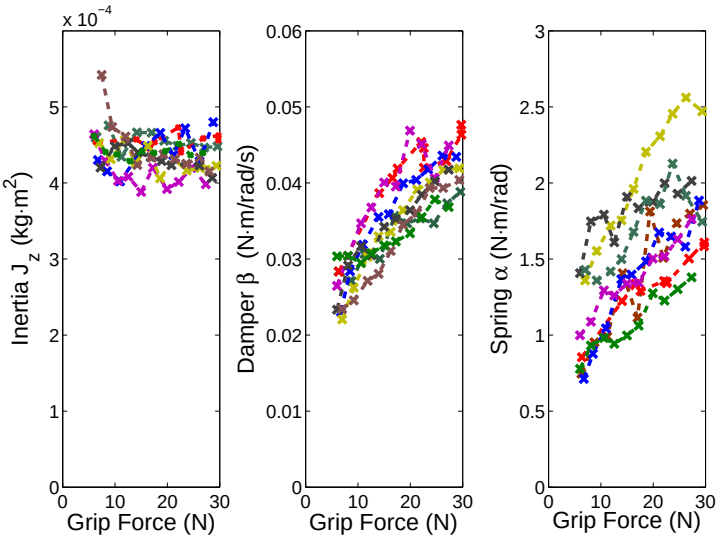

Figure 3.7: Mean values of impedance vs. grip forces for all participants.

To capture the relationship between grip force and impedance values, we can fit a constant value to the mean of the inertia estimate and linear functions to the mean values of the damping and spring estimates. The fitted functions that describe how impedance parameters change with grip force will be used later to produce a description of impedance that applies during grasp and twist movements. For the participant whose data is depicted in Figure 3.6, the fitted parameter functions are

$$\begin{aligned} J_z &= 4.41 \times 10^{-4} \ \ \text{kg} \cdot \text{m}^2, \\ \beta &= 8.77 \times 10^{-4} \times f_{\text{grip}} + 2.11 \times 10^{-2} \ \ \text{N} \cdot \text{m/rad/s}, \\ \alpha &= 4.87 \times 10^{-2} \times f_{\text{grip}} + 5.19 \times 10^{-1} \ \ \text{N} \cdot \text{m/rad}, \end{aligned} \tag{3.6}$$

where f_{grip} is the grip force measured by the load cell and the unit is Newton. The fitted parameter functions for all subjects are summarized in Table 3.1.

3.4.2 Grasp and Twist Movement Results

We plot the grip force and the hand position data for one subject in Figure 3.8. Here the time 0 is defined as the moment when the hand starts to move based on

Table 3.1: Fitted functions for all subjects' impedance profiles

Participant	$J_z = J_0$	$\beta = \beta_1 \times f_{\text{grip}} + \beta_0$		$\alpha = \alpha_1 \times f_{\text{grip}} + \alpha_0$	
Number	J_0	β_1	β_0	α_1	α_0
1	4.55×10^{-4}	4.56×10^{-4}	2.51×10^{-2}	4.81×10^{-2}	5.22×10^{-1}
2	5.13×10^{-4}	5.17×10^{-4}	2.40×10^{-2}	5.93×10^{-2}	1.66×10^{-1}
3	4.54×10^{-4}	5.80×10^{-4}	2.98×10^{-2}	3.28×10^{-2}	6.61×10^{-1}
4	4.41×10^{-4}	8.77×10^{-4}	2.11×10^{-2}	4.87×10^{-2}	5.19×10^{-1}
5	4.12×10^{-4}	8.12×10^{-4}	2.53×10^{-2}	3.21×10^{-2}	8.49×10^{-1}
6	4.31×10^{-4}	8.71×10^{-4}	1.90×10^{-2}	5.54×10^{-2}	10.50×10^{-1}
7	4.30×10^{-4}	7.70×10^{-4}	2.03×10^{-2}	2.33×10^{-2}	13.95×10^{-1}
8	4.48×10^{-4}	8.53×10^{-4}	1.71×10^{-2}	3.26×10^{-2}	11.09×10^{-1}
9	4.61×10^{-4}	6.22×10^{-4}	2.68×10^{-2}	3.14×10^{-2}	11.31×10^{-1}

the measurement of wheel position. The upper figure shows the grip force and the lower figure shows the hand position of all trials. Each pair of grip force and hand position data corresponds to a single grip and twist movement trial. Different colors of trajectories stand for different categories defined in Section 3.3.4.2. Very rarely, the participant may experience slips during the movement and the corresponding data are excluded from our analysis. In Figure 3.8, we have 50 Light trajectories, 42 Heavy trajectories, 13 Light-Heavy trajectories, and 9 Heavy-Light trajectories.

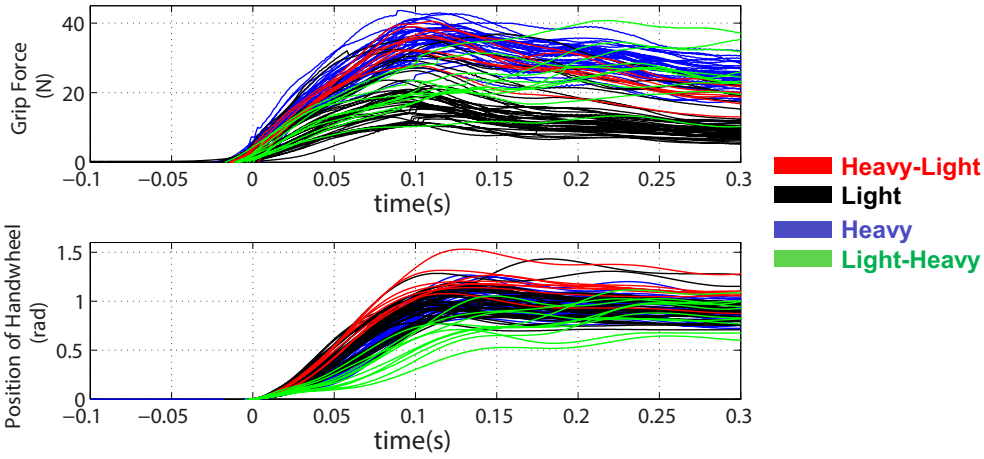

Figure 3.8: Grip force and hand position data of Subject 4.

Taking a closer look at these data, we averaged the grip force and hand position trials of each category as shown in Figure 3.9. The solid lines stand for the mean value and the shaded areas represent the 95% confidence interval. The upper figure shows the average grip force for these four categories in different colors. For Light and Heavy load torques, we have two distinct grip force trajectories. It is clear that the

participant needs to grip harder for heavy load torques than for light load torques. This phenomenon is consistent with results in [46].

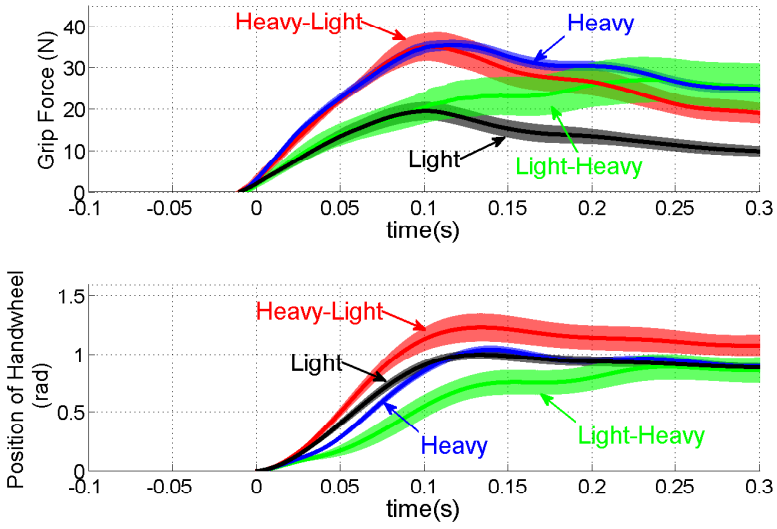

Figure 3.9: Averaged grip force and hand position data of Subject 4. The solid lines stand for the mean value and the shaded areas represent the 95% confidence interval.

Figure 3.9 also illustrates the catch trial grip force properties for our grasp and twist tasks. We can see from the average grip force trajectory of Heavy-Light catch trial data, the grip force follows the grip force of the previous Heavy trial at the beginning and then the participant realizes the actual torque is light at about 0.10s and starts to decrease the grip force to the level of a Light trial in the end. Similar trends are found in the grip force trajectories of Light-Heavy catch trial data. Because the previous trial is Light and the current load is the Heavy torque, the grip force of Light-Heavy starts like the Light grip force and then changes to Heavy.

Other participants' grip force trajectories are very similar to the results in Figure 3.9. We also observed that the trend of the separation of catch trial from its previous trial was more obvious in Light-Heavy catch trials than Heavy-Light ones. Thus, we measure the time when the grip force of Light-Heavy is separated from Light for all participants and the results are reported in Table 3.2. The results in Table 3.2 show that the time for all participants is very consistent, with a mean value of 0.1108s and standard deviation of 0.0119s.

Table 3.2: Time when the grip force of Light-Heavy is separated from Light for all participants

Participant Number	Time when feedback comes in (s)
1	0.101
2	0.097
3	0.102
4	0.107
5	0.103
6	0.116
7	0.125
8	0.132
9	0.114
mean (all participant)	0.1108±0.0119

3.4.3 Model Validation Using Catch Trial Movements

Figure 3.9 also shows the trajectories of hand movement. All other participants' hand movement trajectories are similar to the results in Figure 3.9. Although we instructed participants to turn the wheel at the same rate, the Light trial hand trajectory is clearly above the Heavy trial trajectory showing the participants' hands move faster for the Light load than the Heavy load. All participants' hand trajectories have the same order from the top to bottom: Heavy-Light, Light, Heavy, and Light-Heavy. For each participant separately, we use the averaged trajectories of Light and Heavy together with grip forces of Light and Heavy to estimate θ_r for normal trials. Figure 3.10 shows the estimated θ_r for heavy and light load torques as well as θ_z(Heavy) and θ_z(Light) that were used to estimate θ_r trajectories. We can see that although the hand movement θ_z(Heavy) is lagging behind θ_z(Light) in time, the motor plan θ_r(Heavy) is ahead of θ_r(Light) in order to compensate for the heavy load.

We have identified the proposed model with position source θ_r and impedance parameters α, β, J_z (from the measured grip force and (3.6)) for both the Heavy and Light loads. We now use this model to predict the catch trial hand movement trajectories: Heavy-Light and Light-Heavy. From the grip force analysis of Heavy-Light data, the subject starts the movement using the pre-planned grip force for heavy load torques and it is also reasonable to assume that the participant uses the position source θ_r for Heavy at the beginning. Hence the way to calculate the Heavy-Light trajectory θ_z is to use θ_r and grip force (impedance) for heavy torques, and apply the light τ_{load}. Similarly, the predicted trajectory θ_z for Light-Heavy is to use θ_r and

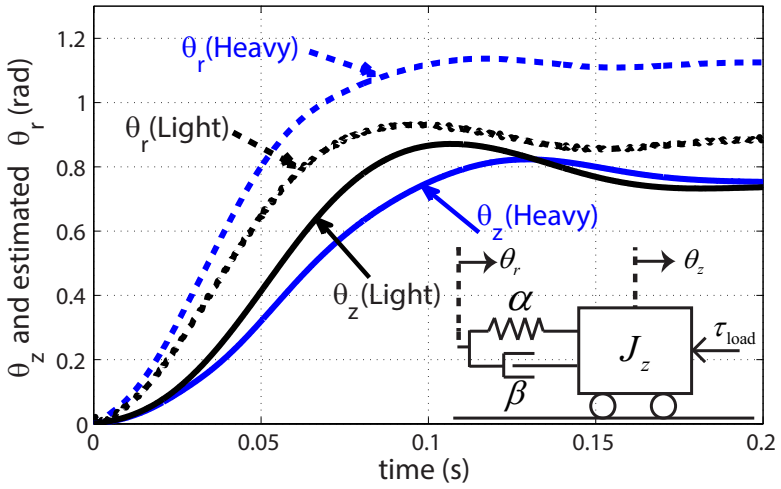

Figure 3.10: θ_z and estimated θ_r.

grip force for light torques, and apply the heavy τ_{load}. We notice that the participant will use feedback information to determine the actual torque as we can see from the changes of grip force in catch trial data, which also indicate the possible change of θ_r. However, our current model only focuses on the use of feedforward control to predict the catch trial trajectories before the time at which feedback comes into play. Hence in our prediction we assume no change in the position source and grip force in calculating catch trial trajectories.

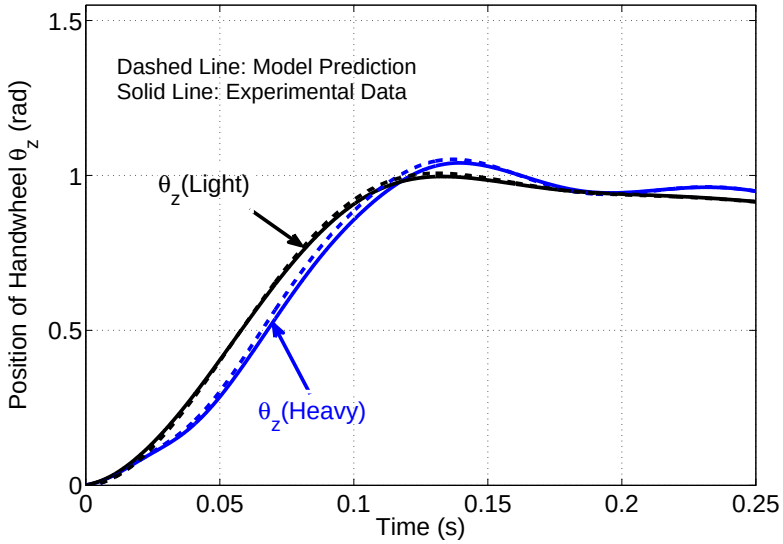

Figure 3.11: Experimental data vs model prediction of Normal Light and Heavy trials for Subject 4.

Figure 3.11 shows that the predicted trajectories of θ_z(Light) and θ_z(Heavy) are very close to the experimental data because we use the experimental data to estimate θ_r for heavy and light torques. This also verifies the effectiveness of the algorithm for θ_r estimation. The small differences result from the calculation error of $\dot{\theta}_z$ and $\ddot{\theta}_z$ in estimating θ_r due to encoder resolution.

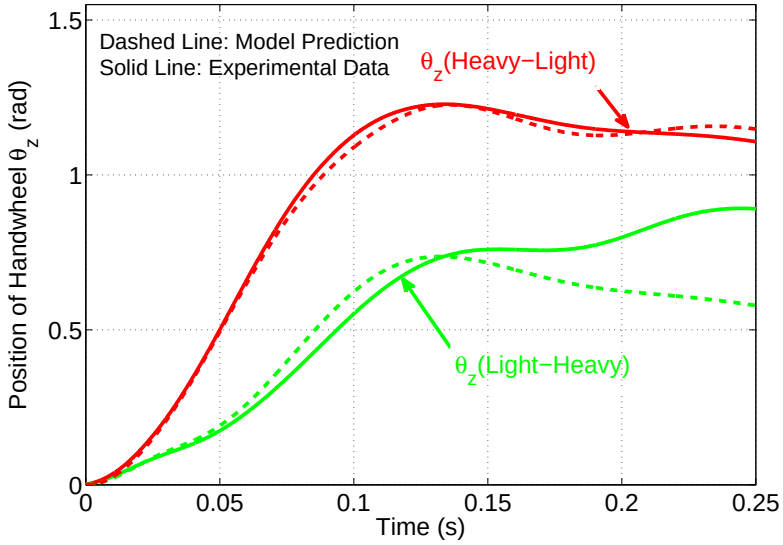

Figure 3.12: Experimental data vs model prediction of catch trials for Subject 4.

To validate the model, we will compare the predicted catch trial trajectories with the experimental data. The results are shown in Figure 3.12. The predicted trajectory of catch trial θ_z(Light-Heavy) matches the experimental data up to 0.13s, which is roughly the time when the participant uses feedback information to change grip force and position source. Similar trends can be seen for the θ_z(Heavy-Light) trajectory. The predicted trajectory matches the experimental result up to 0.25s and then these two curves are separated.

In order to compute the similarity between our model prediction and the experimental catch trial data, we define a "fitness score", by estimating the percentage of the catch trial trajectories predicted by the model. The fitness score depends on the difference between the experimental catch trial data and the model prediction, normalized by experimental data. Similar model validation metrics are used in [84, 23]. The two fitness scores for θ_z(Heavy-Light) and θ_z(Light-Heavy) are shown

in the following equations.

$$\begin{aligned}\text{Fitness score}_{\text{Heavy-Light}} &= 1 - \frac{\|\theta_z(\text{Heavy-Light}) - \hat{\theta}_z(\text{Heavy-Light})\|}{\|\theta_z(\text{Heavy-Light})\|},\\ \text{Fitness score}_{\text{Light-Heavy}} &= 1 - \frac{\|\theta_z(\text{Light-Heavy}) - \hat{\theta}_z(\text{Light-Heavy})\|}{\|\theta_z(\text{Light-Heavy})\|}.\end{aligned} \tag{3.7}$$

Here, θ_z(Heavy-Light) is the experimental trajectory for Heavy-Light catch trial and $\bar{\theta}_z$(Heavy-Light) is the mean value of θ_z(Heavy-Light); $\hat{\theta}_z$(Heavy-Light) is the model prediction trajectory for Heavy-Light catch trial; θ_z(Light -Heavy) is the experimental trajectory for Light-Heavy catch trial and $\bar{\theta}_z$(Light -Heavy) is the mean value of θ_z(Light -Heavy); $\hat{\theta}_z$(Light-Heavy) is the model prediction trajectory for Light-Heavy catch trial; The notation $\|\cdot\|$ denotes the Euclidean norm of a vector. We only calculate the fitness scores in(3.7) up to 0.10s before the feedback takes effect for all participants. The following table shows the fitness score to calculate the fit of our model to the experimental data for all participants. The mean of the fitness score for Heavy-Light catch trial is 92.66% with standard deviation of 5.49%. The mean of fitness score for Light-Heavy catch trial is 76.38% with standard deviation of 13.35%.

Table 3.3: Model fit for all participants

Participant Number	Fitness score$_{\text{Heavy-Light}}$	Fitness score$_{\text{Light-Heavy}}$
1	93.83%	85.01%
2	96.73%	89.77%
3	97.92%	80.17%
4	96.88%	85.65%
5	94.82%	75.60%
6	82.99%	69.47%
7	86.33%	74.93%
8	96.57%	81.93%
9	96.08%	71.53%
mean (all participants)	92.66±5.49%	76.38±13.55%

Our model in Figure 3.4 is structurally simple. It contains a position source, a spring-damper-mass impedance representation, and the external loads. Yet the impedance model is both user-specific and time varying. The impedance model is user-specific because each user has his or her own fitted functions shown in Table 3.1. The impedance value also depends on grip forces and we show in Figure 3.8 and Figure 3.9 that the grip forces are not constant. Hence the impedance values

(β and α) are time varying during the twist movement. Now we will first simplify the impedance model to a non-user-specific one and then further simplify it to be a non-user-specific and time-invariant one. We want to see if the model prediction will become worse after these simplifications and if so, how bad the simplified models are compared with the user-specific and time varying model.

3.4.3.1 Non-user-specific and Time Varying Impedance Model

To obtain the non-user-specific impedance model, we fit the mean values of all subjects' impedance in Figure 3.7 and the results are

$$\begin{aligned} J_z &= 4.50 \times 10^{-4} \ \ \mathrm{kg \cdot m^2}, \\ \beta &= 6.47 \times 10^{-4} \times f_{\mathrm{grip}} + 2.43 \times 10^{-2} \ \ \mathrm{N \cdot m/rad/s}, \\ \alpha &= 3.74 \times 10^{-2} \times f_{\mathrm{grip}} + 8.90 \times 10^{-1} \ \ \mathrm{N \cdot m/rad}. \end{aligned} \tag{3.8}$$

With the impedance profiles in (3.8) for all subjects, the fitness scores for catch trials are shown in Table 3.5. The mean of the fitness score for Heavy-Light catch trial is 92.51% with standard deviation of 3.60%. The mean of the fitness score for Light-Heavy catch trial is 75.45% with standard deviation of 8.59%.

Table 3.4: Non-user specific and time varying impedance model fit for all subjects

Participant Number	Fitness score$_{\text{Heavy-Light}}$	Fitness score$_{\text{Light-Heavy}}$
1	91.61%	77.55%
2	94.23%	76.04%
3	95.09%	74.28%
4	95.95%	78.11%
5	94.98%	74.69%
6	88.00%	78.02%
7	87.01%	83.04%
8	96.27%	83.16%
9	90.27%	57.99%
mean (all participants)	92.51±3.60%	75.45±8.59%

3.4.3.2 Non-user-specific and Time-invariant Impedance Model

To further simplify the impedance models, we use constants to fit the mean values of all subjects' impedance in Figure 3.7 and the results are

$$\begin{aligned} J_z &= 4.50 \times 10^{-4} \ \ \mathrm{kg \cdot m^2}, \\ \beta &= 3.65 \times 10^{-2} \ \ \mathrm{N \cdot m/rad/s}, \\ \alpha &= 15.97 \times 10^{-1} \ \ \mathrm{N \cdot m/rad}. \end{aligned} \tag{3.9}$$

With the impedance profiles in (3.9) for all subjects, the fitness scores for catch trials are shown in Table 3.5. The mean fitness score for Heavy-Light catch trial is 92.35% with standard deviation of 4.01%. The mean fitness score for Light-Heavy catch trial is 66.04% with standard deviation of 12.58%.

Table 3.5: Non-user-specific and time-invariant model fit for all subjects

Participant Number	Fitness score$_{\text{Heavy-Light}}$	Fitness score$_{\text{Light-Heavy}}$
1	91.95%	70.64%
2	91.82%	58.35%
3	96.88%	70.66%
4	97.98%	70.21%
5	90.97%	79.57%
6	85.51%	58.55%
7	90.88%	73.62%
8	96.13%	74.64%
9	89.07%	38.16%
mean (all participants)	92.35±4.01%	66.04±12.58%

3.4.3.3 Comparison of the Three Models

Now we have the results of three models:

- Model 1: User-specific and time varying impedance model;
- Model 2: Non-user-specific and time varying impedance model;
- Model 3: Non-user-specific and time-invariant impedance model.

We want to compare the how well these three models's prediction fit the experimental data. Figure 3.13 and Figure 3.14 shows the fitness scores for Heavy-Light and Light-Heavy catch trials respectively. The bar indicates the mean values and the error bar indicates 95% confidence intervals. The red dot stands for each participant's fitness

score. We can see the fitness scores of Heavy-Light catch trials do not differ a lot and the fitness scores of Light-Heavy catch trials have certain discrepancies.

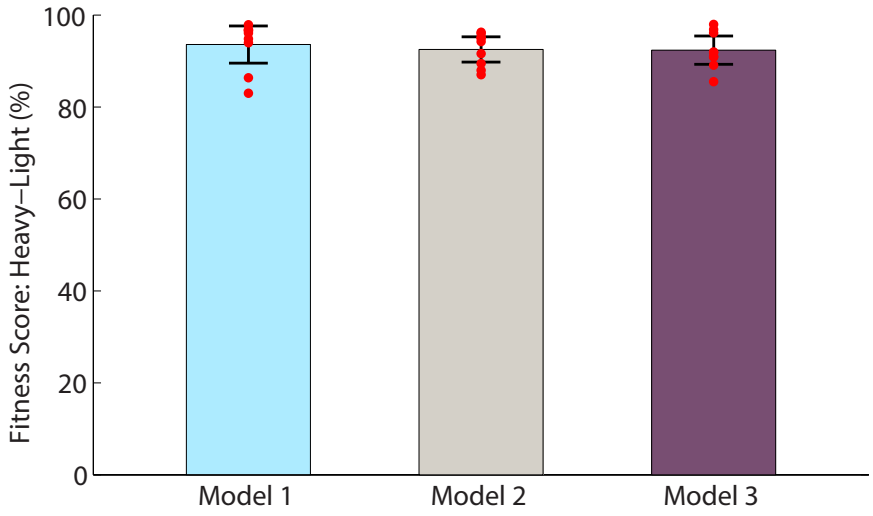

Figure 3.13: Comparison of fitness scores for Heavy-Light catch trials. The bar indicates the mean values and the error bar indicates 95% confidence intervals. The red dot stands for each participant's fitness score.

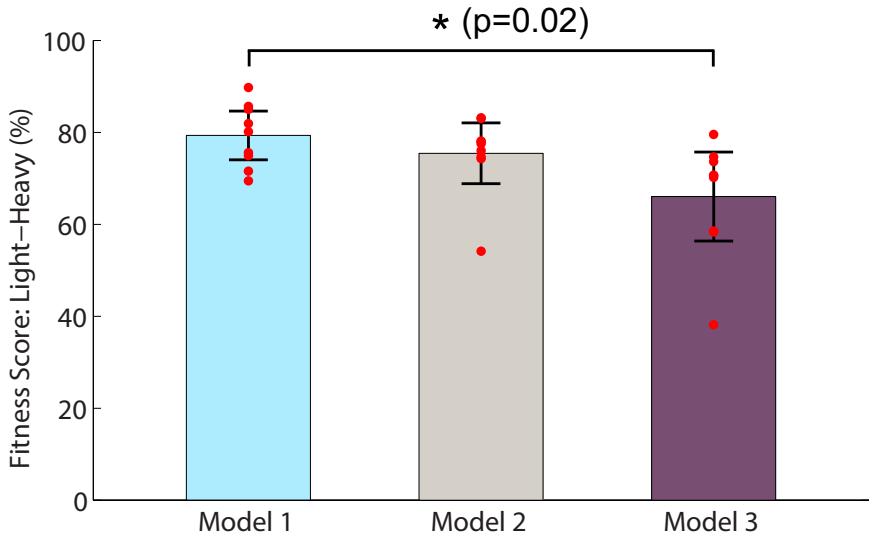

Figure 3.14: Comparison of fitness scores for Light-Heavy catch trials. The bar indicates the mean values and the error bar indicates 95% confidence intervals. The red dot stands for each participant's fitness score.

We further applied one-way ANOVA tests for statistical analysis to the data in Figures 3.13 and 3.14. For Heavy-Light fitness scores, ANOVA reported that there was no significant difference among the three models ($F(2, 24) = 0.216$, $p =$

0.807). For Light-Heavy fitness scores, there was a statistically significant difference ($F(2, 24) = 4.511$,$p = 0.022$). A Tukey post-hoc test revealed that the means of Model 1 and Model 3 are significantly different ($p = 0.02$) while no models have means significantly different from Model 2.

3.5 Discussion

We have proposed a model of the neuromuscular system that can predict motion of the hand in the grasp and lift (twist) task. Our model takes the form of a Norton network with a motion source and series-connected impedance and describes both the actuation behavior and the bending under load observed in the grasp and lift task. Our work is different than most of the existing grasp and lift literature, which focuses on the coordination of grip force and load force [48, 47, 46]. We focus instead on the position trajectory of the lifted (twisted) object rather than on the coordination between grip and load forces. We further made use of the coordination between grip and load forces to design experiments containing catch trials in order to validate our model. The predicted position trajectory of our model for unexpected loads matched the experimental data well (Figure 3.12 and Table 3.3)

3.5.1 A Generalized Norton Equivalent Circuit Model

The motion source in our model is analogous to the current source in the Norton equivalent electrical circuit [40]. The spring-damper-mass impedance is comparable to the electrical impedance in a Norton equivalent circuit. Our input estimation approach is built on the assumption that impedance is dependent on grip force. This is novel compared with existing motion source estimation methods. The motion source estimation method in [37] is based on the development of an online algorithm that eliminates the interaction force between the human body and environment, which is similar to the idea of "short-circuiting the electrical terminal" in a Norton equivalent circuit. A potential shortcoming of a method that avoids identifying the impedance such as that used in [37] is that any dependance of the model on a time-varying impedance is lost. Any dependence of impedance on the conditions imposed as part of the estimation method is also lost. The motion source identified in [37] may not be generalized to model common human active movement with interactive forces or torques between the human body and environment. Ample evidence has shown the strong adaptability of humans' impedance in different tasks [1]. Hence it is unlikely that the motion source for different tasks would be the same. Also, the motion source

identified in [37] was not validated by other experiments.

3.5.2 Relation to the Equilibrium-Point Hypothesis

Our model and the motion source identification method are similar to some of the work involving the equilibrium-point hypothesis [31, 32] but are also distinct from it in important ways. While the focus of the equilibrium-point hypothesis work is on the existence and properties of the equilibrium-point, the focus of our work is to build a simple yet competent model to describe human movement.

Several papers by Gomi, Kawato, and Flash [27, 31, 32] have compared the joint stiffness measured at rest and the joint stiffness measured during motion. Their results show that the stiffness measured during movement is usually larger than the stiffness measured at rest. In order to capture the difference and obtain accurate impedance values for motion source identification, we allow for a dependence of the impedance values on grip force. The difference between the stiffness at rest and during movement may be explained by the different grip force employed. On the other hand, identifying impedance during movement provides another approach to estimate the motion source [31, 32]. In the approach used in references [31, 32], the impedance values (including viscosity and stiffness matrices) were identified at discrete point-to-point movement positions and the motion source was estimated based on the interpolated impedance values.

The catch trial data in our work was used to validate the proposed model and the fitness scores in Table 3.3 illustrated the effectiveness of our model. Such validation of estimated models were not provided in the equilibrium-point hypothesis work [31, 32, 37].

3.5.3 Twist Impedance during Motion is Estimated While Stationary

The dependance of the identified impedance values on grip force in Figure 3.7 matches the results of existing work on human body/joint impedance [34, 35]. The nearly linear increase in damping and stiffness with increasing grip force and relatively constant inertia compare well to results on the impedance that other researchers [35, 34] have identified of the hand or fingers in contact with stationary objects. During grasp and lift tasks, a set of muscles are engaged to generate the lifting force that is perpendicular to the grip force. Note that the grip force is produced in part by some of the same muscles and neural circuits used to generate a twist torque.

It is reasonable that the relationship between the stationary impedance and grip

force remains valid during active movement, which is an assumption in our model. However, we have not tested this assumption through additional experiments. For human active movement that is very fast or sensitive to perturbations during movement, the impedance should be estimated through separate experiments.

3.5.4 Comparison with Simplified Models

Successful models should account for variation in impedance. We tested the fitness scores of Heavy-Light and Light-Heavy for three models: the user-specific and time varying model, the non-user-specific and time varying model, and the neither user-specific nor time varying model. The results of Light-Heavy fitness scores in Figure 3.14 show that 1) there is a statistically significant difference between the user-specific and time varying model and the neither user-specific nor time varying model; 2) there is no statistically significant difference between the user-specific and time varying model and the non-user-specific and time varying model. This indicates that the variation of impedance should at least be accounted for in the model.

The significant decrease of the fitness scores using constant impedance values is not surprising considering the highly nonlinear dynamics of the human body. A large amount of work has shown that the impedance values differ significantly depending on the grip force and posture [97, 35]. The estimated impedance during movement reported in [31, 32] were also highly variable.

3.5.5 The Effect of Feedback and Feedforward Control

The grip force produced by our participants for normal trials and catch trials in Figure 3.9 is consistent with the work in [47, 46]. The change of grip force in catch trials indicated the effect of feedback control through the CNS. The results in Table 3.2 reported the time at which feedback apparently comes into play. The reason why the change of grip force in Figure 3.9 is more obvious in Light-Heavy catch trials is that the participants need to increase the grip force to accommodate the Heavy load in order to avoid slips and achieve the rise time requirement. For the Heavy-Light trial, even if the participants do not decrease the grip force, slips can still be avoided and the rise time requirement can be achieved due to the Light load. Hence the change of grip force in Heavy-Light trials is not obvious.

As we only considered human feedforward control in this chapter, it is not surprising to see in Figure 3.12 that the prediction of the Light-Heavy trajectory did not match the experimental data after 0.13s. The predicted Heavy-Light trajectory

matched the experimental data for up to at least 0.25 s because this participant uses the motor plan and grip force for the Heavy load even when he or she realized the load is Light. This can be observed from this participant's grip force trajectories in Figure 3.9.

The overshoot of the position signal in Heavy-Light catch trials is consonant with the results in [47]. However, the undershoot of the position signal in Light-Heavy catch trials in our work was not found in [47] probably due to the different time synchronization method and the speed that objects were lifted. Also, our work has an identified model to predict the overshoot and undershoot.

3.5.6 Generalization of the Model to Different Areas

The model of a motion source and variable impedance in Figure 3.2 may be generalized to describe other biological and mechatronic movements. Some recent results by Hogan [40] have demonstrated the possibility of generalizing the Norton equivalent circuit to model nonlinear systems in robotics and mechatronics.

3.6 Conclusion

We studied the grip force development and hand trajectories in grasp and twist tasks. We built a simple model to investigate feedforward control during this task. This model depends on parameter values identified individually for each subject and subsequently used to explain the hand trajectories for catch trials with unexpected torque changes. The proposed model can fit the experimental results before feedback takes effect. The grip force development for catch trials indicates the possibility of a change in motion source after 0.11s. Hence in future work we shall study how the motion source in our model depends on feedback signals beyond 0.11s.

Either a motion source or an impedance alone cannot fully describe the human body's interactive dynamics during active movement. However, this fact is frequently ignored in different areas e.g. the active-steering control system design [2, 95, 68, 4]. Most human models in these models only contain passive driving point impedance or if they contain active control, they lack backdrive impedance. The integration of a motion source and impedance can enable these models to predict active movement and interactions with the environment such as lane changing.

Extending our model to study human interaction with cyber-physical systems is also one of our future research directions. Of particular interest to us is to further investigate the dissipativity phenomenon when human users interact with virtual

harmonic oscillator systems, which has been studied in our previous work [105]. The results in this chapter describes how impedance values change with grip force, which was not considered in our previous oscillator work [105].

CHAPTER IV

Human Control Strategies in Pursuit Tracking with a Disturbance Input

4.1 Introduction

Human tracking performance while pursuing a moving target by manipulating a control device such as a joystick has been studied since the early years of human-machine and aircraft pilot research [70]. Tracking experiments with a random input or pseudo random (sum-of-sins) reference and/or disturbance are often used to model real-world situations, e.g. driving a car along a windy road or flying an airplane. Human operators can use various control strategies during tracking tasks. McRuer *et al.* [54] proposed a scheme that he called *successive organization of perception*. Three types of control strategies are classified in this scheme depending on the predictability of the reference signals and skill development of the human operator: compensatory, pursuit, and precognitive control. The lowest level is compensatory control, in which only the tracking error is visually available and the human operator largely relies on a feedback control loop to achieve tracking performance. In pursuit control, past experience may provide the human operator with information about what to expect in the near future if the input is predictable, but closed-loop feedback control with visual feedback is also needed to correct his or her response. If the human operator has complete information about the reference signal's future, he or she may use precognitive control. A visual stimulus can then serve to trigger a properly sequenced response on the part of the operator. Closed-loop feedback control is not needed and hence precognitive behavior is essentially open loop control.

Early research on manual tracking behavior in pilot modeling has primarily focused on the feedback control model with a compensatory display [63], wherein the reference signal or disturbance were subjectively random-appearing. The human op-

erator behavior for these simple yet important tasks was largely captured in McRuer's crossover model [64]. Even nowadays, some human/machine interface research has found new applications of McRuer's models in various areas, e.g., the operation of a crane [79].

With a pursuit display, a human operator may use both feedback and feedforward control [100, 64, 3, 23]. With merely the reference signal as input, it is not possible to identify both feedback and feedforward controllers simultaneously in a human operator using classical spectral measurement techniques [100, 36, 23]. Instead, an "equivalent open-loop" controller that depends on both feedback and feedforward controllers was used in [100, 36] to study human tracking performance. Experimentally identifying the feedforward controllers has been a challenging problem. So far, there are only two proposed methods appearing in the literature that attempted to solve this problem. The first method was proposed by McRuer *et al.* in [100]. These authors hypothesized that an implied or indirectly measured feedforward controller can be calculated from the assumption that the feedback controller for the pursuit display was the same as the estimated feedback controllers for the corresponding compensatory display. The experimental results reported in [100] showed that under this assumption the feedforward was close to the inverse of the controlled dynamics.

Another approach to identify both feedback and feedforward controllers is to add a disturbance signal as a second input [3, 23]. In [3], the authors studied human manual tracking performance with a pursuit display and a disturbance input. However, no mathematical models were developed to fit the data using classical spectral measurement techniques. In [23], the authors investigated human control behavior in pursuit tracking of a ramp signal while being perturbed by a quasi-random multisine disturbance signal. Well-established time-domain identification methods were used to fit the time-domain data with ARX models that contains both parameterized feedback and parameterized feedforward controllers. The results showed that the feedforward controller is similar to the inverse of the controlled system dynamics.

In this chapter we propose a novel identification method that simultaneously estimates the feedback and feedforward controller. The method uses classical spectral measurement techniques and does not need the assumption made in [100]. We develop this method by taking advantage of the fundamental limitations theory [89], which lies at the very heart of feedback theory since it reveals performance constraints in feedback systems. The Bode sensitivity integral and complementary sensitivity integral are famous examples of such constraints. In [92], Gunter Stein provided theo-

retical explanation and application examples to illustrate the importance of respecting these constraints. The results in Chapter II also illustrated the importance of Bode integrals in the control of transient behavior in coupled oscillators. Another important constraint in fundamental limitations theory is the complementarity constraint [89, Chapter 1], which is of fundamental importance to feedback control design. In control systems, the complementarity constraint is used to illustrate a design tradeoff between disturbance rejection and measurement noise suppression. We will make use of the complementarity constraint to illustrate the relationship between reference tracking and disturbance rejection and then separate the feedback and feedforward control.

We aim to identify the feedback and feedforward control strategies of human operators in tracking single sine and pseudo random reference signals while being perturbed by a pseudo random disturbance signal. We will use frequency domain methods to identify non-parametric models for feedback and feedforward control. Furthermore, we will investigate a human operator's ability to reject disturbances using feedback control. Our experimentally identified non-parametric models for feedback and feedforward controllers show that a human operator's tracking of sine signals is largely dependent on feedforward control while tracking of pseudo random signals relies mostly on feedback control. The different control strategies in tracking single sine and pseudo random signals may be the key to explain several phenomena in human tracking activities. The phase lag difference in tracking single sine waves and sum-of-sines signals has been reported in the literature [41, Section 13]. The identified feedback and feedforward controllers in human tracking can explain the difference in phase lag identified in the present work and likely also in previous work.

The remainder of this chapter is organized as follows. Section 4.2 reviews the compensatory control model and feedforward control model in the literature on human manual tracking. Section 4.3 details the experimental procedures to track single sine waves and pseudo random signals. The identification method to estimate the feedback and feedforward controllers is also provided. The results about the identified human operator models are shown in Section 4.4. A discussion is offered in Section 4.5 and concluding remarks are given in Section 4.6.

4.2 Human Operator Models in Manual Control

Depending on the display type as well as the properties of reference and disturbance signals, the tracking strategies of human operators can be characterized as fully compensatory or combined feedforward and compensatory.

4.2.1 Compensatory Control Model

A model of compensatory human behavior is shown in Figure 4.1. The compensatory model describes the behavior of human operators when only the error signal is available to the human operator and the reference/disturbance signals are unpredictable.

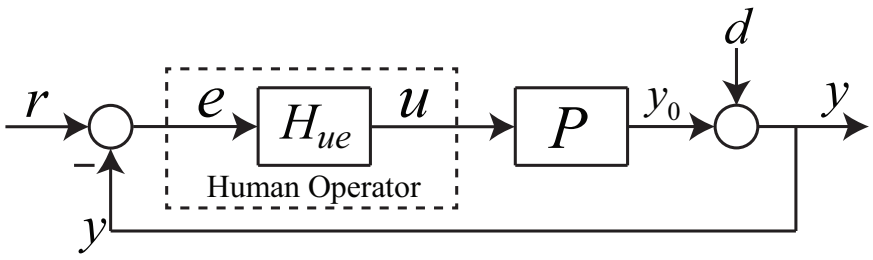

Figure 4.1: Human operator model: Compensatory.

The feedback model in Figure 4.1 is a unity feedback system. Define the *feedback open loop* transfer function

$$L(s) = H_{ue}(s)P(s), \tag{4.1}$$

and the *sensitivity* and *complementary sensitivity* functions by

$$S(s) = \frac{1}{1 + L(s)}, \tag{4.2}$$

$$T(s) = \frac{L(s)}{1 + L(s)}, \tag{4.3}$$

respectively. Then the human operator model in Figure 4.1 can be described by

$$Y(s) = T(s)R(s) + S(s)D(s). \tag{4.4}$$

A useful and widely used model to describe a human operator's compensatory control in Figure 4.1 is McRuer's crossover model. The crossover model has been used to analyze manual control performance in a variety of circumstances [65]. The crossover model assumes that a human operator and plant together approximate an integrator k_c/s with a time delay τ around the crossover frequency ω_c, that is

$$L(s) \approx \frac{k_c e^{-s\tau}}{s}. \tag{4.5}$$

The compensatory control structure in Figure 4.1 also places a fundamental limit between reference tracking and disturbance rejection performance. Here $T(s)$ is the

transfer function for pursuit tracking (in the Laplace domain, $\frac{Y(s)}{R(s)} = T(s)$) and $S(s)$ is the transfer function for disturbance rejection ($\frac{Y(s)}{D(s)} = S(s)$). Furthermore, the sum of $T(s)$ and $S(s)$ must be unity:

$$T(s) + S(s) = 1. \tag{4.6}$$

This identity is called "complementarity constraint" and is well-known in the theory of fundamental limitations [89] due to its fundamental importance to feedback control system analysis.

A robust feedback control system provides good tracking performance between $r(t)$ and $y(t)$, and it also suppresses disturbances $d(t)$. We will show in Section 4.4 that human operators can reject low-frequency disturbances very well, that is $S(j\omega) \approx 0$ when ω is small. To have $S(j\omega) \approx 0$, the feedback loop gain $|L(j\omega)|$ is very large at low frequencies. $S(j\omega) \approx 0$ also implies $T(j\omega) \approx 1$ from (4.6), which implies human operators can achieve good tracking and disturbance rejection performance for low frequencies using only the feedback control. Near the crossover frequency, $L(s)$ will have a slope of -20dB/decade and $T(s)$ is not close to 1. Hence, human operators' tracking and disturbance rejection performance will be worse. For signals with much higher frequencies than the crossover frequency, human operators will lose the ability to track reference signals and suppress disturbance due to neuromuscular limits. In other words, the feedback control loop has a bandwidth limitation that is roughly the same as the crossover frequency in McRuer's model.

4.2.2 Feedforward Control Model

If the reference signal is predictable and both reference and output signals are available, human operators may use combined feedforward and compensatory control strategies [100, 23] as shown in Figure 4.2. Then the response of the signals in the loop is

$$Y(s) = T_{\text{pursuit}}(s)R(s) + S(s)D(s), \tag{4.7a}$$

$$E(s) = T_{\text{error}}(s)R(s) - S(s)D(s), \tag{4.7b}$$

where $T_{\text{pursuit}}(s)$ is the summation of two transfer functions and defined as

$$T_{\text{pursuit}} = T(s) + H_{ur}(s)P(s)S(s), \tag{4.8}$$

and $T_{\text{error}}(s)$ is defined as

$$T_{\text{error}}(s) = 1 - T_{\text{pursuit}}(s) = [1 - H_{ur}(s)P(s)]\, S(s). \tag{4.9}$$

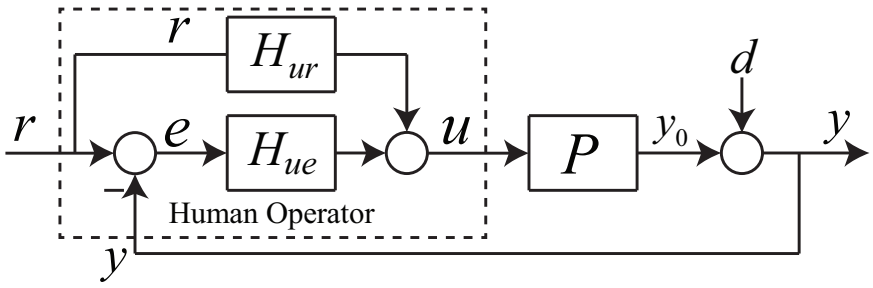

Figure 4.2: Human operator model: Combined compensatory and feedforward.

Compared with the compensatory model, the combined feedforward and compensatory control can use both feedback and feedforward controllers to achieve pursuit tracking and can only use the feedback controller to reject disturbances. The transfer function for feedback loop tracking is $T(s)$ and the transfer function for feedforward loop tracking is $H_{ur}(s)P(s)S(s)$. The addition of the feedforward loop can improve the tracking performance. Some papers [65, 23] assume that the feedforward controller of the human operator will invert the dynamic system that he or she is controlling, that is $H_{ur}(s)P(s) \approx 1$. In this case, the control action $u(t)$ is mostly from the feedforward controller $H_{ur}(s)$.

We can see from (4.7) that the feedforward control loop cannot reject disturbances. Rather, disturbances can only be suppressed through the feedback loop. The relationship between $T(s)$ and $S(s)$ in (4.6) still holds in the combined feedforward and compensatory control setup. Moreover, the feedforward loop tracking transfer function $H_{ur}(s)P(s)S(s)$ is also affected by $S(s)$. As discussed in Section 4.2.1, $S(s)$ is very small at low frequencies and then $H_{ur}(s)P(s)S(s)$ is small too. In other words, the contribution of feedforward loop tracking is attenuated by $S(s)$ at low frequencies, even if the feedforward controller is the inverse of the system dynamics. Hence, the addition of a feedforward tracking loop may not significantly improve tracking performance at low frequencies compared with the compensatory control model. The feedforward controller will improve the tracking performance at frequencies around the crossover frequency where the compensatory control loop starts to lose authority to achieve perfect tracking.

Our objective in this chapter is to design algorithms to simultaneously identify the feedback controller $H_{ue}(s)$ and feedforward controller $H_{ur}(s)$ in Figure 4.2 based

on the control system analysis in this section.

4.3 Methods

To identify the human operator model, a manual visual tracking experiment has been conducted.

4.3.1 Apparatus

The tracking task was presented on a LCD display in a "pursuit" configuration as shown in Figure 4.3. The animation update rate was 50 Hz. The display is measured 55×36 cm with 1920×1200 pixel resolution and was placed at a distance of around 120 cm from the participants' eyes.

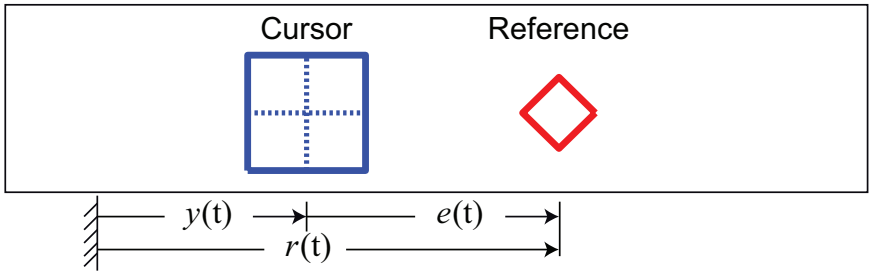

Figure 4.3: Display type for tracking tasks.

The manual tracking experiment was implemented in Matlab. Participants used a motorized haptic wheel [105] shown in Figure 4.4 to generate their control inputs, i.e., $u(t)$. Participants used a range of ± 90 degrees from the wheel's initial position. The angular position of the wheel, which was the control input $u(t)$, was measured by an optical encoder attached to the motor (Avago Technologies, HEDL-556x series). The resolution of the angular position was 0.09 degree (4000 counts per revolution). The rotational stiffness of the wheel was set to 0.14 N·m/rad over the full rotational range. The inertia of the wheel and rotor was 4.5×10^{-4} kg·m and the damping coefficient was 0.0013 N·m/(rad/s). These values were identified from separate system identification experiments.

A PC computer with a Sensoray Model 626 data acquisition card was used to record the data including the reference, error, control, disturbance, and output signals. All the signals were saved at 200 Hz for later analysis. The torque servo rate was 10 kHz.

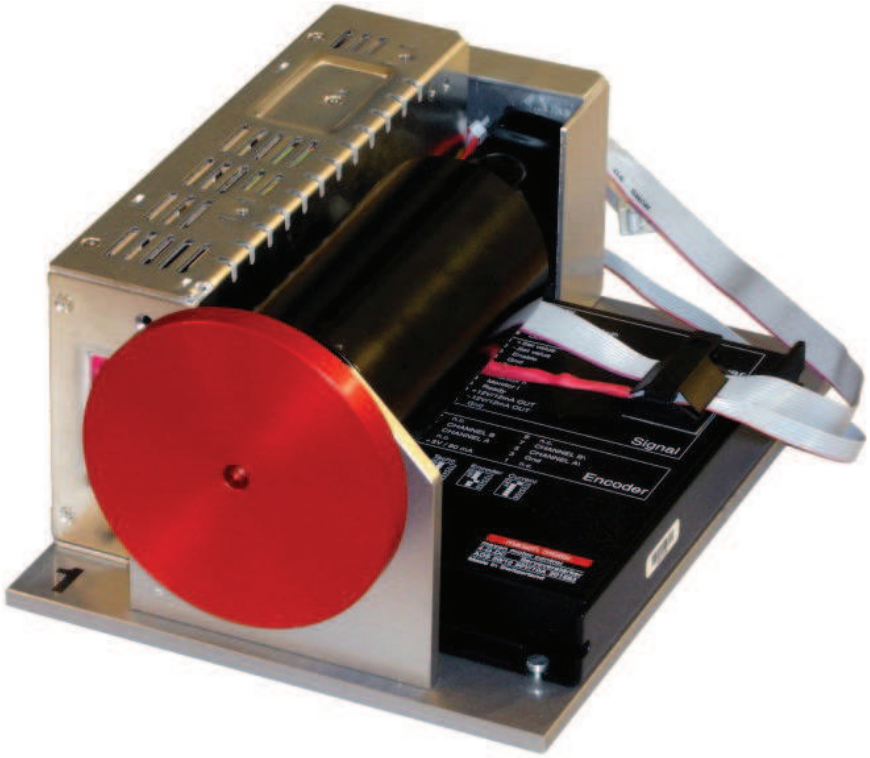

Figure 4.4: Single axis haptic interface used at ETH Zurich.

4.3.2 Experimental Design

Single-integrator dynamics for the plant $P(s)$ were considered in the present experiment: $P(s) = K_p/s$, where the input is $u(t)$ (the angular position of the wheel in degrees) and the output is $y_0(t)$ (the position of the cursor in pixels). The gain K_p was chosen to be $K_p = 40$. With this gain value, subjects usually turn the wheel within a comfortable range (± 90 degrees) and also can have fine control of the cursor.

The pseudo random reference function is a sum-of-sines signal and has 9 frequency components:

$$r(t)_{\text{pseudo random}} = \sum_{i=1}^{9} A_i \sin\left(\omega_i^r t + \phi_i\right), \tag{4.10}$$

where the amplitude A_i and frequency ω_i of these components are shown in Table 4.1 and ϕ_i is randomly generated at the beginning of each trial. For the single sine reference signal, the frequencies of individual reference signals are the same as ω_i^r in Table 4.1 and the amplitude is 540 pixels for all single sine reference signals.

The disturbance signal is a sum-of-sines signal that has 10 frequency components. The frequency components are different from the reference signals and the amplitude of the disturbance signals is smaller than that of the reference signals. These values

Table 4.1: Frequency components of the sum-of-sines reference input

Frequency Number i	Frequency ω_i^r (rad)	Amplitude A_i (pixel)
1	0.18	230.85
2	0.349	218.79
3	0.628	187.11
4	0.977	163.26
5	1.606	136.44
6	2.583	110.79
7	4.189	84.69
8	6.772	58.68
9	10.961	32.67

are shown in Table 4.2. For comparison, the amplitudes and frequencies of $r(t)$ and $d(t)$ are plotted in Figure 4.5.

Table 4.2: Frequency components of the disturbance signal

Frequency Number i	Frequency ω_i^d (rad)	Amplitude B_i (pixel)
1	0.10	57.71
2	0.265	54.70
3	0.488	46.78
4	0.801	40.82
5	1.292	34.11
6	2.095	27.70
7	3.386	21.17
8	5.481	14.67
9	8.867	8.168
10	12.481	4.5

4.3.3 Protocol and Participants

Eight subjects, all males, aged 20–31 years, were instructed to minimize the tracking error $e(t)$ presented on the display. All participants reported normal or corrected-to-normal vision, and no neurological or motor deficit. All participants gave written informed consent. The experiment was approved under the University of Michigan's Health and Behavioral Sciences Institutional Review Board. The IRB Registration Number was IRB00000245.

Prior to the formal tracking tasks, subjects were invited to perform a training session in which they could familiarize themselves with the tracking apparatus and tasks. The training session lasted 4 minutes during which the first 2 minutes were for

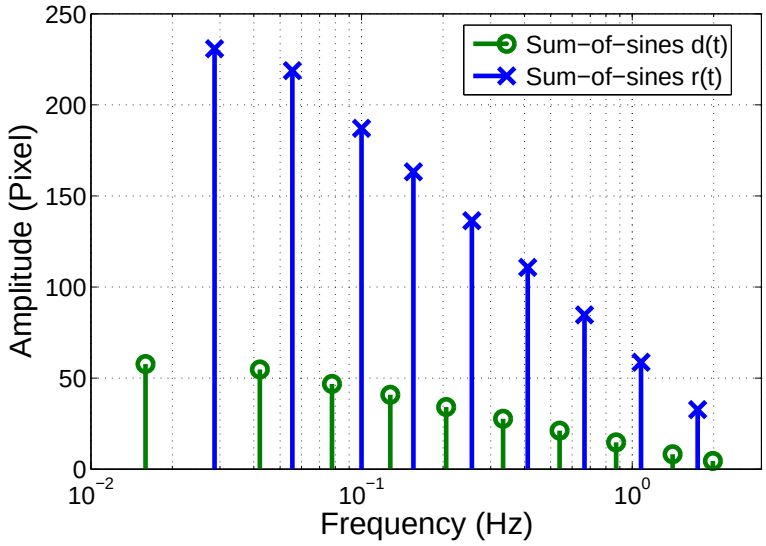

Figure 4.5: The amplitude and frequency of sum-of-sines $r(t)$ and $d(t)$.

tracking sum-of-sines signals and the second 2 minutes were for tracking single sine waves with different frequencies.

Subjects performed 10 formal tracking tasks after training. Nine of the 10 tracking tasks were to track the single sine waves with frequencies from ω_1^r to ω_9^r respectively. The 10th tracking task was to track the pseudo random reference signal in (4.10). The order of these tasks for each subject was randomized. Table 4.3 lists the reference signals and disturbance signals for each task.

Table 4.3: Reference and disturbance signals for each task

Task	$r(t)$ (pixel)	$d(t)$ (pixel)
Task 1	$540 \sin(\omega_1^r t + \phi_1)$	$\sum_{i=1}^{10} B_i \sin(\omega_i^d t + \phi_i)$
Task 2	$540 \sin(\omega_2^r t + \phi_2)$	
Task 3	$540 \sin(\omega_3^r t + \phi_3)$	
Task 4	$540 \sin(\omega_4^r t + \phi_4)$	
Task 5	$540 \sin(\omega_5^r t + \phi_5)$	
Task 6	$540 \sin(\omega_6^r t + \phi_6)$	
Task 7	$540 \sin(\omega_7^r t + \phi_7)$	
Task 8	$540 \sin(\omega_8^r t + \phi_8)$	
Task 9	$540 \sin(\omega_9^r t + \phi_9)$	
Task 10	$\sum_{i=1}^{9} A_i \sin(\omega_i^r t + \phi_i)$	

Each trial comprising one tracking task lasted 240s, of which the last 220s were used as the measurement data. On average, the whole experiment took about one hour for each participant.

4.3.4 Model Identification Methods

In this chapter, we will focus on the identification of the feedforward control model $H_{ur}(s)$ in Figure 4.2. The disturbance signal is indispensable in order to identify both the feedback and feedforward controllers [100]. For the identification, the frequencies of $d(t)$ should be different from the frequencies of $r(t)$ as shown in Figure 4.5. We also do not assume any model structures for $H_{ur}(s)$ and $H_{ue}(s)$. Instead, we will estimate these controllers' frequency response.

In Figure 4.2, there are six variables r, e, u, y_0, d, y. Given that $P(s)$ is known, there are only three independent variables. The signals $r(t)$ and $d(t)$ are two input variables. We use $y_0(t)$ as the output for identification instead of $y(t)$. Then we have

$$Y_0(s) = T(s)R(s) + H_{ur}(s)P(s)S(s)R(s) - T(s)D(s).$$

Rearranging (4.3.4) yields

$$\frac{Y_0(s)}{D(s)} = -T(s), \tag{4.11}$$

$$\frac{Y_0(s)}{R(s)} = T(s) + H_{ur}(s)P(s)S(s). \tag{4.12}$$

To identify $T(s)$, a fast Fourier transform (FFT) with a Hanning window was applied to both signals $d(t)$ and $y_0(t)$. Then the frequency estimate of $T(s)$ can be evaluated as

$$\hat{T}(j\omega) = -\frac{\hat{Y}_0(j\omega)}{\hat{D}(j\omega)}, \quad \text{at frequencies } \omega_1^d, \omega_2^d, \cdots, \omega_m^d, \tag{4.13}$$

where $\hat{Y}_0(j\omega)$ is the FFT of $y_0(t)$ and $\hat{D}(j\omega)$ is the FFT of $d(t)$. The frequency response of $T(s)$ at frequencies $\omega_1^r, \omega_2^r, \cdots, \omega_n^r$ can be obtained through interpolation of $\hat{T}(j\omega)$ at frequencies $\omega_1^d, \omega_2^d, \cdots, \omega_m^d$. The estimate of the feedback controller $H_{ue}(s)$ can be obtained from $\hat{T}(s)$ based on (4.3). The estimate of $S(s)$ can be obtained as:

$$\hat{S}(s) = 1 - \hat{T}(s).$$

The feedforward controller can be identified at frequencies $\omega_1^r, \omega_2^r, \cdots, \omega_n^r$ using (4.12)

$$\hat{H}_{ur}(s)\hat{P}(s) = \frac{\frac{\hat{Y}_0(s)}{\hat{R}(s)} - \hat{T}(s)}{\hat{S}(s)}.$$

4.4 Results

4.4.1 Phase Lag Difference in Pursuit Response

The phase lag differs when tracking single sine and pseudo random signals with the pursuit and disturbance display. These phenomena have been observed in humans [41, Section 13]. The frequency response of $T_{\text{pursuit}}(s)$ is estimated by calculating the ratio of FFTs of the output signal $y(t)$ and reference signal $r(t)$: $\frac{\hat{Y}(j\omega)}{\hat{R}(j\omega)}$. In the frequency domain, perfect pursuit tracking means $T_{\text{pursuit}}(s) = 1$ (0 dB in magnitude response and 0 degree in phase response). Figure 4.6 depicts the average frequency response estimates of $T_{\text{pursuit}}(s)$ for all subjects. Line segments are drawn between data points to make the curves easier to visualize, not to infer interpolation between the points. The error bars indicate the lower and upper bounds with 95% confidence intervals, to indicate between-subject variability[1]. The pursuit response $T_{\text{pursuit}}(s)$ in Task 10 (black line) can be estimated at frequencies $\omega_1^r, \omega_2^r, \cdots, \omega_9^r$ because the sum-of-sines reference signal has components at these frequencies. Each data set of Task 1 to Task 9 can be used to estimate the pursuit response $T_{\text{pursuit}}(s)$ at a single frequency (red line) ω_1^r to ω_9^r, respectively. Figure 4.7 depicts average frequency response estimates of $T_{\text{error}}(s)$ for all subjects.

From Figure 4.6, we can see that human operators can track low-frequency signals very well (close to 0 dB in magnitude response and 0 degree in phase response) up to 0.06 Hz in our experimental setup. The tracking performance shows little difference in tracking single sine waves and pseudo random signals up to 0.06 Hz. As frequency increases, the phase lag discrepancy becomes obvious over the range of 0.1 to 1 Hz. Over this range, the tracking performance for single sine waves is much better than for pseudo random signals. From Figure 4.7, we can see the magnitude response of $T_{\text{error}}(s)$ is smaller in tracking single sines than in tracking pseudo random.

4.4.2 Disturbance Rejection Through Feedback Loop

Disturbance rejection can only be achieved through the feedback loop. Human operators are able to reject low-frequency disturbances but lack the ability to reject high-frequency disturbances. Figure 4.8 shows the average FFTs of $d(t)$ and $y(t)$ for tracking pseudo random signals in Task 10 for all subjects. The error bars indicate the lower and upper bounds with 95% confidence intervals. We can see that although $d(t)$ has significant low-frequency components (less than 0.05 Hz), these components have

[1]These notations also apply to Figures 4.8 to 4.14 in this section.

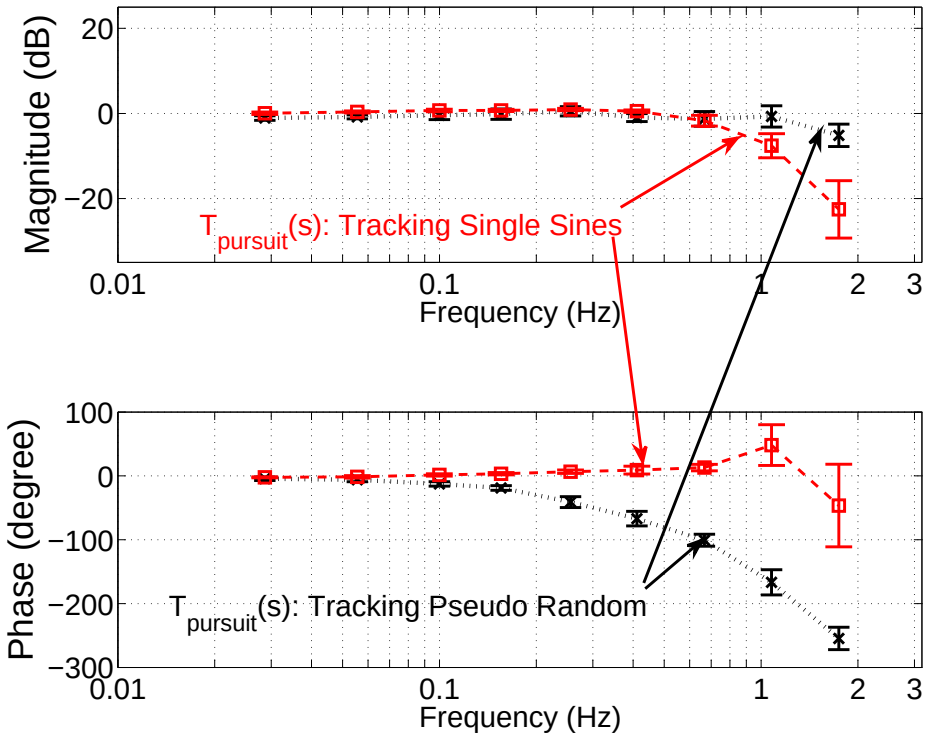

Figure 4.6: A comparison in pursuit responses $T_{\text{pursuit}}(s)$ between tracking single sine (red) and pseudo random (black) signals shows significant phase lag discrepancy.

mostly been suppressed in $y(t)$ through the feedback control loop. Human operators start to lose the ability to reject the disturbance signal as the frequency increases (0.05 to 0.3 Hz). For components with frequencies higher than 0.3 Hz, human operators cannot suppress them at all because of the feedback loop's bandwidth limitation. This limitation may be due to sensory delays, cognitive information processing limits, or neuromuscular response limits.

As discussed in Section 4.2, the transfer function from $d(t)$ to $y(t)$ is $S(s)$, which describes the ability to reject disturbances. Figure 4.9 shows the estimated $S(s)$ for tracking single sine and pseudo random signals. Despite the varied low-frequency components in $y(t)$, we averaged the frequency response estimates of $S(s)$ in Tasks 1-9 for all subjects. Again, the error bars indicate the 95% confidence intervals. We can see that the magnitude of $S(s)$ is small at very low frequencies and then increases to 1 with increasing frequency. Also, the estimated $S(s)$ looks very similar for both tracking pseudo random and single sine waves, at least for the frequency range 0.1 to

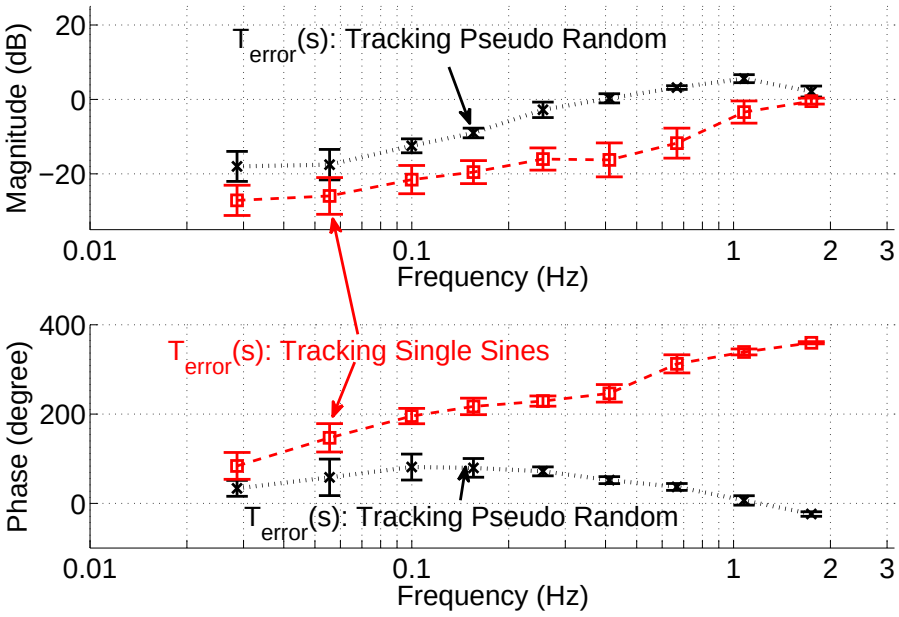

Figure 4.7: A comparison in $T_{\text{error}}(s)$ between tracking single sine (red) and pseudo random (black) signals shows the difference in tracking performance.

2 Hz.

We can further derive the estimated feedback open-loop transfer function $L(s)$ based on $S(s)$. The average estimates of frequency responses for all subjects are shown in Figure 4.10. The estimated $L(s)$ is almost identical for tracking both pseudo random and single sines. Also we can see that $L(s)$ resembles McRuer's crossover model. The crossover frequency is about 0.3 to 0.4 Hz and the phase is about 135 degrees.

The transfer function of feedback loop tracking $T(s)$ can be derived from $S(s)$ based on the identity (4.6). The estimated $T(s)$ is shown in Figure 4.11. We can see that $T(s)$ makes little difference between tracking single sine and pseudo random signals, and there is little phase lag difference in $T(s)$ although both estimated frequency responses have an obvious phase lag starting from 0.1 Hz.

As discussed in Section 4.2.2, the pursuit response $T_{\text{pursuit}}(s)$ consists of two parts: $T(s)$ and $H_{ur}(s)P(s)S(s)$. We then compare estimated $T(s)$ with $T_{\text{pursuit}}(s)$ and see if the feedback control is the dominant one. Figure 4.12 shows the comparison results between $T(s)$ and $T_{\text{pursuit}}(s)$ in Task 10 for tracking pseudo random signals. From Figure 4.12, there is no pronounced difference between $T(s)$ and $T_{\text{pursuit}}(s)$. This indicates that feedback control is dominant in tracking pseudo random signals. Figure

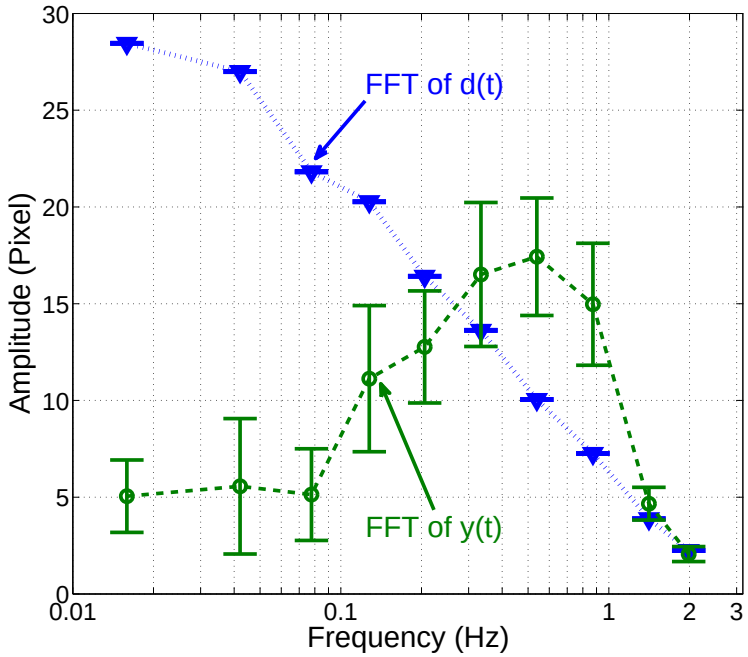

Figure 4.8: A comparison in amplitude between FFTs of $d(t)$ and $y(t)$ at frequencies $\omega_1^d, \omega_2^d, \cdots, \omega_m^d$ illustrates human operators can reject low-frequency disturbances but lack the ability to suppress high-frequency disturbances in Task 10.

4.13 shows the comparison results between $T(s)$ and $T_{\text{pursuit}}(s)$ in Task 1-9 for tracking single sine signals. There are significant differences in both magnitude response (above 0.7 Hz) and phase response (above 0.06 Hz) between $T(s)$ and $T_{\text{pursuit}}(s)$. This indicates that for tracking single sine signals with frequency above 0.06 Hz, the feedback control is not the dominant one and the feedforward controller $H_{ur}(s)$ may be used to compensate for the difference between $T(s)$ and $T_{\text{pursuit}}(s)$.

4.4.3 Estimated Feedforward Control in Human Operators

From our analysis in Section 4.4.2, the feedback controllers in human operators are not the cause for the phase lag difference discussed in Section 4.4.1. Using the method in Section 4.3.4, we can identify the feedforward controller $H_{ur}(s)$. Figure 4.14 shows the estimated frequency responses of $H_{ur}(s)P(s)$. The black line represents the mean values of frequency responses at ω_1^r to ω_9^r in Task 10 and the error bars stand for the lower and upper bounds with 95% confidence intervals. The results of frequency responses in Task 1 to 9 are shown in red.

The difference of frequency responses of $H_{ur}(s)P(s)$ in tracking single sine and

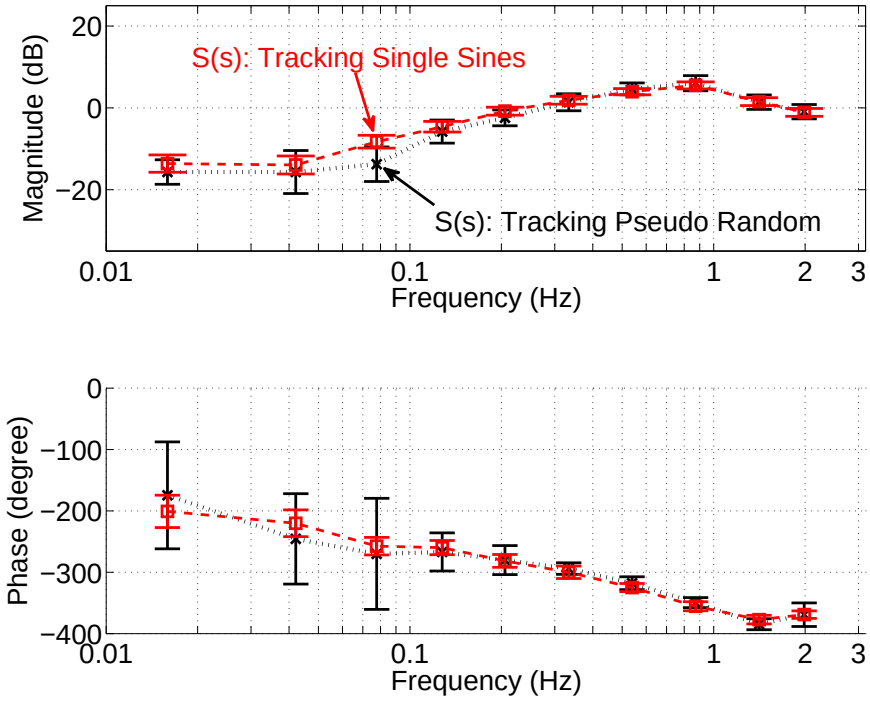

Figure 4.9: Frequency response estimates of $S(s)$ determine the ability to reject disturbances in tracking single sine (red) and pseudo random (black) signals.

pseudo random is obvious. In tracking single sine waves, $H_{ur}(s)P(s)$ is close to 1 over the range of 0.06 to 0.7 Hz while $H_{ur}(s)P(s)$ is not close to 1 in tracking pseudo random signals. Over this frequency range, the control action $u(t)$ for pursuit tracking is mostly generated by the feedforward controller in tracking single sines signals. In other words, if the signal is a single sine wave, human operators can generate the proper control signal $u(t)$ based on the model of $P(s)$ and prediction of $r(t)$ so that $H_{ur}(s)P(s) \approx 1$. If the signal is pseudo random, human operators will lose the ability to predict the reference signal and cannot use feedforward control to generate the proper $u(t)$. The difference in feedforward control is the cause of the phase lag difference in Section 4.4.1.

4.5 Discussion

The identification method in this chapter takes advantage of the relationship between disturbance rejection and pursuit tracking through fundamental limitations

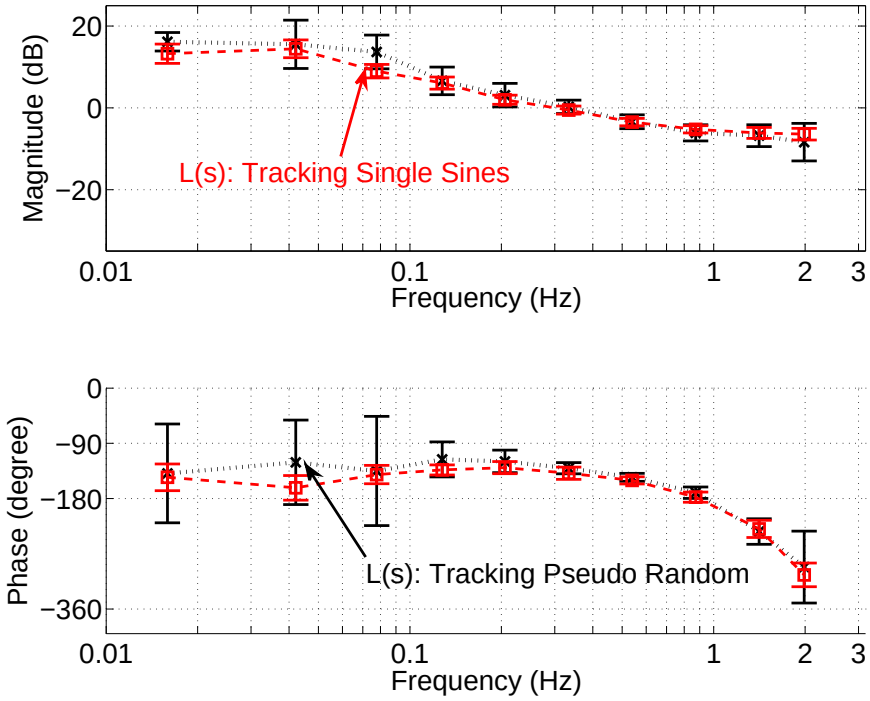

Figure 4.10: Frequency response estimates of $L(s)$ for tracking single sine (red) and pseudo random (black) signals are similar and resemble McRuer's crossover model.

theory. Although the complementary constraint in (4.6) is well-known in control system design, this fundamental constraint has not been used to identify feedback and feedforward controllers in the existing literature on human operator modeling [100, 64, 3, 23].

4.5.1 Feedback Control

The feedback control identified in this chapter matched McRuer's crossover model. From Figure 4.10, we can see that the crossover frequency is about 0.3 Hz and the phase at crossover frequency is about -135 degrees. Fitting these values to the crossover model in (4.5), we obtain that $\omega_c \approx 0.3$ Hz, $k_c \approx 1.89$, and $\tau \approx 0.32$ s. The corresponding parameter values reported in [64] by McRuer are $\omega_c \approx 0.75$ Hz and $\tau \approx 0.12 - 0.26$ s, which indicate higher crossover frequency and shorter time delays. The differences between McRuer's values and our values are likely due to the fact that the participants in McRuer's work were highly experienced civilian and naval test pilots while our participants were mostly university students.

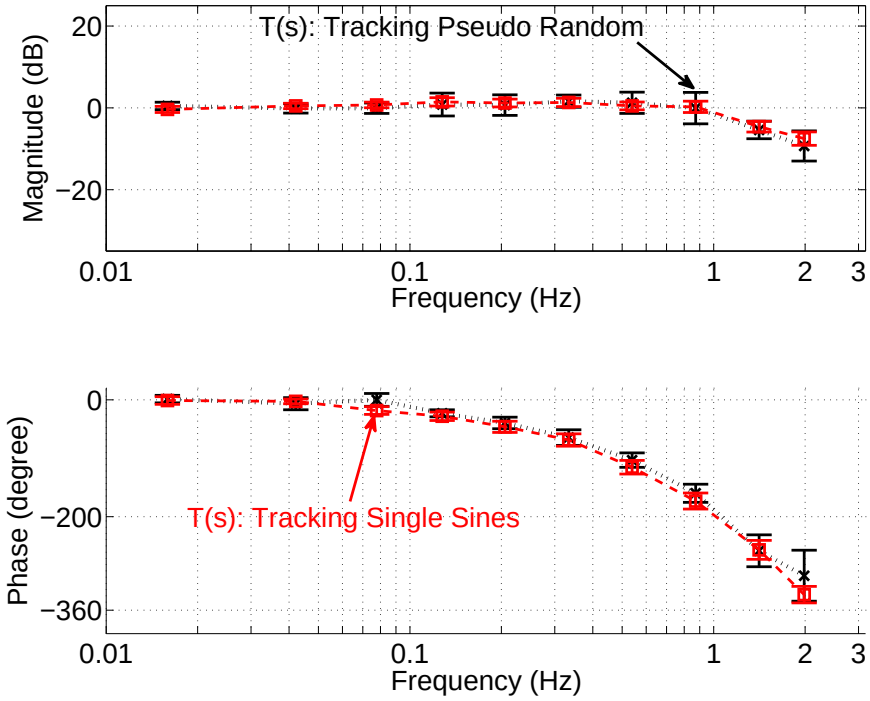

Figure 4.11: Frequency response estimates of $T(s)$ for tracking single sine (red) and pseudo random (black) signals are almost identical.

We also notice that the variation of the phase response of $S(s)$ and $L(s)$ in Figure 4.9 and Figure 4.10 for tracking pseudo random signals is larger at low frequencies than high frequencies. The data reported in [100] exhibit similar phenomena. One possible reason for this large variation is that the gain of $L(s)$ is very large at these low frequencies, which guarantees that the feedback tracking transfer function $T(s)$ is close to one no matter what values the phase responses have (see Figure 4.11). Since the function $T(s)$ is not sensitive to the phase response of $L(s)$ and $S(s)$, it is not surprising that humans may exhibit different phase response at these frequencies.

4.5.2 Feedforward Control

The identified feedforward control when tracking predicable signals in this chapter is consistent with the ARX model and MLE estimation results in [23] over the frequency range of 0.06 to 0.6 Hz. Our estimated frequency response of feedforward control in Figure 4.14 at frequency around 0.03 Hz is different from the results of the ARX model in [23]. The data at ω_1^r in Figure 4.14 indicate that $H_{ur}(s)P(s)$ is not

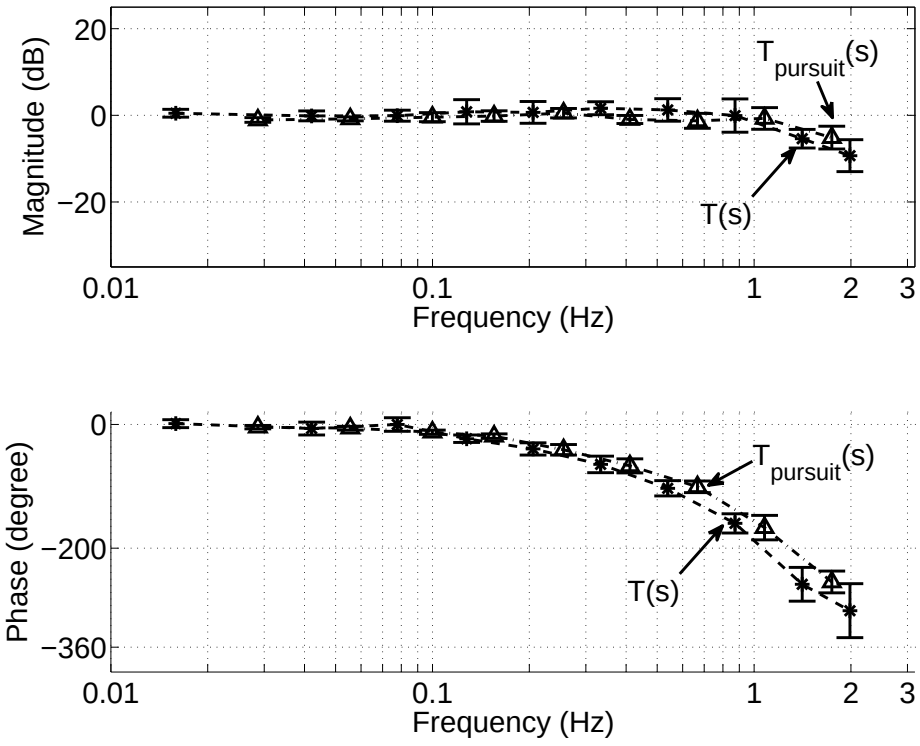

Figure 4.12: The overlay of frequency response estimates of $T(s)$ and $T_{\text{pursuit}}(s)$ in Task 10 indicates feedback control is dominant for tracking pseudo random signals.

as close to unity as other frequencies such as ω_2^r to ω_6^r. This illustrated that human operators may use feedback control to achieve good tracking performance at this low frequency as ω_1^r is way below the crossover frequency. This trend is not found in [23] probably due to the different reference signals (ramp in [23] and sinusoidal signals in our work) as well as the different identification methods employed in [23].

McRuer *et al.* identified the feedforward control in human operators [100] based on the untested hypothesis that feedback controllers are the same for compensatory and pursuit tracking. The results of the feedforward control in [100] generally coincide with the identified feedforward control in this work. However, there are some differences. The identified $H_{ur}(s)P(s)$ in our work is very close to one with nearly 0 dB in magnitude response and 0 degree in phase response over the frequency range of 0.06 to 0.6 Hz (Figure 4.14). In [100], the magnitude of the identified $H_{ur}(s)P(s)$ is not so close to 0 dB (-6 dB when $P(s)$ is a pure gain) and the phase can be 20 to 60 degrees at certain frequencies. The fact that $H_{ur}(s)P(s)$ in [100] is not close to

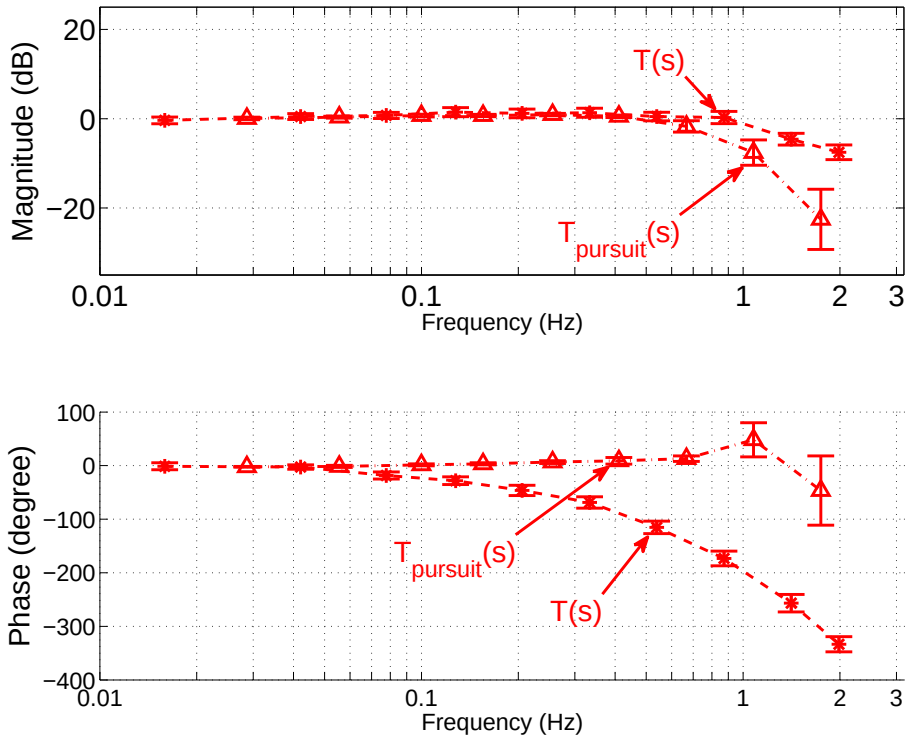

Figure 4.13: The difference in frequency response estimates of $T(s)$ and $T_{\text{pursuit}}(s)$ in Tasks 1-9 indicates the use of feedforward control for tracking single sine signals.

1 may be due to the hypothesized assumption. The assumption may not be totally true. The results in [23] show that the estimated feedback control gain is lower for the ramp pursuit tracking conditions than for the compensatory tracking conditions.

4.5.3 Limitations

Finally, it is acknowledged that the current study only focuses on the steady-state response. Whether the identified models are also applicable to transient responses has not been tested. How the models (especially the feedforward control) vary with other signals or different plant dynamics have not been investigated, although some results on the variation of feedback control have been reported in [64].

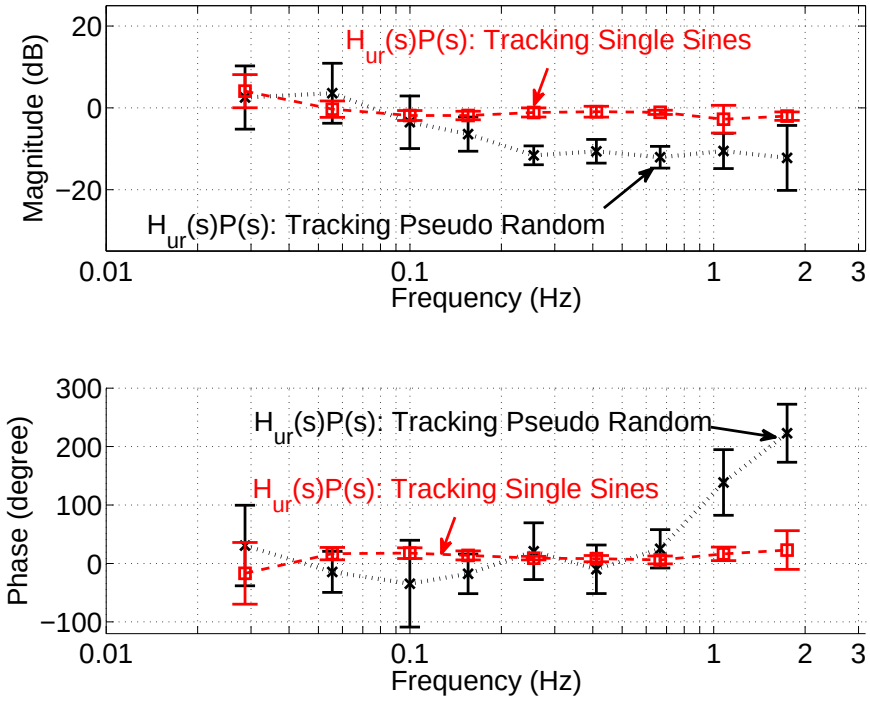

Figure 4.14: $H_{ur}(s)P(s)$ is close to 1 over a broad frequency range for tracking single sine signals.

4.6 Conclusion

In this chapter, we designed experiments and proposed identification methods to estimate both feedback and feedforward control in human manual tracking tasks. Our models explained the phase lag difference in tracking pseudo random and single sine signals. Using the theory of fundamental limits, we also showed the relationship between disturbance rejection and pursuit tracking. In future work, we will investigate the model variation for different plant dynamics.

The identification method can be incorporated with other observable brain processes through the fMRI or EEG techniques to characterize the motor performance. With these brain processes, researchers have examined which brain regions contribute to feedback and feedforward motor control processes [86]. Also, the pursuit tracking tasks in this chapter have been used as common tasks to study the impairment of voluntary movement by patients suffering from Parkinson's disease [29, 8, 18, 71]. So far, linear dynamic system approaches to separate the feedback and feedforward behaviors have not been used in human motor control. The proposed novel meth-

ods can be further extended for clinical rating scale development and rehabilitation performance estimation for neurodegenerative disorders [71, 5].

CHAPTER V

Conclusion and Future Work

5.1 Conclusion

Multi-agent systems are capable of displaying a larger and more interesting set of behaviors than single-agent systems. Common to the multi-agent systems is information exchange through virtual connection rather than physical linkage. String instability is one example of a behavior that emerges from a multi-agent system with virtual links (e.g. vehicle platooning). Only very recently have infeasible specifications been delineated for agents using arbitrary control policies, using analysis from the theory of fundamental design limitations, where the agent model contains a single or double integrator. Significant gaps remain in the determination of fundamental design limits for cyber-physical systems with more complex agent models such as harmonic oscillators. Our model in this dissertation is a second order, linear oscillator model that allows us to study how applied forces translate into oscillator motion. We have contributed theoretical tools to the study of string instability in coupled harmonic oscillator strings. We developed a new Bode-like integral relation that must be satisfied by the complementary sensitivity function in oscillator systems using the Cauchy integral theorem. We also derived a relationship between time domain specifications (steady-state and transient errors) to track a ramp-enveloped sinusoidal signal and frequency domain constraint (bound in magnitude response). We can say that certain design specifications will necessarily lead to string instability in oscillator systems based on our results. We also studied how constant time delays in the communication networks affect string instability. A time-headway operator is further proposed to improve string stability in the oscillator strings. Heterogeneous harmonic oscillators have also been considered.

When mechanical linkages are replaced by electronic communication and control systems (virtual links), certain undesirable phenomena can arise that may be difficult

to anticipate. In simple cases the lack of dissipativity in the cyber link unmasks instabilities that were present but suppressed in the system with a mechanical or physical link. The system of particular interest for us in this work is a system containing a human in the loop. We can call these "cyber-physiological" systems, to highlight the role of biomechanics in such systems. But even further, the physiological part of such systems contains control loops implemented in very complex and not-to-be-deciphered neural circuits. We have developed appropriate models that capture phenomena observable in cyber-physiological systems, especially those related to the realization of certain "links" in neural circuits, certain links in electronic circuits (and embedded control code), and yet other links in physical components.

Our model is partially inspired by the idea of Norton theorem in electrical engineering. Similar to the construction of Norton equivalent circuit at electrical terminals, the developed model is based on the observed mechanical behaviors of motion and force at the point of contact between human body and environment. The model contains a motion source and variable driving point impedance. Hence it features both a forward path dynamics (describing how the motion source affects the active movement) and interactive dynamics (describing how external loads affect the active movement). Experimentally validating such a model in human active movement tasks has not been undertaken in the literature. We applied system identification techniques and modeling principles guided by controls to experimentally identify the proposed model. We have used a prototypical manual task, the grasp and twist task, which involves a significant amount of coordination that produces interesting observable phenomena under perturbations and unexpected catch trials. In terms of the grasp and twist task, the proposed simple model has captured all the necessary aspects of motion planning, force control, biomechanics, and feedforward control.

Some tasks in our everyday life require the use of both virtual links and physical interactions like driving a vehicle along the highway. Similar to driving tasks, human operators can manipulate an integrator plant and manually track a single sine wave very well with almost unity amplitude ratio and zero phase lag as long as the frequency of the sine wave is not too high. However, the pattern of responses across single sine signals of different frequencies does not resemble the pattern of response across random appearing sum-of-sines signals for moderate to high frequencies. There is a significantly larger phase lag in tracking a pseudo random signal than tracking a single sine wave for moderate to high frequencies. This phenomenon suggests that humans utilize different control strategies for predictable tasks than for unpredictable tasks.

How to identify human control strategies especially the feedback and feedforward control has been studied for more than sixty years and so far most work with experimental support has been limited to the identification of feedback control. The identification of feedforward control has been a very challenging problem. A few papers that appeared very recently attempted to tackle this problem experimentally in the viewpoint of system identification. On the other hand, the well-established theory of fundamental limitations has proved its pivotal role in control system analysis but has not been utilized in human operator modeling. In this dissertation, we took advantage of theory of fundamental limitations to reveal the relationship between disturbance rejection and pursuit tracking using feedback control, which has been neglected in the literature of human operator modeling. Based on this relationship, we can further separate the feedforward control from the pursuit tracking performance. Specifically, we designed experiments and methodologies to identify non-parametric feedback and feedforward controllers in human operators for manual tracking with an explicit display of the sinusoidal reference signals and a disturbance input. Our results show that the feedback controller resembles McRuer's "crossover model", and the feedforward controller attempts to invert the system dynamics that the human operator is manipulating if the reference signal is predictable.

5.2 Future Work

5.2.1 Synchronization of Oscillators

The work in string instability of coupled oscillators can be extended in several ways. Extension of the simple string topology to more complex ones such as tree topologies [72] will be very useful, practical, yet challenging. To study more complex topologies, graph theory, which is mostly used in mathematics and computer science, may be needed and incorporated with fundamental limitations theory in controls. Similar to the synchronization of oscillators, the consensus problem in multi-agent systems encountered in control community is mostly focused on the steady-state responses while transient dynamics are still poorly understood. A general framework to incorporate both graph theory and fundamental limitations theory remains to be established.

Another direction is to extend the oscillator model to damped oscillators and nonlinear oscillators (such as the Kuramoto model that appears in much of the oscillator synchronization literature). Similar limitations exist in nonlinear systems, see [89, Chapter 4]. To the best of the our knowledge, using these fundamental limits

to study the transient dynamics in synchronization of nonlinear oscillators has not been considered in the literature.

The third extension of our current work is to consider more complex models of communication channels. In our current work, we merely modelled the communication channels as a constant time delay. In fact, most communication networks include complex features in addition to a constant time delay. The communication network may introduce stochastic time delays, packet dropouts, and noise. The stochastic time delay models build on Markov chains [106] and the signal-to-noise ratio [10] may be composed together with Bode's integrals to study more realistic multi-agent systems.

5.2.2 Human Movement Model with A Motion Source and Grip Force Dependent Impedance

Our work on the model of grasp and twist movements has also led to several future research directions. Our current model assumes that the impedance values depend only on grip force. A more appropriate study design for impedance trend analysis would require a wider selection of variables other than grip force, e.g., the rotational position and velocity of the human subject's hand, the grip force rate, and the amplitude of hand rotation. It has been shown that a smaller rotational range leads to larger impedance values for the dynamics of the human ankle [52]. The forearm posture when grasping the haptic wheel also changes the impedance value significantly.

The assumption that the static impedance values identified through the pulse disturbance are the same as those when turning the wheel was not verified in our current work. Some papers have shown these values can be different [33]. Estimating the dynamic impedance during movement may not be possible in the current grasp and twist setup because the turning time is only about 0.1 second and the time for human subjects to feel the difference in these two load torques is very short. It is still possible to do the impedance identification during the movement [31] if we can upgrade the apparatus and redesign the experiment. There are several ways to modify the experimental setup to prolong the moving time. One way is to change the grasp and twist tasks to a reaching task with a longer moving range. Also the virtual loads are not necessarily to be saturated springs and instead more complex haptic worlds like spring-damper-mass systems can be rendered, provided that more sensors are added to the current device.

Another limitation of our current work is that the impedance model is a second

order system, which combines the dynamics of the human hand and the haptic wheel itself. If we can identify the model of the haptic wheel, we might be able to separate the dynamics of the human hand and haptic wheel. Moreover, the human hand itself may be a fourth order system consisting of two cascaded second order systems and the second order system in this work is only an approximation over a frequency range. How to identify these higher order systems during movement is a challenging problem.

It is also interesting to apply the ideas in this work to real world applications. A simple yet competent model of human motor behavior would enable the design of cyber-physical systems capable of sharing control and collaborating with humans. In particular, predicting human behavior during unexpected conditions is critical to engineering reliable active safety systems.

5.2.3 Feedforward and Feedback Control in Human Pursuit Tracking

The feedback and feedforward model in human pursuit tracking tasks can be improved in various ways. With increased frequency of the single sine wave, it is harder for human subjects to detect disturbance signals. The current human model lacks such a detection representation and we assume the subject can perceive all the disturbance signals. The assumption is not totally valid especially when the reference signals are fast sine waves. The ability of human perception or detection is important in determining the human disturbance rejection and tracking performance. To model human perception using control system methods is challenging yet very useful in human operator models.

In the current work, the plant is a single integrator and it will be valuable to perform experiments for different plants such as unity gain, double integrator, or a single integrator with delays. Application of the identification method to motor control areas could be another future research direction. We have demonstrated a method to model tracking performance with linear dynamical systems, that separates the feedforward and feedback features. As neuroscientists attempt to elucidate the function of different neural structures for various tasks [86], it is natural to consider control system methods like the approach used in this dissertation to provide a theoretical framework for interpreting these studies as the proposed models incorporate concepts of feedback, model selection, and feedforward models.

BIBLIOGRAPHY

BIBLIOGRAPHY

[1] D. A. Abbink and M. Mulder, "Neuromuscular analysis as a guideline in designing shared control," *Advances in haptics*, vol. 109, pp. 499–516, 2010.

[2] T. Akita, K. Satoh, M. Kurimoto, and T. Yoshida, "Development of the active front steering control system," *FISITA paper*, 2000.

[3] R. Allen and H. Jex, "An experimental investigation of compensatory and pursuit tracking displays with rate and acceleration control dynamics and a disturbance input," National Aeronautics and Space Administration, NASA contractor report, 1968.

[4] T. Asao, S. Suzuki, and K. Kotani, "Estimation of drivers steering intention by using mechanical impedance," in *Human Interface and the Management of Information. Information and Interaction Design*, ser. Lecture Notes in Computer Science, S. Yamamoto, Ed. Springer Berlin Heidelberg, 2013, vol. 8016, pp. 3–11.

[5] N. Baradaran, S. N. Tan, A. Liu, A. Ashoori, S. J. Palmer, Z. J. Wang, M. M. Oishi, and M. J. McKeown, "Parkinsons disease rigidity: relation to brain connectivity and motor performance," *Frontiers in Neurology*, vol. 4, 2013.

[6] P. Barooah, P. G. Mehta, and J. P. Hespanha, "Mistuning-based control design to improve closed-loop stability margin of vehicular platoons," *IEEE Transactions on Automatic Control*, vol. 54, no. 9, pp. 2100–2113, Sep. 2009.

[7] M. Bennett, M. F. Schatz, H. Rockwood, and K. Wiesenfeld, "Huygens's clocks," *Proceedings: Mathematics, Physical and Engineering Sciences*, pp. 563–579, 2002.

[8] C. Bloxham, T. Mindel, and C. Frith, "Initiation and execution of predictable and unpredictable movements in Parkinson's disease," *Brain*, vol. 107, no. 2, pp. 371–384, 1984.

[9] H. W. Bode, *Network analysis and feedback amplifier design*. D. van Nostrand, New York, 1945.

[10] J. H. Braslavsky, R. H. Middleton, and J. S. Freudenberg, "Feedback stabilization over signal-to-noise ratio constrained channels," *IEEE Transactions on Automatic Control*, vol. 52, no. 8, pp. 1391–1403, 2007.

[11] J. W. Brown and R. V. Churchill, *Complex Variables and Application*. McGraw-Hill Science/Engineering/Math, 2008.

[12] E. Burdet, R. Osu, D. W. Franklin, T. E. Milner, and M. Kawato, "The central nervous system stabilizes unstable dynamics by learning optimal impedance," *Nature*, vol. 414, no. 6862, pp. 446–449, 2001.

[13] O. Celik and S. Ertugrul, "Predictive human operator model to be utilized as a controller using linear, neuro-fuzzy and fuzzy-ARX modeling techniques," *Engineering Applications of Artificial Intelligence*, vol. 23, no. 4, pp. 595–603, 2010.

[14] N. Chopra and M. W. Spong, "On exponential synchronization of kuramoto oscillators," *IEEE Transactions on Automatic Control*, vol. 54, no. 2, pp. 353–357, Feb. 2009.

[15] D. J. Cole, "A path-following driver–vehicle model with neuromuscular dynamics, including measured and simulated responses to a step in steering angle overlay," *Vehicle System Dynamics*, vol. 50, no. 4, pp. 573–596, 2012.

[16] J. B. Conway, *Functions of One Complex Variable*, 2nd ed. Springer-Verlag, 1978.

[17] E. J. Davison, "The robust control of a servomechanism problem for linear time-invariant multivariable systems," *IEEE Transactions on Automatic Control*, vol. 21, no. 1, pp. 25–34, Feb. 1976.

[18] B. Day, J. Dick, and C. Marsden, "Patients with Parkinson's disease can employ a predictive motor strategy," *Journal of Neurology, Neurosurgery & Psychiatry*, vol. 47, no. 12, pp. 1299–1306, Dec. 1984.

[19] M. Desmurget and S. Grafton, "Forward modeling allows feedback control for fast reaching movements," *Trends in Cognitive Sciences*, vol. 4, no. 11, pp. 423–431, 2000.

[20] J. M. Dolan, M. B. Friedman, and M. L. Nagurka, "Dynamic and loaded impedance components in the maintenance of human arm posture," *IEEE Transactions on Systems, Man, and Cybernetics*, vol. 23, no. 3, pp. 698–709, 1993.

[21] F. Dörfler and F. Bullo, "Synchronization in complex networks of phase oscillators: A survey," *Automatica*, vol. 50, no. 6, Jun. 2014.

[22] F. Dörfler, M. Chertkov, and F. Bullo, "Synchronization in complex oscillator networks and smart grids," *Proceedings of the National Academy of Sciences*, vol. 110, no. 6, pp. 2005–2010, 2013.

[23] F. M. Drop, D. M. Pool, H. J. Damveld, M. M. van Paassen, and M. Mulder, "Identification of the feedforward component in manual control with predictable target signals," *IEEE Transactions on Cybernetics*, vol. 43, no. 6, pp. 1936 – 1949, Dec. 2013.

[24] J. I. Elkind, "Characteristics of simple manual control systems," Ph.D. dissertation, Massachusetts Institute of Technology, 1956.

[25] P. M. Fitts, "The information capacity of the human motor system in controlling the amplitude of movement." *Journal of Experimental Psychology*, vol. 47, no. 6, p. 381, 1954.

[26] J. R. Flanagan and A. M. Wing, "The role of internal models in motion planning and control: evidence from grip force adjustments during movements of hand-held loads," *The Journal of Neuroscience*, vol. 17, no. 4, pp. 1519–1528, 1997.

[27] T. Flash, "The control of hand equilibrium trajectories in multi-joint arm movements," *Biological Cybernetics*, vol. 57, no. 4-5, pp. 257–274, 1987.

[28] T. Flash and N. Hogan, "The coordination of arm movements: an experimentally confirmed mathematical model," *The Journal of Neuroscience*, vol. 5, no. 7, pp. 1688–1703, 1985.

[29] K. Flowers, "Some frequency response characteristics of Parkinsonism on pursuit tracking," *Brain*, vol. 101, no. 1, pp. 19–34, Mar. 1978.

[30] M. J. Fu and M. C. Cavusoglu, "Human-arm-and-hand-dynamic model with variability analyses for a stylus-based haptic interface," *IEEE Transactions on Systems, Man, and Cybernetics, Part B: Cybernetics*, vol. 42, no. 6, pp. 1633–1644, 2012.

[31] H. Gomi and M. Kawato, "Equilibrium-point control hypothesis examined by measured arm stiffness during multijoint movement," *Science*, vol. 272, no. 5258, pp. 117–120, 1996.

[32] ——, "Human arm stiffness and equilibrium-point trajectory during multi-joint movement," *Biological Cybernetics*, vol. 76, no. 3, pp. 163–171, 1997.

[33] H. Gomi, Y. Koike, and M. Kawato, "Human hand stiffness during discrete point-to-point multi-joint movement," in *Proceedings of the 14th Annual International Conference of the IEEE Engineering in Medicine and Biology Society*, vol. 4, 1992, pp. 1628–1629.

[34] A. Z. Hajian and R. D. Howe, "Identification of the mechanical impedance at the human finger tip," *Journal of Biomechanical Engineering*, vol. 119, no. 1, pp. 109–114, Feb. 1997.

[35] C. Hasser and M. Cutkosky, "System identification of the human hand grasping a haptic knob," in *Proceedings of the 10th Symposium on Haptic Interfaces for Virtual Environment and Teleoperator Systems*, Orlando, FL, USA, Mar. 2002, pp. 171–180.

[36] R. A. Hess, "Pursuit tracking and higher levels of skill development in the human pilot," *IEEE Transactions on Systems, Man, and Cybernetics*, vol. 11, no. 4, pp. 262–273, 1981.

[37] A. J. Hodgson and N. Hogan, "A model-independent definition of attractor behavior applicable to interactive tasks," *IEEE Transactions on Systems, Man, and Cybernetics, Part C: Applications and Reviews*, vol. 30, no. 1, pp. 105–118, Feb. 2000.

[38] N. Hogan, "Impedance control: An approach to manipulation: Part II-Implementation," *Journal of Dynamic Systems, Measurement, and Control*, vol. 107, no. 1, pp. 8–16, 1985.

[39] ——, "Mechanical impedance of single-and multi-articular systems," in *Multiple Muscle Systems*. Springer, 1990, pp. 149–164.

[40] ——, "A general actuator model based on nonlinear equivalent networks," *IEEE/ASME Transactions on Mechatronics*, vol. PP, no. 99, pp. 1–11, 2013.

[41] R. J. Jagacinski and J. Flach, *Control theory for humans: Quantitative approaches to modeling performance*. Taylor & Francis, 2011.

[42] A. Jain and C. C. Kemp, "Pulling open novel doors and drawers with equilibrium point control," in *Proceedings of the 9th IEEE-RAS International Conference on Humanoid Robots*, 2009, pp. 498–505.

[43] P. Jenmalm, S. Dahlstedt, and R. S. Johansson, "Visual and tactile information about object-curvature control fingertip forces and grasp kinematics in human dexterous manipulation," *Journal of Neurophysiology*, vol. 84, no. 6, pp. 2984–2997, 2000.

[44] P. Jenmalm and R. S. Johansson, "Visual and somatosensory information about object shape control manipulative fingertip forces," *Journal of Neuroscience*, vol. 17, no. 11, pp. 4486–4499, 1997.

[45] G. Jian-Yue, X. Xin-Jian, W. Zhi-Xi, and W. Ying-Hai, "Synchronization of coupled oscillators on newman–watts small-world networks," *Chinese Physics Letters*, vol. 23, no. 6, p. 1410, 2006.

[46] R. S. Johansson, J. L. Backlin, and M. K. Burstedt, "Control of grasp stability during pronation and supination movements," *Experimental Brain Research*, vol. 128, no. 1-2, pp. 20–30, 1999.

[47] R. S. Johansson and G. Westling, "Coordinated isometric muscle commands adequately and erroneously programmed for the weight during lifting task with precision grip," *Experimental Brain Research*, vol. 71, no. 1, pp. 59–71, 1988.

[48] R. Johansson and G. Westling, "Roles of glabrous skin receptors and sensorimotor memory in automatic control of precision grip when lifting rougher or more slippery objects," *Experimental Brain Research*, vol. 56, no. 3, pp. 550–564, 1984.

[49] D. Johnson, "Origins of the equivalent circuit concept: the current-source equivalent," *Proceedings of the IEEE*, vol. 91, no. 5, pp. 817–821, May 2003.

[50] M. R. Jovanović and B. Bamieh, "On the ill-posedness of certain vehicular platoon control problems," *IEEE Transactions on Automatic Control*, vol. 50, no. 9, pp. 1307–1321, Sep. 2005.

[51] M. Kawato, "Internal models for motor control and trajectory planning," *Current Opinion in Neurobiology*, vol. 9, no. 6, pp. 718–727, 1999.

[52] R. Kearney and I. Hunter, "Dynamics of human ankle stiffness: variation with displacement amplitude," *Journal of Biomechanics*, vol. 15, no. 10, pp. 753–756, 1982.

[53] R. E. Kearney, R. B. Stein, and L. Parameswaran, "Identification of intrinsic and reflex contributions to human ankle stiffness dynamics," *IEEE Transactions on Biomedical Engineering*, vol. 44, no. 6, pp. 493–504, 1997.

[54] E. S. Krendel and D. T. McRuer, "A servomechanisms approach to skill development," *Journal of the Franklin Institute*, vol. 269, no. 1, pp. 24–42, Jan. 1960.

[55] K. J. Kuchenbecker, J. G. Park, and G. Niemeyer, "Characterizing the human wrist for improved haptic interaction," in *Proc. ASME Int. Mechanical Engineering Congress and Exposition*, vol. 2, 2003, p. 42017.

[56] Y. Kuramoto, "Self-entrainment of a population of coupled non-linear oscillators," in *International symposium on mathematical problems in theoretical physics*, 1975, pp. 420–422.

[57] H. Lee, P. Ho, M. Rastgaar, H. Krebs, and N. Hogan, "Multivariable static ankle mechanical impedance with active muscles," *IEEE Transactions on Neural Systems and Rehabilitation Engineering*, vol. 22, no. 1, pp. 44–52, Jan. 2014.

[58] H. Lee and N. Hogan, "Investigation of human ankle mechanical impedance during locomotion using a wearable ankle robot," in *Proceedings of the 2013 IEEE International Conference on Robotics and Automation (ICRA)*, 2013, pp. 2651–2656.

[59] C.-Y. Liang and H. Peng, "Optimal adaptive cruise control with guaranteed string stability," *Vehicle System Dynamics*, vol. 32, no. 4-5, pp. 313–330, 1999.

[60] C. C. Macadam, "Understanding and modeling the human driver," *Vehicle System Dynamics*, vol. 40, no. 1-3, pp. 101–134, 2003.

[61] L. Masia, V. Squeri, G. Sandini, and P. Morasso, "Measuring end-point stiffness by means of a modular mechatronic system," in *Proceedings of the 2012 IEEE International Conference on Robotics and Automation (ICRA)*, 2012, pp. 2471–2478.

[62] T. A. McMahon, *Muscles, Reflexes, and Locomotion*. Princeton University Press, 1984.

[63] D. T. McRuer, D. Graham, E. Krendel, and W. Reisener Jr, "Human pilot dynamics in compensatory systems. theory, models and experiments with controlled element and forcing function variations," *Wright-Patterson AFB (OH): Air Force Flight Dynamics Laboratory*, 1965.

[64] D. T. McRuer and H. R. Jex, "A review of quasi-linear pilot models," *IEEE Transactions on Human Factors in Electronics*, no. 3, pp. 231–249, 1967.

[65] D. T. McRuer and D. H. Weir, "Theory of manual vehicular control," *IEEE Transactions on Man-Machine Systems*, vol. 10, no. 4, pp. 257–291, Dec. 1969.

[66] R. H. Middleton and J. H. Braslavsky, "String instability in classes of linear time invariant formation control with limited communication range," *IEEE Transactions on Automatic Control*, vol. 55, no. 7, pp. 1519–1530, Jul. 2010.

[67] R. E. Mirollo and S. H. Strogatz, "Synchronization of pulse-coupled biological oscillators," *SIAM Journal on Applied Mathematics*, vol. 50, no. 6, pp. 1645–1662, 1990.

[68] H. Nakamura, D. Abbink, and M. Mulder, "Is grip strength related to neuromuscular admittance during steering wheel control?" in *Proceedings of the 2011 IEEE International Conference on Systems, Man, and Cybernetics (SMC)*, 2011, pp. 1658–1663.

[69] G. J. Naus, R. P. Vugts, J. Ploeg, M. Van de Molengraft, and M. Steinbuch, "String-stable cacc design and experimental validation: A frequency-domain approach," *IEEE Transactions on Vehicular Technology*, vol. 59, no. 9, pp. 4268–4279, 2010.

[70] M. Noble, P. M. Fitts, and C. E. Warren, "The frequency response of skilled subjects in a pursuit tracking task," *Journal of Experimental Psychology*, vol. 49, no. 4, p. 249, Apr. 1955.

[71] M. M. Oishi, P. TalebiFard, and M. J. McKeown, "Assessing manual pursuit tracking in Parkinsons disease via linear dynamical systems," *Annals of Biomedical Engineering*, vol. 39, no. 8, pp. 2263–2273, Aug. 2011.

[72] R. Olfati-Saber, J. A. Fax, and R. M. Murray, "Consensus and cooperation in networked multi-agent systems," *Proceedings of the IEEE*, vol. 95, no. 1, pp. 215–223, Jan. 2007.

[73] R. Olfati-Saber and R. M. Murray, "Consensus problems in networks of agents with switching topology and time-delays," *IEEE Transactions on Automatic Control*, vol. 49, no. 9, pp. 1520–1533, 2004.

[74] A. Pentland and A. Liu, "Modeling and prediction of human behavior," *Neural Computation*, vol. 11, no. 1, pp. 229–242, 1999.

[75] L. E. Peppard, "String stability of relative-motion PID vehicle control systems," *IEEE Transactions on Automatic Control*, vol. 19, no. 5, pp. 579–581, Oct. 1974.

[76] R. Pew, J. Duffendack, and L. K. Fensch, "Sine-wave tracking revisited," *IEEE Transactions on Human Factors in Electronics*, no. 2, pp. 130–134, 1967.

[77] D. Piovesan, A. Pierobon, P. DiZio, and J. R. Lackner, "Experimental measure of arm stiffness during single reaching movements with a time-frequency analysis," *Journal of Neurophysiology*, vol. 110, no. 10, pp. 2484–2496, 2013.

[78] D. Pool, M. Van Paassen, and M. Mulder, "Modeling human dynamics in combined ramp-following and disturbance-rejection tasks," in *Proc. AIAA Guidance, Navig., Control Conf., Toronto, Canada*, 2010.

[79] J. J. Potter and W. E. Singhose, "Effects of input shaping on manual control of flexible and time-delayed systems," *Human Factors: The Journal of the Human Factors and Ergonomics Society*, Mar. 2014.

[80] M. Rahman, R. Ikeura, and K. Mizutani, "Investigating the impedance characteristic of human arm for development of robots to co-operate with human operators," in *Proceedings of the 1999 IEEE International Conference on Systems, Man, and Cybernetics*, vol. 2, 1999, pp. 676–681.

[81] W. Ren, "Synchronization of coupled harmonic oscillators with local interaction," *Automatica*, vol. 44, no. 12, pp. 3195–3200, Dec. 2008.

[82] W. Ren, R. W. Beard, and E. M. Atkins, "Information consensus in multivehicle cooperative control," *IEEE Control Systems Magazine*, vol. 27, no. 2, pp. 71–82, Apr. 2007.

[83] J. Rosero, J. Ortega, E. Aldabas, and L. Romeral, "Moving towards a more electric aircraft," *IEEE Aerospace and Electronic Systems Magazine*, vol. 22, no. 3, pp. 3–9, 2007.

[84] A. C. Schouten, E. De Vlugt, J. B. van Hilten, and F. C. Van der Helm, "Quantifying proprioceptive reflexes during position control of the human arm," *IEEE Transactions on Biomedical Engineering*, vol. 55, no. 1, pp. 311–321, Jan. 2008.

[85] S. H. Scott, "Inconvenient truths about neural processing in primary motor cortex," *The Journal of Physiology*, vol. 586, no. 5, pp. 1217–1224, 2008.

[86] R. Seidler, D. Noll, and G. Thiers, "Feedforward and feedback processes in motor control," *Neuroimage*, vol. 22, no. 4, pp. 1775–1783, 2004.

[87] P. Seiler, A. Pant, and K. Hedrick, "Disturbance propagation in vehicle strings," *IEEE Transactions on Automatic Control*, vol. 49, no. 10, pp. 1835–1841, Oct. 2004.

[88] R. Sepulchre, D. Paley, and N. Leonard, "Collective motion and oscillator synchronization," in *Cooperative Control*, 2005, pp. 189–205.

[89] M. M. Seron, J. H. Braslavsky, and G. C. Goodwin, *Fundamental Limitations in Filtering and Control*. Springer-Verlag New York, Inc., 1997.

[90] S. E. Shladover, C. A. Desoer, J. K. Hedrick, M. Tomizuka, J. Walrand, W.-B. Zhang, D. H. McMahon, H. Peng, S. Sheikholeslam, and N. McKeown, "Automated vehicle control developments in the PATH program," *IEEE Transactions on Vehicular Technology*, vol. 40, no. 1, pp. 114–130, 1991.

[91] J. E. Speich, L. Shao, and M. Goldfarb, "Modeling the human hand as it interacts with a telemanipulation system," *Mechatronics*, vol. 15, no. 9, pp. 1127–1142, 2005.

[92] G. Stein, "Respect the unstable," *IEEE Control Systems*, vol. 23, no. 4, pp. 12–25, Aug 2003.

[93] S. H. Strogatz, "Exploring complex networks," *Nature*, vol. 410, no. 6825, pp. 268–276, 2001.

[94] D. Swaroop and J. K. Hedrick, "String stability of interconnected systems," *IEEE Transactions on Automatic Control*, vol. 41, no. 3, pp. 349–357, Mar. 1996.

[95] Y. Tanaka, Y. Kashiba, N. Yamada, T. Suetomi, K. Nishikawa, T. Nouzawa, and T. Tsuji, "Active-steering control system based on human hand impedance properties," in *Proceedings of the 2010 IEEE International Conference on Systems Man and Cybernetics (SMC)*, 2010, pp. 1697–1702.

[96] K. P. Tee, E. Burdet, C.-M. Chew, and T. E. Milner, "A model of force and impedance in human arm movements," *Biological Cybernetics*, vol. 90, no. 5, pp. 368–375, 2004.

[97] T. Tsuji, P. G. Morasso, K. Goto, and K. Ito, "Human hand impedance characteristics during maintained posture," *Biological Cybernetics*, vol. 72, no. 6, pp. 475–485, 1995.

[98] A. Tustin, "The nature of the operator's response in manual control, and its implications for controller design," *Journal of the Institution of Electrical Engineers-Part IIA: Automatic Regulators and Servo Mechanisms*, vol. 94, no. 2, pp. 190–206, 1947.

[99] S. E. Vozar, "A framework for improving the speed and performance of teleoperated mobile manipulators," Ph.D. dissertation, The University of Michigan, 2013.

[100] R. J. Wasicko, D. T. McRuer, and R. E. Magdaleno, "Human pilot dynamic response in single-loop systems with compensatory and pursuit displays," Air Force Flight Dyn. Lab. Res. and Technol. Div. Air Force Syst. Command, Wright-Patterson AFB, OH, Tech. Rep. AFFDL-TR-66-137, Dec. 1966.

[101] D. M. Wolpert and Z. Ghahramani, "Computational principles of movement neuroscience," *Nature Neuroscience*, vol. 3, pp. 1212–1217, 2000.

[102] R. S. Woodworth, "Accuracy of voluntary movement." *The Psychological Review: Monograph Supplements*, vol. 3, no. 3, p. i, 1899.

[103] C. W. Wu and L. O. Chua, "Application of graph theory to the synchronization in an array of coupled nonlinear oscillators," *IEEE Transactions on Circuits and Systems I: Fundamental Theory and Applications*, vol. 42, no. 8, pp. 494–497, 1995.

[104] T. Yamashita, "Effects of sine wave combinations on the development of precognitive mode in pursuit tracking," *The Quarterly Journal of Experimental Psychology*, vol. 42, no. 4, pp. 791–810, 1990.

[105] B. Yu, J. S. Freudenberg, R. B. Gillespie, and J. A. Cook, "Dynamic coupling between a human user and haptic virtual environment," in *Proceedings of the 51st IEEE Conference on Decision and Control*, Maui, HI, USA, Dec. 2012, pp. 2489–2494.

[106] B. Yu, Y. Shi, and J. Huang, "Modified generalized predictive control of networked systems with application to a hydraulic position control system," *Journal of Dynamic Systems, Measurement, and Control*, vol. 133, no. 3, p. 031009, 2011.

[107] Y. Zhang, Y. Yang, and Y. Zhao, "Finite-time consensus tracking for harmonic oscillators using both state feedback control and output feedback control," *International Journal of Robust and Nonlinear Control*, vol. 23, no. 8, pp. 878–893, May 2013.